Digital signal processing optical receivers for the mitigation of physical layer impairments in dynamic optical networks

José Manuel DELGADO MENDINUETA

A thesis submitted to the University College London (UCL) for the degree of Doctor of Philosophy

Optical Networks Group
Department of Electronic and Electrical Engineering
University College London (UCL)

September 2011

I, José Manuel Delgado Mendinueta, confirm that the work presented in this thesis is my own. Where information has been derived from other sources, I confirm that this has been indicated.

Abstract

It is generally believed by the research community that the introduction of complex network functions—such as routing—in the optical domain will allow a better network utilisation, lower cost and footprint, and a more efficiency in energy usage. The new optical components and sub-systems intended for dynamic optical networking introduce new kinds of physical layer impairments in the optical signal, and it is of paramount importance to overcome this problem if dynamic optical networks should become a reality. Thus, the aim of this thesis was to first identify and characterise the physical layer impairments of dynamic optical networks, and then digital signal processing techniques were developed to mitigate them.

The initial focus of this work was the design and characterisation of digital optical receivers for dynamic core optical networks. Digital receiver techniques allow for complex algorithms to be implemented in the digital domain, which usually outperform their analogue counterparts in performance and flexibility. An AC-coupled digital receiver for core networks—consisting of a standard PIN photodiode and a digitiser that takes samples at twice the Nyquist rate—was characterised in terms of both bit-error rate and packet-error rate, and it is shown that the packet-error rate can be optimised by appropriately setting the preamble length. Also, a realistic model of a digital receiver that includes the quantisation impairments was developed. Finally, the influence of the network load and the traffic sparsity on the packet-error rate performance of the receiver was investigated.

Digital receiver technologies can be equally applied to optical access networks, which share many traits with dynamic core networks. A dual-rate digital receiver, capable of detecting optical packets at 10 and 1.25 Gb/s, was developed and characterised. The receiver dynamic range was extended by means of DC-coupling and non-linear signal clipping, and it is shown that the receiver performance is limited by digitiser noise for low received power and non-linear clipping for high received power.

DON'T PANIC

—Douglas Adams, *The Hitchhiker's Guide to the Galaxy*

Acknowledgements

"Yo soy yo y mi circunstancia"

—José Ortega y Gasset, *Meditaciones del Quijote*

I OWE A GREAT debt to my supervisor, DR. BENN THOMSEN. Not only he is a very supportive and helpful person, but also a great supervisor who always stands next to you when you really need him. I thank him for giving me the opportunity to carry out the PhD at UCL, and also for trusting me. I know that sometimes this is complicated.

During all my life, women have played a fundamental role in my education. First, my piano teacher, MARÍA VICTORIA MARTÍN ADÁNEZ. I vividly remember the strong argument about the convergence of geometric series with my high school math teacher, PAQUITA ALONSO PÉREZ, in which I wrongly stated that an infinite sum of numbers could never converge. Now, I thank PROF. POLINA BAYVEL for her profound knowledge of how research should be done, and for her constant quest to bring out the best of every person.

I also express my gratitude with THE REST OF THE ONG MEMBERS and FELLOW PHD STUDENTS, both in the 808 room (whose name remarkably resembles 101 room) and around and about Roberts building. There are too many names to be written here, so I shall write none and, thus, nobody will be upset. Thank you all for being part of my circumstance.

Not everything in life is work, indeed very applicable to a PhD student—particularly in the late stages. I consider myself very lucky of having such a good friends around me like MANOLO, RAQUEL, PABLO, MERCEDES, AÍNA, and many others. I specially thank ALFONSO MORCHÓN for allowing me to sleep in his living room during the first couple of weeks I was in London.

And last but not least, I want to express my gratitude to my parents, MANUEL and JOSEFINA. They encouraged me to start my education in music, and made a really big effort toward me and my sisters—SANDRA and MARÍA—to receive the best possible education. I also thank my grandparents, which are not among us anymore. I greatly admire my grandfather RAMÓN MENDINUETA MÓNACO, for showing me the true meaning of wisdom, patience and love. He would be proud of me, wherever he is.

Contents

List of Figures

List of Tables

1 Introduction

THE ADVENT of new bandwidth-hungry applications—such as high-definition video and audio streaming, online real-time gaming, or peer-to-peer file sharing—in conjunction with the ubiquitous convergence of telecommunications services has pushed steadily the demand for higher line-rate networks in all their flavours, namely, carrier trunk networks [Tkach, 2010; Gerber and Doverspike, 2011], access networks [O'Byrne, 2010; Krogfoss et al., 2011], and wireless networks [Schneiderman, 2011].

In the context of core optical networks, recent research has concentrated on increasing the capacity of current wavelength division multiplexed links. Complex optical modulation formats—such as polarisation multiplexed QPSK [Lavery et al., 2011], OFDM [Youn et al., 2011], or 16-QAM [Gnauck et al., 2011], which require coherent optical receivers[1] [Savory, 2010; Ip et al., 2008]—have become a reality. In a coherent optical receiver, the electrical signal coming from the photo-detectors is sampled and digital signal processing algorithms for impairment compensation and clock and data recovery are carried out in the digital domain. A fundamental enabling technology is the availability of ultra-fast analog to digital converters capable of digitising electrical signals carrying data at optical line-rates [Dedic, 2010]. Complex modulation formats together with coherent detection and digital signal processing enable the upgrade of currently deployed fibre cables to carry more data and at a longer distance, increasing the capacity of Wavelength Division Multiplexed (WDM) optical links.

[1] non-coherent OFDM is also possible [Benlachtar et al., 2009]

Besides the benefits of the increased optical transport capacity and energy-per-bit reduction, all the network switching and routing is still performed in the electrical domain. Although it was speculated ten years ago that electronics would not be able to support the growing traffic demand [Hunter and Andonovic, 2000; Modiano and Narula-Tam, 2000; Tariq et al., 2000], reality has proved otherwise [Cisco Systems, 2011; O'Mahony et al., 2008]. Electronic switching has many advantages over optical switching—such as random access memory, that allows for packets to be stored and forwarded later, in order to avoid contention. However, router power consumption and on-chip heat dissipation have become important issues [Geer, 2005]. For example, the clock speed of microprocessors can not be increased further than 4 GHz with current technological processes, which originated the development of multi-core processors [Geer, 2005] that make use of *dark silicon*—not all the transistors on a chip can be used at a time [Esmaeilzadeh et al., 2011]. The development of faster optical links will require the design of even faster line-cards and electronic switching matrices, and it is expected that these problems will aggravate further.

A potential solution to tackle these issues is to better utilise the enormous bandwidth available in the optical fibre transmission medium by implementing more complex networking functions into the optical domain, thus circumventing the optical-electronic conversion bottleneck as much as possible—or ideally at all [Berthold, 2008; Ben Yoo, 2006]. It is generally believed by the research community that this will allow for a network cost reduction, bandwidth increasing, better network utilisation and throughput, ability to cope with network traffic changes, and reduced energy consumption and footprint [Qiao et al., 2010; Peng et al., 2010; Jue et al., 2009; Blumenthal et al., 2000].

A first approach to dynamic optical networking consists of routing wavelength channels avoiding electronic processing at intermediate nodes. This is known in the literature as **Optical Circuit Switching (OCS)** or **Wavelength Routed Optical Networks (WRONs)** [Baroni and Bayvel, 1997; Ramaswami and Sivarajan, 1995]. The network-wide end-to-end wavelength channels are referred as **lightpaths**. WRONs have been devoted considerable attention during the last 15 years and currently there are commercial products available [Berthold, 2008]. The design of WRONs is relatively simple; starting from a measured or predicted traffic demand, a set of lightpaths are routed and a different wavelength is assigned to each. This problem is named the Routing and Wavelength Assignment (RWA) problem and it is a NP-complete problem [Chlamtac et al., 1992]. Hence, many sub-optimal algorithms have been investigated to solve the RWA problem in an affordable time [Banerjee and Mukherjee, 2000; Hyytiä, 2004; Azodolmolky et al., 2009]. Moreover, WRON networks offer protection and resilience by means of lightpath re-routing, and can adapt to changing traffic conditions by reconfiguring previously established lightpaths [Banerjee and Mukherjee, 2000]. In

order not to disrupt operating lightpaths when reconfigurations are taking place, optical attenuators in every wavelength-selective switch keep the optical power constant over timescales that are much longer than the optical line-rate, and so the design of the physical layer and the optical receiver is simplified as a continuous-mode approach can be used. In spite of all the advantages of WRON networks over point-to-point WDM networks with electronic switching in every node, WRONs networks do have some disadvantages, such as the poor adaptability to changes in the traffic matrix and long reconfiguration times [Berthold, 2008].

The drawbacks of WRONs can be overcome if layer-3 Internet Protocol (IP) datagrams or packets can be directly mapped into the optical domain [Jue et al., 2009]. This leads to **Optical Packet Switching (OPS)**, in which data packets are switched entirely into the optical domain on a packet-by-packet basis without any optoelectronic conversion. The control information is stored in the optical packet itself in the form of an optical label [Koonen et al., 2007; Blumenthal et al., 2000], and this label is processed electronically to reconfigure the optical switch. Also, several all-optical OPS alternatives have been proposed [Ramos et al., 2005; Rangarajan et al., 2004; Blumenthal et al., 2003]. The main benefit of OPS is that it uses the optical bandwidth at its lowest granularity, in an efficient and flexible fashion. However, OPS have numerous disadvantages, such as the technological challenges it requires—ultra fast optical switches—and the lack of scalable optical memory to enable efficient contention resolution, without which packet loss becomes problematic.

The challenging optical component requirements needed for the realisation of OPS networks prevent the development of commercially available products at an affordable cost and, thus, competing with current electronic switching or WRONs will not be possible in the foreseeable future [Ramaswami, 2006]. However, there is an intermediate solution between OCS and OPS that provides a granularity better than a wavelength channel and also relaxes the optical switching speed and optical component requirements, and so simplifies the actual implementation with current technologies. This approach is known in the literature as **Optical Burst Switching (OBS)** [Qiao and Yoo, 1999, 2000; Turner, 1999; Battestilli and Perros, 2003; Düser, 2003].

OBS aggregates layer-3 datagrams at the edge of the optical network to form optical bursts of variable size [Aracil et al., 2007; Düser, 2003]. When a large-enough burst is aggregated or a timeout expires—the latter in order to reduce network end-to-end latency—a control packet is sent on a separate signalling wavelength. The purpose of this control packet is to setup an end-to-end lightpath by reconfiguring the optical switches that the optical burst has to traverse to reach its destination. Although many different signalling protocols have been proposed in the literature, all of them can be classified into two main kinds,

1. OBS Type-I, in which the burst route is not acknowledged. The signalling packet

is sent before the actual burst transmission and every optical switch traversed by that signalling packet is configured for the burst forwarding. After some time offset, the edge node starts the burst transmission in the hope that every switch in the path is correctly configured. However, if there are not enough switching resources available, the entire burst can be discarded due the contention. This can significantly degrade the throughput of the network, particularly for high network loads [Yao et al., 2003]. In order to avoid this, Type-I OBS makes use of relatively small optical bursts, in the order of kilobytes to megabytes [Bayvel and Düser, 2004].

2. OBS Type-II, in which there is a centralised control node or a distributed control mechanism which acknowledges the burst path before transmission and, thus, burst loss through contention is avoided in the network core—however, there could be still data loss at the edge queue if there are not enough network resources. As the burst loss in the network core is avoided, larger optical bursts allow for a better utilisation of network resources, and Type-II OBS signalling protocols use burst with sizes ranging from megabytes to even terabytes [Bayvel and Düser, 2004].

Dynamic optical networks enabling technologies

Core dynamic optical networks require four fundamental optical components in order to become a reality [Puttnam, 2008],

I Burst-mode transmitters, consisting of a tunable laser which is capable of promptly tuning to a specific wavelength and remaining stable whilst at a particular wavelength.

II Fast optical switches, able to quickly reconfigure and route an specific wavelength channel from an input port to a particular output port whilst keeping impairments such as attenuation, noise, and crosstalk as low as possible. In addition, other channels should be kept undisturbed.

III Burst-mode optical amplifiers, that amplify optical signals with high gain and keep the noise figure as low as possible, and most importantly for dynamic optical networks, do not show gain transients as a function of the instantaneous input optical power.

IV Burst-mode receivers, that are able to correctly detect the presence of incoming optical bursts which exhibit burst-to-burst power fluctuations and in-burst power variations. Also, the burst-mode receiver must carry out clock and data recovery on a burst-by-burst basis.

The requirements of all these components, and consequently the technological challenges to be addressed in their design, depend on the network granularity and the signalling method used [Buchta and Patzak, 2008]. For example, an optical switch capable of reconfiguring in ms time is adequate for OCS. However, OPS requires a switching speed of the order of ns.

Optical access networks

So far in this introduction, only core optical networks have been described as potential candidates for the benefits of dynamic optical networking. Nevertheless, access networks can also benefit from this technology. Indeed, the only currently deployed dynamic optical networking technology is for optical access networks where Time Division Multiple Access (TDMA) is used to multiplex users in the upstream direction [Effenberger and El-Bawab, 2009].

Besides the similarities between dynamic core and access networks, there are also important differences. Core optical networks make use of optical burst-mode amplifiers and optical switches. In contrast, in order to reduce costs, currently standardised optical access networks lack optical amplification and switching, and make use of optical splitters to share the optical transmission medium in a multicast fashion—from the point of view of the central office to the subscribers, known as downstream—and in a point-to-point time division multiple access—from the point of view of the subscriber transceiver to the central office, known as upstream direction. As the optical medium is shared in the upstream direction, information must be sent in the form of optical packets [Qiu et al., 2004].

Despite these differences, from the burst-mode receiver perspective the physical layer issues of core and access networks can be tackled using similar circuits—for analogue burst-mode receivers—or similar digital signal processing algorithms—for digital burst-mode receivers. This is the main reason for the inclusion of optical access networks in the category of dynamic optical networks.

1.1 Aims of research

The aim of this thesis is twofold. Firstly, the principal physical layer impairments introduced by the burst-mode components working in dynamic operation are identified, and digital receiver techniques—that make use of digital signal processing—are presented as a potential way to overcome them. Secondly, the results of the experimental characterisation of the digital receiver are given in the form of both bit-error rate and packet-error rate, which will help network designers to incorporate these results into the control plane, thus allowing a better understanding of the implications of

the physical layer under dynamic optical network operation.

Previous work by members of the Optical Networks Group at University College London focused on the design of wavelength-routed optical networks [Baroni and Bayvel, 1997], the control plane design and edge aggregation process of wavelength-routed optical burst switching networks [Düser, 2003], the advantages of dynamic versus static operation of wavelength-routed networks [Zapata-Beghelli, 2006], and the aforementioned fundamental components for dynamic optical networks [Puttnam, 2008]. The work of this thesis focuses mainly in the digital realisation of the burst-mode receiver and to produce a better characterisation of this critical component in a way that allows layer-2 network designers to incorporate this physical layer results into packet simulation models of signalling protocols.

Burst-mode receivers for core dynamic networks must be able to accurately detect incoming optical packets by using a preamble whose length should be minimised, in order to increase the physical layer data throughput. In addition, burst-mode receivers should have a large dynamic range, thus being able to correctly receive optical bursts that exhibit significant power variations. Also, the dynamic operation of the optical domain introduces impairments such as instantaneous optical power variations, and intrinsic receiver design—such as AC-coupling—introduces an instantaneous variation of the DC-offset and signal amplitude. A burst-mode receiver should continuously monitor these quantities and vary the optimum detection threshold and the electrical amplifier gain accordingly. The recent advent of fast analog-to-digital converters allows for the application of digital receiver techniques—which have been used in digital modems [Meyr et al., 1997], low speed digital subscriber loops [Song et al., 2002], and software-defined and cognitive radio [Haykin, 2005]—to optical line-rate receivers. The use of complex digital signal processing techniques allows to increase the impairment-tolerance of the digital burst-mode receiver with respect to their analogue counterparts, and consequently to the relaxation of the requirements of other dynamic optical network components.

The digital receiver techniques investigated for core dynamical networks can be readily applied to optical access networks. Indeed, passive optical access networks transmit the information in a continuous-mode fashion in the downstream direction (broadcast), but in the upstream the common sharing of the optical channel imposes a time-division multiplexing medium access control protocol, which leads to the necessity of a burst-mode receiver at the central office premises. Due to the lack of optical amplification—in order to lower the network cost—and to allow a high number of subscribes per passive network segment—which implies high splitting losses at the optical splitter—a burst-mode receiver intended for the upstream direction requires a high-sensitivity. Also, in order to further reduce costs and flexibilise network deployment, a large dynamic range is required. Moreover, having cheap optical transmitters at the

customer premises that have large transmitted optical power tolerance also demands for an increased dynamic range. Another important requirement of access networks from an upgrade point of view is the coexistence of high line-rate users with legacy low-line rate uses. Digital techniques can then be used to implement multi-rate optical receivers that are able to detect and adapt to the line-rate of incoming upstream optical packets from current and legacy subscribers.

1.2 Thesis outline

This thesis is organised as follows. Chapter 2 introduces the reader to the fundamentals of dynamic optical networking, and presents the principal impairments introduced when complex networking functions—such as routing—are introduced into the optical domain, for both core and access dynamic optical networks. Also, there is a survey of the most current work about recently developed burst-mode receivers that will allow for the comparison of the current state-of-the-art with the developed digital burst-mode receiver.

Chapter 3 presents a digital AC-coupled optical receiver intended for dynamic optical core networks. A detailed description of the all-digital receiver architecture is presented. The receiver is characterised and the packet-error rate for a variable preamble length is investigated. In addition, a simulation model suitable for the analysis of digital burst-mode receivers that have to deal with received power variations is developed and experimentally validated. The chapter concludes with an experimental study of the influence of the network traffic load and sparsity on the physical layer packet error-rate performance of the digital burst-mode receiver.

Chapter 4 introduces and characterises a digital dual-rate DC-coupled optical receiver intended for optical access networks. Two main points are investigated here. Firstly, the design and experimental validation of a multi-rate detecting algorithm. Secondly, the dynamic range extension of digital receivers by means of DC-coupling and non-linear clipping by the digitiser. It is shown that this receiver is mainly limited by thermal and quantisation noise for low optical received powers and by the packet and line-rate detector for high optical received powers.

In chapter 5, an optical power equaliser—consisting of a cascade of two semiconductor optical amplifiers—plus a wavelength converter is investigated, using the digital receiver investigated in previous chapters 3 and 4. The purpose of this device is to allow for wavelength consolidation and reach extension of current passive optical network segments in an affordable way.

Finally, chapter 6 summarises the work described in this thesis and also offers the reader some future work suggestions in view of the results of this thesis.

1.3 Original contributions of this thesis

The following list summarises the original contributions carried out and described in this thesis,

- Measurement, for the first time, of the impact of the header length in the ability of a digital receiver to accurately detect optical bursts in a dynamic optical network (chapter 3).
- Investigation of the impact of a high speed analog-to-digital converter, with emphasis on the noise produced by the digitiser, and the development of a realistic model suitable for the study of dynamic networks (chapter 3).
- Assessment of the impact of the network traffic load ρ and the traffic model sparsity on the packet detection of a digital burst-mode receiver, including a physical layer protocol for handling wrongly detected packets (chapter 3).
- Development and investigation of an algorithm for the detection of multiple line-rate optical packets in the context of an optical access network (chapter 4).
- Investigation of the burst-to-burst dynamic range extension of a digital receiver by means of DC-coupling and non-linear signal clipping at the digitiser (chapter 4).
- Development and characterisation—in terms of bit-error rate and packet-error rate—of a digital dual-rate burst-mode receiver designed for 10G-EPON and 1G-EPON optical access standards (chapter 4).
- Characterisation of a optical power equaliser and wavelength-converter intended for the consolidation of current optical access networks into an WDM link, also referred as a long-reach optical access network (chapter 5).

1.4 Publications arising from the work presented in this thesis

The following list cites the publications originated from the work described in this document,

1. Delgado Mendinueta, Cao, Thomsen, and Mitchell, "Performance of an optical equaliser in a 10G wavelength converting optical access network," *OSA Optics Express*, vol. 19, n. 15, pp. B229–B234, Dec. 2011.

2. Cao, Delgado Mendinueta, Mitchell, and Thomsen, "Performance of an optical equaliser in a 10 Gbit/s wavelength converting optical access network," in *Proceedings of the 37th European Conference and Exhibition on Optical Communications (ECOC)*, Geneva, Switzerland, Sep. 2011, paper Mo.1.C.1.

3. Delgado Mendinueta, Mitchell, Bayvel, and Thomsen, "Digital dual-rate burst-mode receiver for 10G and 1G coexistence in optical access networks," *OSA Optics Express*, vol. 19, no. 15, pp. 14060–14066, Jul. 2011.

4. Delgado Mendinueta, Bayvel, and Thomsen, "Digital lightwave receivers: an experimentally validated system model," *IEEE Photonic Technology Letters*, vol. 23, no. 6, pp. 338–340, Mar. 2011.

5. Delgado Mendinueta, Mitchell, Bayvel, and Thomsen, "Digital multi-rate receiver for 10 GE-PON and GE-PON," in *Proceedings of the Optical Fiber Communication Conference and Exhibition (OFC)*, Los Angeles, CA, Mar. 2011, paper NTuD4.

   This paper was awarded an honourable mention in the Corning Outstanding Student Paper Competition.

6. Delgado Mendinueta, Bayvel, and Thomsen, "Impact of network load and traffic sparsity on the performance of a digital burst-mode receiver," *Proceedings of the 36th European Conference and Exhibition on Optical Communications (ECOC)*, Turin, Italy, Sep. 2010.

7. Delgado Mendinueta, Bayvel, and Thomsen, "Dynamic Optical Networks Demonstrators: Reviewed and Classified," in *Proceedings of the London Communications Symposium (LCS)*, Sep. 2009.

8. Delgado Mendinueta, Bayvel, and Thomsen, "Impact of burst header length in the performance of a 10 Gb/s digital burst mode receiver," in *Proceedings of the Optical Fiber Communication and Exhibition (OFC)*, San Diego, CA, Mar. 2009, paper OWA7.

9. Delgado Mendinueta, Bayvel, and Thomsen, "Cluster processing for the study of optical burst-mode digital signal processing receivers and subsystems for dynamic optical burst switching networks," in *Proceedings of the 5th International Conference on Broadband Communications, Networks and Systems (BROADNETS)*, London, United Kingdom, Sep. 2008.

2

Dynamic optical networking fundamentals and literature review

DYNAMIC OPTICAL NETWORKING has been a research subject for more than two decades. During this time, many different approaches, both in the physical layer and in the network control plane, have been proposed. However, introducing high layer networking operations into the optical domain make the whole analysis of dynamic optical networks extremely complex. Thus, most of the published works deal with separated aspects of optical networking, such as the cascadability of a specific optical switching technology, or the scalability of a particular optical switch architecture.

The purpose of this chapter is, thus, to briefly introduce the reader to the concept of dynamic optical networking and to identify the key physical layer issues that arise in this kind of networks. This will be the foundation used in subsequent chapters, which propose the use of digital signal processing technologies for the realisation of receivers for dynamic optical networks.

This chapter is structured as follows. Firstly, the concept of dynamic optical network is described, along with a short classification of the different kinds of dynamic optical networks researched. After this, section 2.2 presents a review of the figures of merit used in the design and testing process of both static and dynamic optical networks. Sections 2.3 and 2.4 identify the enabling technologies, and from them, the physical layer receiver requirements for core dynamic optical networks and optical

access networks, respectively. Next, a review of recently published literature of receivers for dynamic optical networks—the so called burst-mode receivers—is presented. Finally, the chapter concludes with a brief summary.

2.1 Introduction to dynamic optical networks

This section firstly introduces the reader to the concept of dynamic optical network. In order to grasp a better understanding of this long researched field, the several kinds of dynamic optical networks—core and access—are briefly introduced. Finally, a more formal mathematical definition is presented, along with some vocabulary that will be used in this thesis.

2.1.1 Definition of dynamic optical network

In order to properly define the concept of **dynamic optical network**, let's briefly define what a **static optical network** is and then define the former term by contrasting it with the latter.

A **static optical network** uses the optical fibre as a mere physical layer data transportation link in a point-to-point configuration. The most common kind of optical network today is SDH/SONET with ring topology [Maier, 2008]. In Synchronous Digital Hierarchy (SDH) networks, a transponder converts the electrical signal into an optical one and the receiver transponder transforms back the optical signal, after propagation through the fibre, into the electrical domain, and then is forwarded to the SDH upper layers. Thus, there are Optical-Electrical-Optical (O/E/O) converters on every node of the network, and all the switching is done electronically [El-Bawab, 2006].

A **dynamic optical network**, by contrast, extends the point-to-point nature of the optical links, and hence, some kind of *switching is done at the optical layer*. Thus, the key point in a dynamic optical network is that some sort of optical switching is done at the optical domain, and so the optical signal traverses at least one optical switch before being transformed into the electrical domain. Another important idea in dynamic optical networking is the *transmission of the information into small chunks* or packets or bursts. This deviates markedly from the continuous-mode transmission of standard optical links.

2.1.2 The different flavours of dynamic optical networking

To have a better understanding of the broad topic of optical networking it is useful to classify the different kinds on optical networks. One possibility is to classify them in chronological order or generations [Ben Yoo, 2006]. Then, every generational step is

characterised by introducing new features or technologies that solve some problems or issues present in the previous generation. A second option is to classify optical networks according to its degree of transparency [El-Bawab, 2006, p. 24]. **Transparency** could be defined as the ability of the optical layer to transmit optical signals, regardless of the protocol, modulation format, data rate, or line coding. It is clear that electrical networks are **opaque** in nature as the digital transponders should be designed for a specific transmission technology and modulation format. Another possibility is to classify dynamic networks according to the **switching granularity** of the network [El-Bawab, 2006]. Following the electrical domain nomenclature, there are two main kinds of switching granularity: circuit switching and packet switching [Tanenbaum, 1996]. In addition, optical networks associate the concept of circuit with the wavelength channel. Thus, it is more adequate to express these concepts as Optical Circuit Switching and Optical Packet Switching.

The remainder of this section explains the chronological classification of optical networks and the classification according to the switching granularity.

Dynamic network generations

1. The optical fibre point-to-point networks could be named as the **zero generation**. These networks operate with one wavelength channel per fibre, have O/E/O converters on every node of the network, and all switching is done electronically [El-Bawab, 2006]. The most used protocol architecture in this generation is SDH/SONET, typically with Asynchronous Transfer Mode (ATM) on top of it. ATM virtual circuits are used to define a virtual topology that electronic IP routers use transparently.

2. The **first generation** optical networks appeared during the late 1990s. The new feature introduced by this generation is the deployment of WDM in point-to-point links, that vastly increases the transmission capacity [Ben Yoo, 2006]. Still, at every node in the network there are O/E/O converters and all the data is processed and forwarded electronically, but there is considerably more optics than in the previous generation [El-Bawab, 2006]. SDH is still the protocol of choice. It is common to deploy these networks using ring topologies [Maier, 2008]. There are two network elements that came into the scene: the Add-Drop Multiplexer (ADM) and the Optical Cross-Connect (OXC). Essentially, an OXC is a more complex ADM with possibly no tributary ports. Both ADM and OXC devices operate entirely in the electrical domain, as there are O/E/O converters in every fibre port [Ramaswami, 2006].

   An evolution of the first generation optical networks was introduced with the advent of Optical Add-Drop Multiplexers (OADMs). OADMs have the ability

to add, drop, and pass through wavelength channels. OADMs do not perform optical power equalisation and optical performance monitoring, and once the wavelength channels are set up, they stay for a long time because of two major reasons: firstly, changes in the OADMs configuration will have major network disruption and, secondly, network planning is extremely complicated, particularly for big networks [Ramaswami, 2006].

3. The **second generation** optical networks aim is to perform some optical reconfigurability in the optical domain, with the reconfigurability time much longer than the packet round-trip time. This will allow the use of transparent optical paths sharing a wavelength channel across the network, called **lightpaths** [Ben Yoo, 2006]. Two new devices appear: the Reconfigurable Optical Add-Drop Multiplexer (ROADM) and the Wavelength Cross-Connect (WXC) (the optically reconfigurable OXC counterpart). The main evolution of ROADMs over OADMs is that the former performs amplifier gain equalisation, power balancing and optical signal monitoring to mitigate the optical signal impairments. In the same manner, WXCs perform optical circuit switching on the wavelength granularity and space switching technologies are a good candidate for this. Network planning tools have been provided by equipment manufacturers to change network circuits relatively easily, so this kind of networks are becoming a reality nowadays [Ramaswami, 2006].

4. The **third generation** of optical networks is expected to integrate the data networking entirely into the optical layer [Ben Yoo, 2006]. The optical layer switching speed will be fast enough to even directly map the IP packets into the optical domain—avoiding O/E/O conversions in the network core at all—and to increase the overall speed and transport capacity of the network. OPS—and its variants such as optical label swapping [Ben Yoo, 2006]—is an alternative name for third generation optical networks, and it uses store-and-forward routing on a hop by hop basis, with optical synchronisation and optical memory required [Teimoori et al., 2008; Raffaelli et al., 2008].

   To mitigate the hard-to-achieve switching requirements of OPS, a number of hybrid OCS and OPS approaches have been proposed. All of these architectures are known collectively as OBS and will be described in subsequent sections of this chapter.

Dynamic network granularity

The **network granularity**, in the context of optical networking, is defined as the ability of the network to use fractions of one available wavelength channel bandwidth.

Thus, according to the granularity, dynamic optical networks can be divided into the following classes

1. Optical Circuit Switching networks, also known as Wavelength Routed Optical Networks [Ramaswami and Sivarajan, 1995; Baroni and Bayvel, 1997]. WRONs provide end-to-end wavelength channels, called **lightpaths**. Every wavelength only carries a continuous-mode data-link and intermediate nodes do not have access to this wavelength channel (except acting as transit nodes) even if the whole bandwidth is not used. It is assumed that lightpaths will run for a long time, several weeks, months or even years. An incoming wavelength channel should be routed to an output fibre, so only multiplexers/demultiplexers and space switches are required [Düser, 2003]. Additionally, other kinds of optical switching, like Optical Time Division Multiplexing (OTDM) switching [Bonk et al., 2011], can be used. The main issue in designing WRON networks is the RWA problem to assign each lightpath a specific wavelength and route through the network. It has been shown [Baroni and Bayvel, 1997] that for a given traffic matrix, the required number of wavelengths N_λ strongly depends on the network *physical connectivity* α, given by

$$\alpha = \frac{2L}{N(N-1)} \tag{2.1}$$

where L is the total number of physical links and N is the number of nodes in the network.

Some advantages of WRONs are,

(a) WRONs are relatively simple to design, dimension, and operate.

(b) The RWA problem is solved offline, so optimal solutions can be found due to the long processing time available.

(c) WRONs do not have intrinsic delay and jitter is constant.

(d) The transmission mode is continuous-mode. This simplifies the design of the optical physical layer and the optical receiver.

Some disadvantages of WRONs are,

(a) The traffic matrix should be provided a priori.

(b) WRONs do not easily cope with rapidly changing network traffic. Changes in the traffic matrix imply to solve the RWA problem again, and reconfigure the network in accordance.

(c) The RWA problem should be solved and optimised globally and the processing time could be very slow, particularly for large networks with many vertices and edges. Recent research on hardware-accelerated RWA solvers [Qin et al., 2011] can alleviate this issue.

(d) Network reconfiguration could produce short disruption of existing lightpath channels.

(e) The network granularity is the lightpath (typically, 10 or 40 Gb/s in current optical networks). Network capacity between nodes is allocated on a lightpath-by-lightpath basis. This could lead to poor utilisation of the network bandwidth, because not all the data links will consume all the lightpath available bandwidth.

2. Optical Packet Switching networks [Blumenthal et al., 2000; O'Mahony et al., 2006] map IP datagrams, ATM cells, Ethernet frames, or SDH/SONET frames directly into the optical layer, where packets are forwarded on a packet-by-packet basis. OPS networks can be synchronous or asynchronous [Maier, 2008, p. 139]. In synchronous slotted OPS, packets have fixed size (cells) and they are time-placed in time-slots, whereas in asynchronous OPS time is not divided into slots and optical packets can have a variable size. The header size should be as small as possible in order to minimise network overhead and the header processing could be done in the electrical domain [Guillemot et al., 1998; O'Mahony et al., 2001; Stavdas et al., 2003; Monroy et al., 2006] or in the optical domain [Ramos et al., 2005].

   Some advantages of OPS networks are,

   (a) Finer granularity (sub-wavelength) could lead to better network utilisation and the network can react faster to traffic changes (so it is not required to know the traffic demand a priori) [Düser, 2003].

   (b) Also, optical routers/switches have a much less power and size footprint that their electronic counterparts [Ben Yoo, 2006]. However, there is no consensus among the research community about this [Tucker, 2011, 2008].

   (c) OPS maximises the utilisation of network resources and consequently less network capacity and smaller switches are required [O'Mahony et al., 2001].

   (d) Optical transparency at packet granularity could lead to a great integration of a number of heterogeneous tributaries like Ethernet, SDH, and ATM, among others [Düser, 2003].

   Some disadvantages of OPS networks are,

(a) Contrary to WRONs, contention and subsequent packet loss can occur in a core switch if there are no available resources [Yao et al., 2003].

(b) The core node requirements for OPS are much more challenging than for WRONs. Switching time ought to be in the order of nanosecond or pico-seconds.

(c) Enormous optical complexity and cost. Lack of proper optical technology.

(d) Pure random access optical memory does not exist and the proposed solutions [Gambini et al., 1998; Yang et al., 2008; Mack et al., 2009] use fibre delay lines, whose delay is constant and also degrade the signal with noise, crosstalk, attenuation, dispersion and non-linearities.

(e) All-optical header processing is still in development, and if optical headers are processed electronically it is not clear if OPS could compete in cost with electronic switching systems [Ramaswami, 2006].

3. Optical Burst Switching networks [Qiao and Yoo, 1999, 2000; Turner, 1999; Battestilli and Perros, 2003] have been proposed as an intermediate solution between WRONs and OPS networks. OBS has a sub-wavelength granularity (better than WRONs) and the requirements for core nodes switches (switching speed) are much more relaxed than their OPS counterparts.

   There are two basic flavours of OBS, known as two-way reservation (Type II), and one way reservation (Type I) [Bayvel and Düser, 2004]. In Type II OBS, a path request is made to the network and once the requested path is available the network sends an acknowledgement to the edge node and the burst is then transmitted. In Type I OBS, a signalling packet is send with instructions to reconfigure the network core switches for the transmission of the burst, which is sent after some offset time in the hope that the network core has available resources for the burst to reach its destination. Also, in Type II OBS, contention and burst loss only occurs at the edge of the network, whilst in Type I OBS contention and packet loss occurs within the network core, as the burst transmission is not acknowledged. In both OBS network types, the main design parameters are the burst maximum length, the maximum time in the edge-router queue, and also the response time of the central node. OBS allows for a better network utilisation than WRONs. However, if wavelength conversion is not available and the network is sparsely connected, dynamic operation only leads to wavelength savings for low network loads ($\rho < 0.4$) compared to the static case [Zapata-Beghelli and Bayvel, 2008; Zalesky, 2009].

Optical access networks

Optical access networks have been introduced during the last decade as a replacement for currently deployed copper-based broadband technologies, such as Asymmetrical Digital Subscriber Line (ADSL) [Huang et al., 2007]. The two principal optical access standards—IEEE EPON and ITU-T GPON [Green, 2006]—define optical networks which are **passive** and thus they lack both optical amplification and optical switching. Consequently, they are named Passive Optical Networks (PONs).

In a passive optical network—depicted in figure 2.1—the optical media is shared among many users, in a similar fashion as a legacy copper-based Local Area Network (LAN). A passive optical splitter, with high insertion losses, allows the optical signal originating in the central office to reach the customer premises in the downstream direction. However, from the customer to the central office the optical medium is shared among all the subscribers. Thus, a Media Access Control (MAC) protocol, such as TDMA, is mandatory. Moreover, in order to reduce the network latency, the information is split into short packets [Tanenbaum, 1996]. In consequence, many physical layers issues—particularly from the burst-mode receiver design perspective—are shared between the dynamic core optical networks described above and the passive optical access networks.

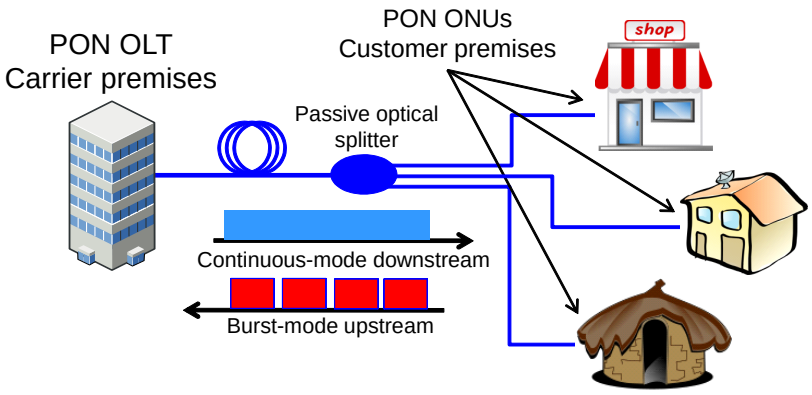

Figure 2.1: A diagram of a typical passive optical network.

2.1.3 A formal definition of a dynamic optical network

A Dynamic Optical Network (DON) can be mathematically described with the help of a graph $\mathcal{N} \triangleq G(V,E)$ and some other network-wide scalar or vectorial properties. The most important of these properties not included in the graph representation are the traffic matrix, the traffic model, and the network granularity.

A **graph** object is composed of a set of vertices V and a set of edges E, depicted in figure 2.2. In this and in subsequent examples, circles represent optical switching nodes that are referred as vertices V, and the blue lines represent optical fibre links

that are represented by the edges E. Both edges and vertices can be unequivocally identified in the graph with a natural number.

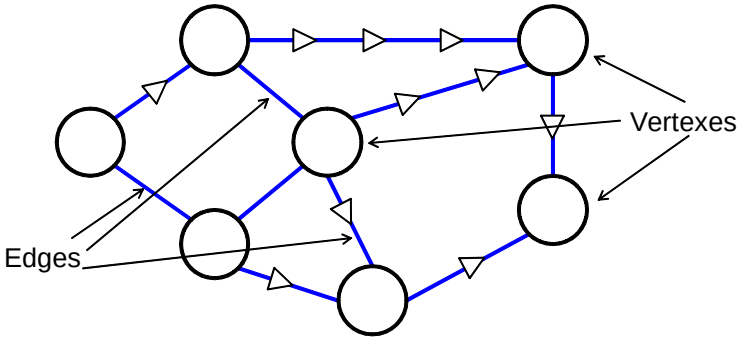

Figure 2.2: An abstract representation of a dynamic optical network. Vertices represent optical switches and edges represent optical WDM links.

This network representation as a graph is possible under a number of assumptions. The graph $G(V,E)$ is an undirected graph, meaning that the edges do not have a particular direction. However, optical networks usually have two fibres on every point-to-point optical link to allow full-duplex operation. Thus, an undirected graph can be used to represent such a network because having two counter propagating fibres in an optical link is abstracted with a single edge. A second assumption is that every switching node will have some tributary input/output ports, as depicted in figure 2.3. Finally, it is worth mentioning that both the edges and the vertices are composed of sets, each set with the properties of a particular node or optical link. For example, a particular vertex can have the number of full-duplex ports (the node degree) and the number of tributary ports as properties, whilst a particular edge will have the span length in km, the total dispersion and the number of optical amplifiers.

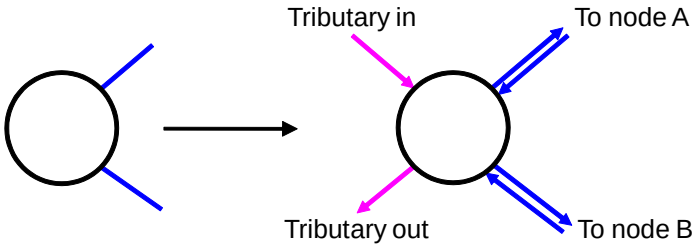

Figure 2.3: Illustration of the differences between the network graph model and the actual optical network with tributary and full-duplex fibre links.

The **traffic matrix** is a vectorial property of the network intended to represent the amount of traffic that nodes in the network send to each other. A number $a_{ij} \in [0,1]$ represents the normalised fraction of the traffic that that node (or vertex) i sends to node j. Under the assumption that one particular node sends as much traffic as it receives from other particular node j, the traffic matrix is symmetric. Otherwise, the traffic matrix is asymmetric. The traffic matrix could be static or stochastic, meaning that the

average volume of traffic $\forall i, j$ is constant or that this traffic volume changes with time, respectively. Finally, the traffic matrix can be simplified into a real number $\rho \in [0,1]$ if we assume that the average traffic volume is equal for every node, that is, $a_{ij} = \rho, \forall i, j$. In other words, all nodes in the network send and receive an equal amount of traffic to each other.

The **traffic model** is defined as the stochastic process with temporal mean a_{ij} that models the behaviour of the network traffic flow for that node. For simplicity, it is usually assumed that all nodes use the same traffic model, but this could not be the case. Common traffic models include Bernoulli, Poisson, and self–similar [Düser, 2003].

2.2 Figures of merit in dynamic optical networks

A Figure Of Merit (FOM) or Performance Metric (PM) is defined as some parameter that quantifies how well an optical link or network delivers data through them. Moreover, these figures of merit are used as key parameters in network design and enable engineers to compare between several choices to draw an optimum decision.

This section introduces the principal figures of merit, its benefits and drawbacks, and motivates the introduction of new figures of merit like the Packet Error Rate (PER), into the optical physical layer, as a logical consequence of performing high-layer network functions—such as routing—into the optical domain.

2.2.1 Continuous-mode figures of merit

A **continuous-mode transmission** is defined as a bit-stream that can be modelled with a random stationary or cyclostationary stochastic process [Meyr et al., 1997]. Intuitively, a continuous-mode transmission is associated with point-to-point optical links and first generation WRONs, where the *lightpaths*, once established, last for a very long time compared to the bit-rate R_b. The FOMs most commonly used when dealing with continuous-mode transmission are the Bit Error Rate (BER), the Q-factor, the receiver sensitivity, the component cascadability, and the power penalty.

The most common continuous-mode FOM is the **Bit Error Rate**, defined as the probability of incorrectly detecting a single bit in the data stream, assuming independence between adjacent bits. In other words, the bit detection process is modelled as a *Bernoulli trial* in which the probability of correct detection is p, and the probability of failure is $\text{BER} = 1 - p$ [Peebles, 1987].

The **Q-factor** is a FOM typically associated with optical communication systems using On-Off Keying (OOK) modulation. The Q-factor is defined as the difference of the mean symbol values divided by the sum of the standard deviation, as

$$Q = \frac{\mu_0 - \mu_1}{\sigma_0 + \sigma_1} \tag{2.2}$$

where μ_x is the mean value of the Probability Density Function (PDF) at the decision point, and σ_x is the standard deviation of the PDF at the decision point, for the symbols `1` and `0`. Moreover, if Gaussian noise is assumed, there is a direct relationship between the Q-factor and the BER of an optical system [Agrawal, 2002]. The advantages of using the Q-factor is that it can be easily measured, compared with the BER, and interpolation methods allow to estimate very low error probabilities accurately [Bergano et al., 1993].

The **sensitivity** is defined as the minimum signal power required to guarantee a BER below a specific threshold, typically 10^{-9} or 10^{-12}, which is considered *error-free* transmission. However, if Forward Error Correction (FEC) is assumed, like in the digital receiver investigated in this work, typically a BER of $\approx 10^{-3}$ is used as the pre-FEC threshold. In passive optical links, the major sources of noise are the photodiode thermal and shot noises [Agrawal, 2002]. However, in optically amplified systems it is likely that the optical noise originating in the optical amplifiers will dominate [Agrawal, 2002]. In both cases, if Gaussian noise is assumed, the sensitivity point for a receiver can be calculated as a function of the photodiode thermal noise, or as a function of the Optical Signal-to-Noise Ratio (OSNR) and the electrical and optical bandwidths [Mikhailov, 2003].

When testing optical components or sub-systems, researchers often measure the BER performance with and without the **device under test**. Typically, the Device Under Test (DUT) introduces a **penalty** (that can be negative in case of optical regenerators) which is defined as the difference in received optical power or OSNR to achieve equal performance with and without the DUT. Thus, the penalty allows to characterise optical devices independently of the optical receiver used in the experiments and allows to fairly compare devices between them.

In an optical link, and particularly in a submarine long-haul optical link, the optical signal traverses up to thousands of optical components. As the frequency response of real optical components such as filters, isolators, de/multiplexers, etc. is not ideal, i.e., completely flat, the cascading of many components have undesirable effects into the transmitted signal spectrum and this leads to a performance degradation. The **cascadability** is defined as the maximum number of optical components of a given type that the optical signal can traverse without significant degradation [Mikhailov, 2003].

2.2.2 OCS figures of merit

As mentioned in section 2.1, OCS/WRON networks and similar second generation networks use continuous-mode FOMs, once the network lightpaths are established.

However, the existence of optical switching implies that some layer-3 functions—like routing—are implemented into the optical domain. Thus, every time a new lightpath should be established, both a wavelength channel and a route should be allocated and there is a **lightpath blocking probability** due to the limited availability of optical network resources, like number of wavelengths.

In the process of reconfiguring an OCS network some of the lightpaths will be darkened, and that will cause an optical power variation along the route of that lightpath. Also, in every network node there are lightpath add/drop operations, so the optical power will vary. In order not to disrupt currently established lightpaths, this power variations should be bounded and much longer that the time constant of the excited carriers of optical amplifiers. Typically, variable optical attenuators are placed for every wavelength after the switch fabric so the total power entering every WDM link is kept constant (possibly using one dummy channel on every WDM link). **Reconfiguration times** can be very long (hours) if lightpath integrity is preserved, or could be much shorter ($\approx ms$) providing there are disruptions in some or all the lightpaths.

2.2.3 Burst-mode figures of merit

A **burst-mode transmission** is defined, opposed to a continuous-mode transmission, as a packetised transmission that exhibits a non-stationary statistical behaviour. Burst-mode transmission is associated with packet networks, in which the information is sent into relatively small (compared with the bit-rate R_b) chucks of information, and every packet has independent clock phase, amplitude, transmission path history, accumulated dispersion, optical filtering, noise figure, etc. [Chandrasekhar and Kilper, 2006]. This is illustrated in the diagram of figure 2.4, where three different and heterogeneous optical paths are represented. In every optical path, the signal is inserted into the network at a switching node with ingress/egress capabilities. Every switching node is characterised by the node degree number, and this degree will have implications in the amount of impairments produced. Switching nodes are interconnected with optical links that have variable length and, thus, variable number of optical amplifiers and optical components. Although the concept represented in figure 2.4 arise in the analysis of transparent optical networks with lightpaths lasting for a very long time, it readily can be applied to OBS and OPS if the duration of the lightpaths is reduced to the range of ms-μs to ns, respectively.

An important FOM in OBS/OPS is the **packet error rate**, defined—in an analogous way to the continuous-mode BER—as the probability of incorrectly detecting an optical packet. While the similarity of the BER and PER is obvious, there is however an important difference: accountable bit errors arise from the incorrect bit detection of a physical-layer-impaired signal at the receiver. In contrast, packet errors arise not

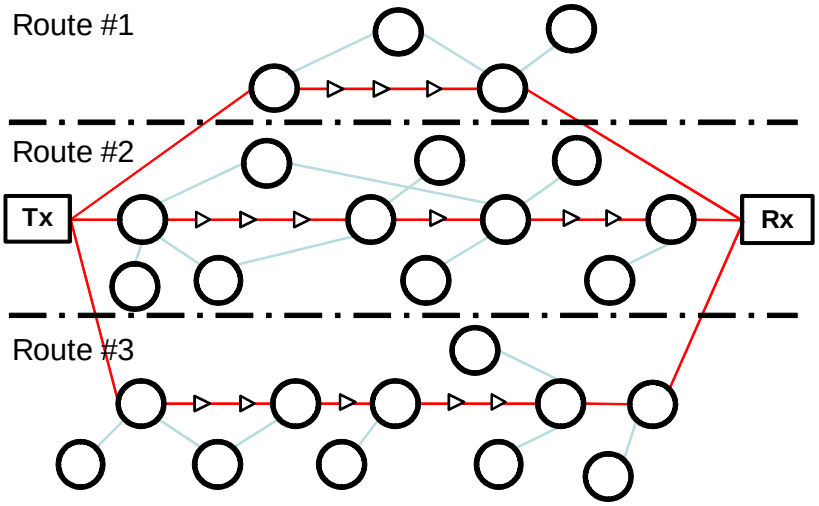

Figure 2.4: Abstract representation of the dynamic network optical paths.

only because of the physical layer impairments and the ability of the receiver packet detector to cope with them, but also from the control plane (signalling protocol) and the amount of resources of the network, due to **packet contention** and **optical switch blocking**.

Packet contention is defined as the condition when two or more packets must use the same wavelength channel on the same output port of an optical switch, and results on one or more packets being discarded (providing that no optical memory such as Fibre Delay Line (FDL) is available). Switching blocking is defined as the ability of a switch fabric to route all the required non-contending packets from all the input ports to the appropriate output ports, for every input/output combination. Both contention and blocking are causes of packet loss, but there is an important difference: contention is caused by the lack of optical resources for the total amount of traffic the optical network should deliver, while blocking is caused by the switching node architecture itself. Moreover, sometimes a blocking switching architecture can be transformed into a non-blocking one by simply adding more switching components (and thus increasing the switch hardware complexity) or by increasing the complexity of the switching fabric control algorithm. In spite of this difference, contention and blocking are related concepts. For example, a dynamic optical network equipped with non-blocking switches is likely to reduce contention.

The **network throughput** is defined as the normalised amount of network resources that successfully transport data. According to [Yao et al., 2003], the network throughput can be calculated as

$$N_t = \frac{N_b}{\frac{C \times t}{d}} \tag{2.3}$$

where N_b is the number of bits correctly delivered, C is the network capacity

(defined as $C = N_l N_\lambda R_b$, where N_l is the number of links, N_λ the number of wavelengths, and R_b is the line-rate), t is the simulated or measured time, and d is the average link distance a burst is likely to travel in the network (averaging all possible routes). Intuitively, the network throughput is a linear function, with slope $m = 1$, of the normalised network load ρ until packet loss starts to dominate and then the slope of the network throughput decreases or even becomes null or negative [Yao et al., 2003].

The PER is the preferred FOM in many control plane resource allocation and protocol studies [Aracil et al., 2007]. In these works, researchers can easily compare the amount of optical network resources required to meet a targeted PER, typically as a function of the network load ρ. Most of these works only deal with contention and blocking as causes of PER, assuming an ideal physical layer that never losses a packet. A step forward is the work by Gauger et al. [2008]. There, a switching node based on the broadcast and select architecture is firstly analysed in terms of contention and blocking by a simulation. A parallel analysis studies the maximum switching-node size and throughput by considering the splitting losses, optical amplification impairments (namely, Semiconductor Optical Amplifier (SOA) noise, gain and saturation effects), and signal crosstalk [Buchta et al., 2008; Buchta and Patzak, 2008]. The physical layer analysis produces a maximum throughput $T_{\max}$ (in Tb/s) and the performance evaluation produces a maximum network load ρ that guarantees a target quality of service. Both parameters can be combined

$$T_{\text{eff}} = T_{\max}\rho_{\max} \tag{2.4}$$

to produce an effective throughput T_{eff}. In this thesis, however, the PER is measured by error counting, and this figure can be combined with layer-3 simulation studies as a conditional probability of losing a packet, arising from the physical layer. This is justified because physical layer parameters, like the optical packet preamble length or the receiver design, have implications in the total PER of the dynamic network.

Additionally, there are other FOMs suitable for dynamic packetised networks, such as dynamic range, tolerance to gain excursions (such as maximum number of burst-mode amplifiers that can be traversed), and average transmission delay. Some of these FOMs will be treated in more detail in the subsequent sections 2.3 and 2.4 for dynamic core networks and optical access networks, respectively.

2.3 Dynamic core networks receiver requirements

The objective of this section is to introduce the reader to the physical layer issues of dynamic core optical networks. There is a brief review of the enabling technologies that will allow the realisation of DONs. Finally, the key requirements of burst-mode

receivers for DONs are summarised.

2.3.1 Enabling technologies for core dynamic networks

The principal enabling technologies for dynamic core networks are described next. Burst-mode receivers for core dynamic networks will be treated in the following section with more detail.

Burst-mode transmitter

Burst-mode transmitters for optical access networks typically use direct laser modulation [Oh et al., 2005]. This introduces undesirable effects for core networks, namely, poor extinction ratio and significant chirp. In addition, a cheap uncooled laser causes wavelength drifts, which is totally unacceptable in a WDM core network. Thus, external modulation with cooled, wavelength-stabilised lasers is preferred.

Wavelength-routed networks (either OCS networks or wavelength-routed OBS networks [Düser and Bayvel, 2002]) require that the optical burst coming out of the transmitter to have a specific wavelength that can vary for every requested lightpath or transmitted burst. In addition, [Düser, 2003] showed that the transmitter setting time—which is closely related with the laser switching and wavelength stabilisation time—is a critical parameter for network performance.

Many different kinds of tunable laser exist [Buus and Murphy, 2006]. However, since fast switching time is a paramount trait in a DON transmitter, Sampled Grating Distributed Bragg Reflector (SGDBR) and Digital Supermode Distributed Bragg Reflector (DSDBR) are currently the best candidates for implementing dynamic network transmitters. SGDBR lasers [Jayaraman et al., 1993] have two different multi-element mirrors on each side of the lasing cavity. Each of these mirrors have a different reflectivity comb spectrum and the laser is tuned at the wavelength where a reflectivity peak coincides on both reflectivity combs [Coldren, 2000]. The operating principle of DSDBR lasers [Ward et al., 2005] is similar. However, rather than having an equal-type gratings with different parameters, the DSDBR laser front mirror is a chirped grating and the rear mirror is a phase grating.

A tunable DSDBR laser is reported in [Ponnampalam et al., 2006] having 6 ms switching time and 5 GHz wavelength-drift due to thermal effects. A wavelength locker mechanism is reported in [Bianciotto et al., 2009; Puttnam et al., 2009], and this substantially improves the locking time to 2 μs and the wavelength stability to 1 GHz.

Burst-mode amplifiers

Erbium Doped Fibre Amplifiers (EDFAs) are currently the most used optical amplification solution, due to the small noise figure and cost [Agrawal, 2002]. However, the finite upper-level lifetime of carriers produces a response in the gain variation as a function of the instantaneous optical power, known as cross gain modulation. The causes of the optical power variation are the add/drop operations in optical switching nodes and the differential attenuation that exists in several optical switching architectures, i.e., the attenuation of the optical signal depends on the particular input/output ports that the optical signal traverses. Two optical signal impairments can be identified,

1. In-burst optical power variations, which is a variation of the instantaneous optical power across the optical burst.

2. Burst-to-burst power variations, which leads to a variation of the burst DC-offset respect to its neighbours. This produces Base-Line Wander (BLW), which is a variation of the instantaneous DC-offset of the signal which can lead to a sensitivity penalty in the burst-mode receiver [Davey et al., 2006].

In order to mitigate the aforementioned impairments, optical amplifiers for DONs should be gain-stabilised in order to prevent gain excursions. A number of techniques for gain stabilisation have been investigated. The principal ones are,

1. **Optical gain clamping**: In this technique, a coupler at the output of the EDFA is used to deliver some Amplified Spontaneous Emission (ASE) noise power into a feed-back loop, which includes an optical attenuator and an optical filter, into the input of the EDFA [Puttnam et al., 2008a]. Using this technique, the output power variations have two components: a steady state power fluctuation (due to spectral hole burning) and relaxation oscillations (associated with the feed-back loop laser cavity) [Luo et al., 1998; Richards et al., 1997]. The advantages of this technique are that no high-speed electronics, extra photodiodes or lasers are required and, thus, it is relatively cost-effective [Puttnam et al., 2008a].

   The investigation conducted in [Puttnam et al., 2008a] shows that 1528 nm is the optimum wavelength for clamping the gain, as this gain peak minimises the amount of attenuation required in the feed-back loop. Also, given a maximum amount of optical power variation at the input of the amplifier, there is an optimum feed-back attenuation value that maximises the Q-factor at the output. This is because low values of attenuation reduce the signal gain, whilst high values of attenuation increase the optical gain but also the gain-transient effects. In cascaded operation, every iteration in the loop requires an extra 0.3 dB feed-back attenuation per node hop. Thus, the feedback cavity design limits the maximum

number of hops the optical signal can traverse without incurring a significant penalty.

2. **Transient-suppressed EDFA**: This is a modified EDFA, in which the active erbium area of the erbium doped fibre is larger than usual [Awaji et al., 2010; Puttnam et al., 2010]. It is worth noting that this does not completely suppress the gain transients, but rather mitigates them by modifying the EDFA gain dynamic behaviour. Thus, transient-suppressed EDFAs can use another technique described here to fully achieve gain-suppression.

3. **Pump power variation**: In this technique, a photodiode placed at the amplifier input monitors the optical input power and this is used to control the driving current of the EDFA pump laser and, thus, the total optical gain [Srivastava et al., 1997]. Additionally, a power monitor can also be added at the output and use a more complex control algorithm [Liu et al., 2006] or a high-speed optical attenuator [Sato et al., 2011], at a price of increasing the amplifier complexity and cost.

4. **Dummy compensation channel**: This technique uses a photodiode to monitor the optical power at the input of the amplifier, and rather than varying the pump power, an auxiliary dummy-channel power is varied in order to keep the total power at the input of the amplifier constant [Tran et al., 2005] and thus suppress the gain transients.

In this work, a gain-clamped EDFA is used as a burst-mode optical amplifier for simplicity.

Optical switches

Figure 2.5.A shows a generic optical switch architecture that could be employed in both core and edge nodes. N represents the number of input/output fibres whilst W stands for the number of wavelength channels. The main difference between edge and core nodes is the existence of some input/output tributary ports in the edge node (see figure 2.3 on page 31). However, from the optical switch design point of view, some of the ports of the figure 2.5.A architecture could be considered as tributary ports and the rest as trunk ports. The main disadvantage of this architecture is that a very large optical switching fabric of size $NW \times NW$ ports is required.

Stacked switch fabrics [El-Bawab, 2006, p. 296] that use W switches of size $N \times N$ can be used to overcome the problem of building a large-port count switch fabric. Figure 2.5.B shows an example of an architecture that employs one optical switching plane

for every wavelength. At the input and at the output of every switching plane all packets have the same wavelength. Figure 2.5.C shows an alternative stacked switch configuration. In this case, the inputs to every switching plane have different wavelengths, so wavelength contention will be presumably much worse than in the previous example.

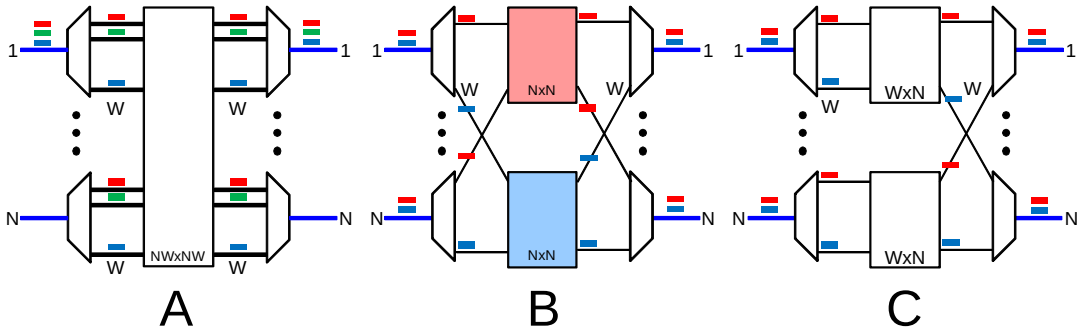

Figure 2.5: Generic optical switching architectures. (A) Large non-blocking switch. (B) Stacked optical switch fabric with same wavelength per switching plane. (C) Stacked optical switch fabric with different wavelengths per switching plane.

After describing the most generic optical switching architectures, the three most common, technically feasible, high switching-speed architectures are introduced next [Gripp et al., 2010; Raffaelli et al., 2008].

- Figure 2.6.A shows a plot of the crossbar architecture. This configuration is found in many planar technologies (e.g., Lead Lanthanum Zirconate Titanate (PLZT) [Sugama et al., 2007], Active Vertical Coupler (AVC) [Vegas Olmos et al., 2006], and SOA switching matrices [Wang et al., 2009; Albores-Mejía et al., 2009]).

- Figure 2.6.B depicts the Broadcast and Select (BS) architecture [Masetti et al., 2003; Chiaroni et al., 1996]. The switch firstly splits the incoming multi-wavelength channel optical signal into N branches. Then, there are W wavelength gates that select one wavelength out of the W available ones. Additional optical amplifiers can be placed in the optical path or optical amplifiers used as optical gates (i.e, SOA gates). The main advantage of this switch is its low complexity. However, the switch requires $N \times W^2$ optical gates, and the attenuation due to the broadcast splitters can be very high for high port counts switching fabrics.

- Figure 2.6.C shows a diagram of a Wavelength Converter and Arrayed Wavelength Grating (WC/AWG) switch architecture [Nicholes et al., 2009; Chia et al., 2001]. This switch works as follows: after demultiplexing the incoming WDM optical signal into separated wavelength channels, a Tunable Wavelength Converter (TWC) changes the wavelength of the signal such that the signal is forwarded to the correct Arrayed Waveguide Grating (AWG) output port. Other wavelength

routing devices could be used instead of an AWG, e.g., a fixed wired combination of optical multiplexers/demultiplexers. The optional Fixed Wavelength Converter (FWC) just before the output multiplexers change the wavelength of the optical signal in order to avoid contention, at the expense of more hardware and higher cost. However, it has been proved [Yao et al., 2003] that wavelength conversion is by far the most effective contention resolution mechanism.

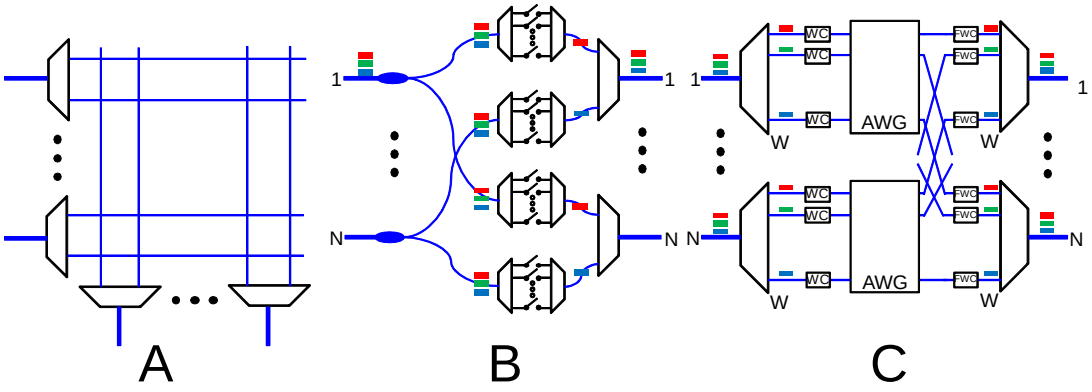

Figure 2.6: The three most common and technically feasible optical switching architectures for OBS/OPS networks. (A) Crossbar matrix. (B) Broadcast and Select. (C) Wavelength Converter plus AWG.

The main physical impairments on BS switching nodes are splitting losses, optical noise originating in active components (such as EDFA or SOA gates), and crosstalk [Buchta and Patzak, 2008]. On the WC/AWG architectures these impairments are crosstalk and wavelength conversion related degradations (like chirp and noise) [Chia et al., 2000].

2.3.2 Receiver requirements for core dynamic networks

Dynamic optical networks in which the information is packetised introduce new kinds of impairments into the optical signal. As has been described in this section, a receiver for a dynamic optical network must be capable of detecting the incoming optical bursts, adapt to burst power variations, rapidly recover the optical burst clock and set an appropriate decision threshold, and compensate for BLW and instantaneous power variations within the optical burst. Such a receiver is called a burst-mode receiver [Eldering, 1993; Su et al., 1997; Kawai et al., 1989].

To summarise, a burst-mode receiver for dynamic core networks must meet the following requirements,

1. **Packet/Burst/Cell detection**: the burst-mode receiver should be able to detect the presence of an incoming optical burst. In order to do that, a preamble—consisting of N bits at the beginning of the burst—with an arbitrary pattern is

used. To keep the network throughput high, the number of preamble bits N should be as small as possible. However, it is likely that having a small N will degrade the performance of the burst detector, so a compromise between detection performance and network throughput should be reached.

2. **Noise immunity**: dynamic core networks are likely to have active optical components (mainly EDFAs) to overcome fibre losses. In addition, the most common high-speed optical switching architectures make use of active optical components like SOAs. All active components add noise to the signal and, thus, the received optical signal will have a poor OSNR—as opposed to passive optical access networks, which lack active optical components.

3. **Gain excursions and BLW tolerance**: the received optical signal will exhibit DC-offset variations within the burst duration (this is referred as BLW) and also variations in the instantaneous power of the signal (due to dynamic gain effects in optical amplifiers). A burst-mode receiver should be able to constantly track the instantaneous DC-offset and amplitude values of the received signal and vary the receiver threshold and gain accordingly.

4. **Dynamic range and sensitivity**: in an optical network with optical amplification the receiver sensitivity is not a main concern, as the optical signal can always be optically pre-amplified to the optimum quantum-limit power. Under this assumption, the noisy current arising from thermal and shot noises are negligible compared with the noisy current arising from the ASE noise which originates in the optical amplifier [Agrawal, 2002, p. 263]. However, the optical signal is likely to have significant power variations between bursts, and so there will be a deviation from the optimum quantum-limit power, which leads to a penalty. It is then desirable for the burst-mode receiver to have a large dynamic range, defined as the difference between the maximum receiver power—also known as the overshoot or saturation point—and the sensitivity.

5. **Response time**: The burst-mode receiver should be able to very rapidly detect the received signal parameters and to adjust itself for the correct detection of the optical burst. In addition, the clock of the incoming burst should be acquired as fast as possible—with a preamble as short as possible—in order to increase the network throughput.

Also, the receiver must carry out symbol timing and data recovery like a continuous-mode receiver. Other technically secondary but important parameters are the receiver cost, the receiver footprint and the total energy consumption.

2.4 Optical access networks receiver requirements

Optical access networks currently deployed or in the process of standardisation lack active optical components and, thus, they are named Passive Optical Networks [Effenberger and El-Bawab, 2009; Shumate, 2008; Effenberger et al., 2007]. There are two main PON standards: the ITU-T GPON family [Qiu et al., 2004; ITU, 2008] and the IEEE Ethernet PON [Tanaka et al., 2010; Kramer, 2009; IEE, 2008, 2009], and besides some MAC differences the network architecture and the optical physical layer of both standards are similar.

2.4.1 Optical access networks

The typical PON architecture, illustrated in figure 2.1 on page 30, contains an Optical Line Terminal (OLT) located at the central-office. The OLT broadcasts a continuous-mode bit-stream in a wavelength channel to multiple subscribers. A passive $1 \times N$ splitter [Borella et al., 1997], where N has typically a maximum value of 16 or 32, distributes the *downstream* signal among the network subscribers. Every subscriber has an Optical Network Unit (ONU) that receives the point-to-multipoint downstream transmission and also transmits the *upstream* information to the OLT. An important point arises: since the downstream is a point-to-multipoint transmission channel a continuous-mode transmission can be used. However, the upstream channel is shared and point-to-point, and unless a MAC arbitration protocol like TDMA is used, collision of packets coming from several ONU will happen at the OLT.

A fundamental enabling technology for the upstream transmission in PONs is, thus, the OLT upstream burst-mode receiver capable of receiving optical packets transmitted from different ONUs. Moreover, every packet will have a different clock, so quick timing acquisition is a must. Also, due to the unknown distance and the absence of optical amplifiers or optical power equalisers, amplitude variations between consecutive packets are expected.

2.4.2 Receiver requirements for access dynamic networks

As opposed to dynamic core networks, optical access networks have several standards and commercial products are already available. Thus, the receiver requirements for these networks are much clearer than in the case of core networks, which are still being researched.

Due to the passive nature of current optical access networks, the main physical layer impairment is the optical attenuation originating at the optical splitter. Ideally, a $1:16$ splitter has an insertion loss of ≈ 12 dB, but realistically this value can be 2 dB higher. Additional sources of attenuation are the optical fibre attenuation (typical max-

imum distances are 20 or 30 km, with attenuations of ≈ 4 and ≈ 6 dB, respectively), splicing losses, and connector losses [Huang et al., 2007]. There are additional penalties that should be considered in the loss budget: Chromatic Dispersion (CD), Relative Intensity Noise (RIN), multipath interference, mode partition noise, and non-linear effects. Dispersion and mode partition noise can be significant if a laser with a broad linewidth is used (like a Fabry-Perot laser). Thus, Distributed Feedback Laser (DFB) lasers are the preferred option for 10 Gb/s PON. Also, the multipath interference could be high if the optical path contains cheap components with high return losses. Finally, non-linearities can became significant if power is very high due to additional wavelength channels used for broadcasting of radio signals [Huang et al., 2007].

In addition, in order to lower the cost of every customer ONU, cheap components having poor figures of merit are used (the electronics/optics at the OLT can be better because the cost is shared among all the PON subscribers). Thus, the OLT receiver has to cope with both a high tolerance in transmitted power—which has an impact in the required dynamic range—and low modulation extinction ratio—which has an impact in the sensitivity of the burst-mode receiver.

The following list enumerates the main parameters required for upstream burst-mode receivers intended for optical access networks [Qiu et al., 2004; Huang et al., 2007; Chang, 2007; Qiu et al., 2009],

1. **Sensitivity**: A high sensitivity is desirable in a PON because of the lack of optical amplification. In addition, increasing the burst-mode receiver sensitivity by 3 dB allows to increase the splitting ratio by the same amount, which almost doubles the number of subscribers [Qiu et al., 2004]. Additionally, the optical path penalties (such as dispersion) are included into the sensitivity in the standards.

2. **Dynamic range** and **Overload**: A high dynamic range is necessary to increase the network flexibility, that is, to have the possibility of ONUs near the central office with ONUs far away (or with high splitting losses) coexisting in the same PON segment. This is referred to as the **differential attenuation**. In addition, there is a relatively high tolerance on the ONU launch power that should be included in the dynamic range. The overload point can be calculated as the addition of the sensitivity plus the dynamic range, so this FOM and the dynamic range are pretty much the same thing [Qiu et al., 2004].

3. **Consecutive Identical Digits**: A large stream of consecutive ones or zeros produces BLW in AC-coupled receivers and prevents the burst clock to be easily estimated. Consequently, the receiver should be able to support a maximum number of Consecutive Identical Digits (CID) [Ohtomo et al., 2010]. DC-coupled

receivers solve both the BLW and CID problems. However, DC-coupling implies the transmission of a DC-offset that should be compensated and that leads to sensitivity penalties.

4. **Response time**: A burst-mode receiver must be able to extract the threshold value on a burst-by-burst basis. The bursts in a PON have a very small guard-band, defined as the idle time between optical bursts, and typically is calculated as the addition of the laser ON and OFF times plus some margin, that is,

$$T_{\text{GB}} = T_{\text{ON}} + T_{\text{OFF}} + T_{\text{IDLE}} \tag{2.5}$$

Additionally, some burst overhead is allowed in order to facilitate the burst-mode reception. The preamble time (also known as setting time) [Nakamura et al., 2005] contains some specific bit-patterns to allow the extraction of the threshold level and to synchronise the Clock and Data Recovery (CDR) circuit. The preamble time is usually decomposed into two parts [Qiu et al., 2004],

(a) Settling time: Adjust amplification gain and offset [Ohtomo et al., 2010].

(b) CDR lock time: Time for the CDR to lock to the packet clock.

In summary, due to the short lengths of both the guard-band and the preamble, the response time of the receiver constitutes a significant design challenge.

Design challenges of analogue burst-mode receivers

Until now, the vast majority of burst-mode receiver designs are analogue-based. Analogue receivers present a number of problems and design challenges which are briefly described next.

Many analogue DC-coupled burst-mode receivers detect the 1 voltage level and the 0 voltage level and set the threshold accordingly, by means of a peak and bottom detectors. A reset signal to erase the offset value is required because of the short gap-band between bursts [Säckinger, 2005, p. 212].

For Avalanche PhotoDiode (APD) optical receivers, a high-sensitivity can be achieved by setting a high APD gain factor M. However, in such a receiver, a loud burst will saturate the Trans-Impedance Amplifier (TIA) and degrade the duty-cycle of the signal. The slow response in the APD does not allow to change the gain parameter M on a burst-by-burst basis. Thus, the M parameter should be kept fixed and optimised accordingly with the transimpedance gain of the TIA [Qiu et al., 2004].

AC-coupled burst-mode receivers usually require line-coding in order to remove the low-frequency component of the transmitted spectrum. If a line-code with significant low-frequency components is used, the high-pass response of the AC-coupling will

produce an unwanted BLW. An alternative to line-coding is to use a small coupling capacitor, such as $RC << 1/R_b$, where R_b is the line-rate. In this case the high-pass characteristic of the coupling increases the noise and, thus, the sensitivity is reduced [Säckinger, 2005].

2.5 Survey of burst-mode receivers

This section reviews the main bulk of literature recently published on the subject of burst-mode receivers. Table 2.1 summarise the main characteristics of the surveyed burst-mode receivers, described in the next paragraphs, along with some older 1.25 Gb/s receivers. The symbol — corresponds to a value not appropriate, missing from reference, or irrelevant. Question marks (?) indicate values not clearly stated in the reference, e.g., a value seen on a plot but no numerical value is written in numbers. The parameters in table 2.1 are the coupling mode (AC or DC), the burst-mode receiver bit-rate, the guard-band, preamble times, the number of supported consecutive identical digits, sensitivity, overshoot point, dynamic range, the institution, and general comments.

Table 2.1: Summary of the surveyed burst-mode receivers main characteristics (coupling, bit-rate, guard-band time, preamble time, consecutive identical bits, sensitivity, overshoot point, dynamic range, company/institution, and miscellaneous comments).

Ref	C	R_b Gb/s	GB [ns]	Pre [ns]	CID [bits]	Sensitivity [dBm]		Overshoot [dBm]		Dyn [dB]	Institution	Comments
Lee et al. [2011]	AC?	2.5 G	64b?	96b?	—	−32.0	@1^{-10}	−4	@1^{-10}	28	ETRI Korea	Single IC
Myouraku et al. [2011]	AC	10 G	5	400	—	−29.5	@1^{-3}	−6	—	> 23.5	NEC	Automatic reset Scrambler
Hara et al. [2010]	AC	10 G	1024	150	—	−28.0	@1^{-3}	−5	@1^{-3}	23	NTT	
Mélange et al. [2010]	DC	10 G	25.6	32	—	−13.0	@1^{-3}	−0.3	—	12.7	Ghent Uni.	With CDR
Nakagawa et al. [2010a]	DC	10 G	0	800	—	−31.2	@1^{-3}	−6	—	25.2	Mitsubishi	Dual-rate rx
	DC	1.25 G	0	400	—	−35.6	@1^{-12}	−9.3	—	26.3		
Ohtomo et al. [2010]	AC	10 G	10	200	—	−29.6	@1^{-3}	−5	—	24.6	NTT	
Shastri and Plant [2010]	—	5 G	64b	0	3100	−24.2	@1^{-10}	—	—	3	McGill Uni.	CDR only
Sugawa et al. [2010]	AC	10 G	500	280	—	−28.6	@1^{-3}	> −6	—	> 22.6	Hitachi	
Takahashi et al. [2010]	AC	10 G	2	10	16	−27.5	@1^{-3}	> −6	—	21.5	NEC	Scrambler
Yin et al. [2010]	DC	5 G	25.6	26.6	—	−15.1	@1^{-10}	+0.5	@1^{-10}	15.6	Ghent Uni.	
Ossieur et al. [2009]	DC	10 G	25.6	23.8	72	−12.5	@1^{-10}	−1.0	—	11.5	Ghent Uni.	No CDR
Nishihara et al. [2008]	AC	10 G	1024	100	—	−18.0	@1^{-12}	−1.5	—	16.5	NTT	
Li et al. [2006]	—	10 G	—	20	—	−15.0	—	−7	—	8	APIC	
Kwon et al. [2005]	AC	1.25 G	32b	512B	—	−24.4	@1^{-12}	−1.5	—	22.9	Samsung	
Nakamura et al. [2005]	AC	1.25 G	32b	20b	—	−30.9	@1^{-11}	> −4	—	> 26	NTT	External reset
Ossieur et al. [2005]	DC	1.25 G	25.6	18	72	−30.6	@1^{-10}	21.6	—	−9	Ghent Uni.	

The reference [Lee et al., 2011] reports a 2.5 Gb/s receiver designed and built in the Electronics and Telecommunications Research Institute, Daejeon, Korea. This receiver is a single-chip BiCMOS and consists of a variable-gain TIA (2 levels of gain: high and low), an automatic offset cancellation module, and burst and gain detectors. An external reset signal is required.

NEC corporation proposed an 10 Gb/s burst-mode receiver, consisting of a 2R burst-mode receiver (a burst-mode TIA and slicer) followed by a burst-mode CDR [Myouraku et al., 2011]. Coupling between these two modules is AC and in order to alleviate the low-frequency cut-off of the AC-coupling, a XOR-gate based scrambling technique (similar to the one used in `1000 BASE-T` Gigabit Ethernet, based on a linear feedback shift register [Spurgeon, 2000, p. 158]) is proposed. A more detailed description of the scrambling technique is to be found in [Takahashi et al., 2010].

NTT corporation has been actively developing burst-mode receivers for a long time (since 1998 at least [Nakamura et al., 1998]). The most current NTT burst-mode receiver [Hara et al., 2010] is a 10 Gb/s AC-coupled chip fabricated in a 0.18 μm BiCMOS process. The coupling capacitors are not integrated and can be optimised for high CID tolerance. [Ohtomo et al., 2010] reports an early version of this AC-coupled receiver, fabricated in a 0.25 μm BiCMOS process. Yet an earlier version of the NTT receiver—reported in [Nishihara et al., 2008] and having a two-step gain TIA and a burst-mode limiting amplifier with automatic offset control—has a much lower sensitivity and dynamic range. Finally, the reference [Nakamura et al., 2005] presents an AC-coupled 1.25 Gb/s receiver with a three-gain step TIA and automatic offset control.

The University of Ghent is another world-class institution in burst-mode receiver technologies for access networks. Ossieur et al. [2005] reports a DC-coupled 1.25 Gb/s single Integrated Circuit (IC) burst-mode receiver with three limiting amplifiers. The DC-offset is compensated digitally and the chip is fabricated using a 0.35 μm BiCMOS process. The reference [Ossieur et al., 2009] presents a PIN-based DC-coupled 10 Gb/s burst-mode receiver consisting of a burst-mode two-step gain TIA and 4-stage burst-mode limiting amplifier with DC-offset compensation and peak-detection. This work does not not include a CDR circuit. Thus, BER measurements were conducted using the known timing of the transmitter. The receiver has automatic burst detection and reset generation. The work reported in [Yin et al., 2010] adds a CDR circuit to the design, but the line-rate is reduced to 5 Gb/s to relax the integration with the CDR section. Finally, the reference [Mélange et al., 2010] reports a complete 10 Gb/s burst-mode receiver with integrated CDR, with a front-end based on the [Ossieur et al., 2009] design.

Mitsubishi Electric Corporation demonstrated the first analog burst-mode receiver for the coexistence of 10 Gb/s and 1 Gb/s EPON ONUs [Igawa et al., 2010; Nakagawa et al., 2010b,a,c, 2009]. The dual-rate receiver consists of three ICs: burst-mode TIA,

burst-mode limiting amplifier, and CDR, fabricated in a 0.13 μm BiCMOS process. The receiver needs an external 10/1 Gb/s switching signal and, thus, the line-rate timing should be known *a priori* (there is no line-rate detection). The electrical front-end is duplicated for 10 and 1 Gb/s line-rates. The CDR section oversamples the signal 4$\times$ (82.5 GS/s), and the power consumption is high (3 W at +3.3 V voltage supply). Nevertheless, this is the first dual-rate burst-mode receiver reported in the literature.

The McGill University of Montreal reported a burst-mode CDR consisting on a classic digital CDR followed by a novel oversampling phase-picking algorithm [Shastri and Plant, 2010]. The authors also built a custom Field Programmable Gate Array (FPGA) based Bit Error-Rate Tester (BERT) capable of measuring both BER and PER. In this work, a detailed theoretical analysis is presented and compared with experimental data. Notably, the locking-time of this CDR is 0 ns (instantaneous). However, the burst-to-burst dynamic range is only 3 dB.

Hitachi reported an AC-coupled 10 Gb/s burst-mode receiver fully compliant with the 10G-EPON protocol [Sugawa et al., 2010]. This receiver uses a two-step gain TIA, and needs a reset signal from the MAC layer circuit.

2.6 Chapter summary

This chapter has reviewed the different types of dynamic optical networks researched during the last two decades. From higher to lower network granularity, optical networks can be classified into OCS, OBS, and OPS. The benefits and disadvantages of these kinds of networks were described. The granularity classification leads to the classification of dynamic optical networks into networks generations, as a decreasing in granularity requires a more demanding optical components, mainly in terms of switching speed.

The figures of merit allow network architects to design optical links and networks and to compare between several alternatives. The introduction of high-layer networking functions in the optical domain requires new figures of merit to be introduced, in order to simplify the network design process. Also, an attempt to integrate control plane simulation and physical layer performance was reviewed.

Dynamic core optical networking introduces new challenges to be tackled by a new set of optical components under research: burst-mode tunable transmitters, burst-mode optical amplifiers, optical switches, and burst-mode receivers. All these components were reviewed in section 2.3, pointing out that having an intelligent burst-mode receiver could relax the requirements for other dynamic optical network components.

Apart from core trunk networks, dynamic optical networking concepts could also be applied to optical access networks. In order to reduce costs, optical access networks are typically passive, thus lacking optical amplification. The burst-mode receiver re-

quirements for access networks were identified in section 2.4.

Finally, a survey of current literature on the topic of burst-mode receivers was presented in section 2.5. It was shown that almost all the proposed prototypes currently researched are analog-based refinements of low bit-rate burst-mode receivers. In the next chapters, digital signal processing technologies will be proposed for the realisation of optical burst-mode receivers.

3

Digital burst-mode receivers for dynamic core networks

OPTICAL BURST/PACKET SWITCHING will be a key technology in next generation dynamically-reconfigurable optical networks that are able to adapt in response to changing traffic demand [Bayvel and Düser, 2004] and also in PONs [Ossieur et al., 2005; Kramer, 2009; Tanaka et al., 2010]. OBS switching provides granularity on the sub-wavelength scale and network reconfigurability in response to traffic demands on a microsecond to second time-scale. The use of OBS can result in a more efficient utilisation of the limited transmission resources in core networks. Additionally, optical burst switching also allows the system to adaptively switch off network capacity as the network load reduces, thus improving the energy consumption.

In addition to tunable wavelength burst transmitters and optical amplification that is insensitive to rapidly changing input powers [Puttnam et al., 2008a], dynamic optical networks require optical receivers capable of accurately recovering the timing information and data from asynchronous optical bursts that exhibit large power fluctuations between them. The recent availability of high speed Analog to Digital Converters (ADCs) has enabled the use of Digital Signal Processing (DSP) techniques in both coherent and Direct Detection (DD) lightwave communication systems. In coherent optical systems, DSP has been used to compensate for chromatic dispersion, polarisation state tracking, and carrier recovery [Savory, 2008, 2010; Fludger et al.,

2008]. Long haul DD systems have also used DSP to overcome residual CD and Polarisation Mode Dispersion (PMD) by employing soft decision Viterbi decoders [Benlachtar et al., 2007]. In the context of dynamic optical networks, such as OBS and PON, DSP can be used to compensate for high power variations, BLW, and fast equalisation and clock and data recovery.

A 10 Gb/s digital burst-mode receiver, suitable for receiving asynchronous bursts with burst-to-burst power variations of up to 7 dB whilst maintaining a Payload Bit-Error Rate (pBER) better than 10^{-3}, was demonstrated by Dr. Benn Thomsen and Dr. Ben Puttnam [Thomsen et al., 2007; Puttnam, 2008]. This digital burst-mode receiver is based on an AC-coupled photodiode followed by asynchronous analogue-to-digital conversion at 20 GS/s. However, in [Thomsen et al., 2007] and [Puttnam et al., 2008b], the digital signal processing was carried out offline with receiver performance characterised in terms of the Required Optical Signal-to-Noise Ratio (ROSNR). This was performed using a sequence of only a few bursts, captured using a real time oscilloscope. Whilst this accurately characterises the ability of the digital signal processing algorithm to compensate for the signal distortions caused by BLW within the burst, it does not address the performance of the burst detector that is used to determine the start of the burst. Thus, if the burst detector does not correctly detect the start of a burst then the entire burst is lost and a packet error occurs, which has an impact on the OBS control plane. Additionally, the PER, which is an interesting metric for layer-2 designers, was not characterised.

In order to fully characterise a burst-mode receiver it is therefore necessary to characterise both the errors that occur due to failure to detect an entire burst, i.e., the PER, and errors that occur within the payload, i.e., the pBER. The main purpose of this chapter is therefore to develop a tool to fully study and characterise a digital burst-mode receiver. Using this tool, an investigation of the traffic pattern sparsity and network load will be conducted as well.

This chapter is organised as follows. Firstly, section 3.1 introduces the reader with the fundamentals of digital receivers for optical line-rates, the several DSP algorithms used, and also describes the digital receiver architecture used in this and subsequent chapters. After that, section 3.2 presents the solution devised for the measurement of the PER, which involves a cluster of computers to produce results in an affordable amount of time. Section 3.3 describes an experimental-based model used to obtain the main parameters of the digital receiver chain. Then, section 3.4 studies the influence of the network load and sparsity on the digital burst-mode receiver performance. Finally, the chapter is summarised within section 3.5.

3.1 Design and theory of a digital burst-mode receiver for optical burst-switching networks

An optical receiver intended for dynamic optical networks must deal with non-stationary conditions in the received signal. Contrasting with a continuous-mode transmitted bit-stream, information in a DON is transmitted on a burst-by-burst basis. Each burst of information (other names are packet, or cell) contains a relatively small number of payload bits and it is delimited by a preamble and a tail. In addition, every burst has a different relative clock and that means that the receiver should lock to this clock very rapidly on a burst-by-burst basis. Also, DONs have idle periods of time when no information is transmitted at all (idle channel) and consequently the receiver should have a waiting-state in which the channel is monitored for an incoming burst, and when a burst is detected the receiver's CDR section is properly initialised and started.

In section 2.5, a number of recently developed burst-mode receivers was surveyed and it was found that the vast majority of them are pure *analogue* receivers. In this chapter, in contrast, the approach to the realisation of a burst-mode receiver is to make use of digital technologies for all the receiver subsystems. Figure 3.1 shows a simplified diagram of such a digital receiver. It consists of an **analog front-end** and a DSP section. The analog front-end consists of a photodiode followed by a TIA. After that, an analog filter removes out-of-band noise, shapes the signal, and acts as anti-aliasing filter. Then, the signal is converted into the digital domain (at two samples-per-bit) by a high speed ADC converter. The DSP section carries out the task of burst-detection and once a burst is detected, it performs CDR and possibly other impairment mitigation. This DSP section is typically implemented on an Application-Specific Integrated Circuit (ASIC) and designed in a hardware description language such as Very-high-speed-integrated-circuit Hardware Description Language (VHDL). However, during prototyping and experimentation, such as the work described in this thesis, high-level offline processing solutions are preferred. High-level language implementations, i.e., MATLAB or `C`, allow for faster development of the DSP algorithms and also facilitate the task or correcting both programming and algorithmical errors.

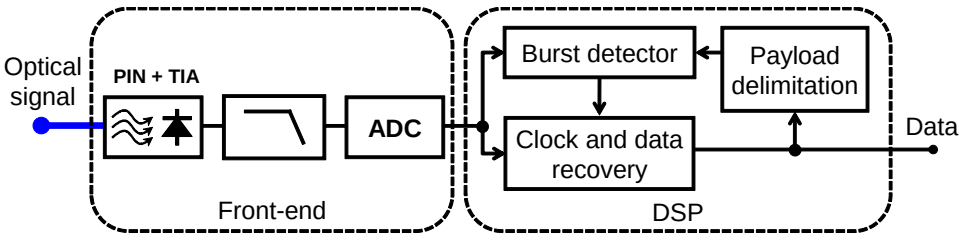

Figure 3.1: Diagram of the proposed digital burst-mode receiver.

In this section, the focus is on the detailed description of the theoretical found-

ations of digital burst-mode receiver and on the description of the developed digital burst-mode receiver that will be characterised later in this chapter. This digital burst-mode receiver was proposed initially by Dr. Benn Thomsen and Dr. Ben Puttnam and updated and improved by the author. This receiver will be fully characterised, in terms of BER and PER, in sections 3.2 and 3.4.

3.1.1 Digital burst-mode receiver architecture

Figure 3.2 shows the complete architecture of the developed digital burst-mode receiver, detailing all the digital processing algorithms. There are three enclosed subsystems that correspond to the Burst Detector (BD), the CDR, and the frame delineation subsystem, which correspond to the subsystems depicted in figure 3.1.

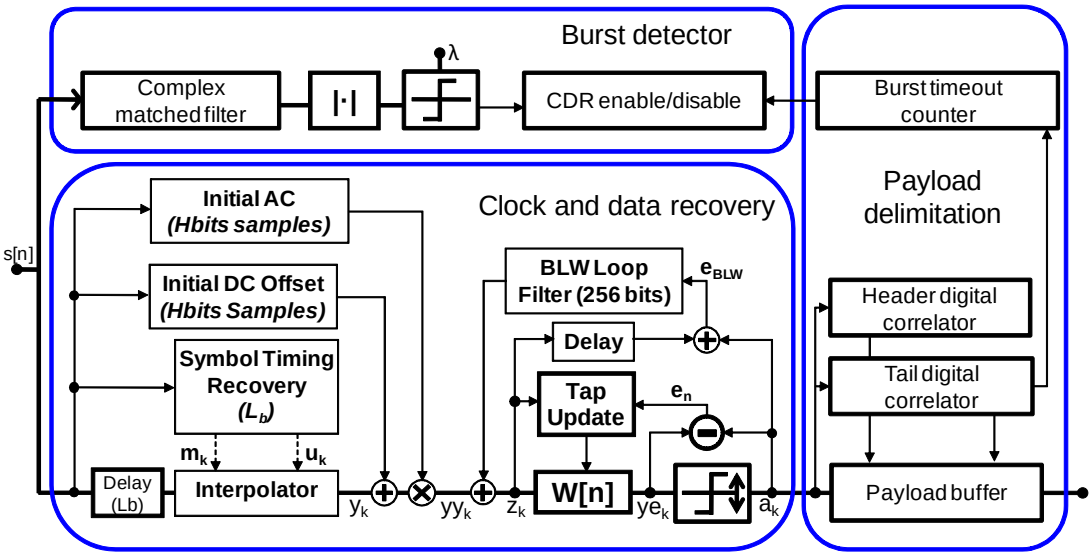

Figure 3.2: Complete digital burst-mode receiver schematic diagram. It consists of a burst detector, a clock and data recovery, and a payload delimitation subsystems.

Both the theoretical foundations and the implementation of all the receiver subsystems will be described next, always taking figure 3.2 as the main reference.

3.1.2 Burst-detector

The purpose of the **burst-detector** is to continuously monitor the communication channel and to detect the presence of an incoming burst, and then activate the CDR section of the digital receiver to start the processing of the burst payload and forward the received payload bits to the upper layers of the protocol-stack. A deterministic bit sequence, called the **burst preamble** or **burst header**, is placed at the beginning of the optical burst. Consequently, the burst detection problem could be translated into the problem of the detection of a deterministic signal embedded into a noisy environment

[Jaranowski and Królak, 2005]. The aforementioned problem has been studied extensively in the literature, firstly in the 1940s as part of the radar development [Turin, 1960] and later in the context of digital communication theory [Haykin, 2001].

Probabilistic criteria

The intuitive concept behind statistical signal detection is that the statistical characteristics of a random variable are modified depending if the signal is present or not [Jaranowski and Królak, 2005; Turin, 1960]. Thus, the *null hypothesis* $\mathcal{H}_0$ is that the signal $s(t)$ is not present and the *alternative hypothesis* $\mathcal{H}_1$ is that $s(t)$ is present. A *hypothesis test* or *decision rule* is a rule to split the partition of the observables into two complementary sets, $\mathcal{R}$ and $\overline{\mathcal{R}}$, so that if the observable is in $\mathcal{R}$ then $\mathcal{H}_0$ is chosen, and if the observable is in $\overline{\mathcal{R}}$, then $\mathcal{H}_1$ is chosen. Clearly, two different kind of errors can arise: type I error is selecting the hypothesis $\mathcal{H}_1$ when $\mathcal{H}_0$ is true (also known as *false alarm*), and the type II error is selecting $\mathcal{H}_0$ when $\mathcal{H}_1$ is true (also known as *missed target*). Several criteria can be used to optimise the statistical test: the Bayesian approach, the Minimax approach, and the Neyman-Pearson approach [Jaranowski and Królak, 2005]. An important result is that all these criteria led to the *likelihood test*, which in turn leads to the **matched filter** in the particular case that the noise $n(t)$ is Additive White Gaussian Noise (AWGN) [Turin, 1960].

Mean-square optimisation criterion

Under the mean-square optimisation criterion, a known continuous signal of finite energy, $s(t)$, which contains an AWGN $n(t)$, with one-side Power Spectral Density (PSD) of N_0 W/Hz, should be linearly filtered and the output of this linear filter should be maximised when the signal is present and minimised otherwise. One criterion for such optimisation is to maximise the filter output Signal-to-Noise Ratio (SNR), defined as the quotient of the signal and noise powers at the output of the filer. Using the Schwarz inequality it can be proved [Haykin, 2001] that the matched filter impulse response is

$$h(\tau) = ks(\Delta - \tau) \tag{3.1}$$

where Δ and k are arbitrary constants. The SNR at the output of the filter, for a white noise and at the *optimum sampling point*, is [Turin, 1976]

$$\mathrm{SNR}_o = \frac{2\mathcal{E}}{N_0} = 2TW\mathrm{SNR}_i \tag{3.2}$$

where $\mathcal{E}$ is the energy of $s(t)$, T is the temporal duration of $s(t)$, W is the noise bandwidth of the matched filter, and SNR_i is the SNR at the input of the matched filter.

Non-coherent signal detector

It should be noted that equation 3.2 gives the output SNR of the matched filter at the *optimum sampling point*. This implies that the timing at the burst-detector must be known. Timing information at the burst-detector is not known because the transmission distance and thus the delay Δ in equation 3.1, is a random variable. Additionally, taking asynchronous samples introduces a fractional delay of value μ_k. This problem can be solved by using a complex matched filter followed by an envelope detector. It can be proved that the performance of this non-coherent matched filter for a square-law detector, under the assumption of high SNR, is [Turin, 1976]

$$\mathrm{SNR}_o \approx \frac{\mathcal{E}}{2N_0} = \frac{TW}{2}\mathrm{SNR}_i \tag{3.3}$$

Shape of $s(t)$

The performance of the matched filter used as a burst-detector is proportional to the energy $\mathcal{E}$ of the signal $s(t)$. Consequently, all signals of duration T with the same energy will perform equally well. However, since timing information is not available, the output signal of the Matched Filter (MF) should be considered at all instants of time and not only at the optimum sampling point, whose location is unknown. Thus, depending on the properties of the MF output signal, $y(t)$, the performance of the burst-detector can be improved (or worsened).

Assuming that $\Delta = 0$, the output of the matched filter for the noise-free case is

$$y(t) = \int_{-\infty}^{+\infty} s(-\tau)\, s(t-\tau)\, d\tau \tag{3.4}$$

which corresponds to the autocorrelation of the deterministic signal $s(t)$. Clearly, it holds that $y(0) = \mathcal{E}$ and also that the Fourier transform of $y(t)$ equals the energy spectral density $|S(f)|^2$. Let's define W_α and W_β as the widths, using whatever energy criteria, of the signals $y(t)$ and $|S(f)|^2$. It can be proved that [Turin, 1960]

$$W_\alpha W_\beta \approx 1 \tag{3.5}$$

which has great implications for the choice of the shape of the signal $s(t)$ and the performance of the burst-detector. With all these definitions, there are three properties of $s(t)$ that can be considered [Turin, 1960]: A) *accuracy* B), *resolution*, and C) *ambiguity*. To detect a signal with accuracy the SNR_o should be maximised and W_α should be minimised. Resolution refers to the case where several targets are present in the signal and, thus, W_α should be reduced. Ambiguity refers to the secondary lobes of the signal $y(t)$, which can trigger the detector. The worst case is for a periodic $s(t)$, which will result in $y(t)$ having an undesirable periodic feature.

To summarise, minimising W_α, which is equivalent to maximising the resolution and is required to increase the accuracy, requires making the bandwidth of the correlator large, thus decreasing the SNR_o. Thus, there is a compromise between maximising the MF performance and accurately determining the precise instant of the burst occurrence.

Burst detector implementation

The burst detector section consists of a complex correlator tuned to a frequency of half the line-rate. In an initial state, only the BD operates to detect a burst arrival over the background noise of the guard band or the idle channel. The BD comprises a Finite Impulse Response (FIR) complex MF, followed by a modulus operator, and a decision circuit. The decision circuit requires a threshold λ that should be optimised in order to minimise the PER.

In this work, a preamble that consists of a `1010...` binary sequence was chosen, which produces a main spectral tone of half the line-rate. As stated above in this section, the SNR at the output of the MF will be maximised, due to the periodic nature of this preamble, at a cost of losing detection resolution and increasing the detection ambiguity. However, in this particular case the decision is justified, as the problem is similar to a radar `ON` and `OFF` case, with the advantage that in our case, the *targets* (that is, the optical bursts) are far apart from each other, for this is guaranteed by the OBS network scheduler. The coefficients of the MF FIR implementation are given by the well-known Discrete Fourier Transform (DFT) equation

$$X_k = \sum_{n=0}^{N-1} x[n]\, e^{-\frac{j2\pi kn}{N}} \tag{3.6}$$

where N is the length of the digital filter and $k \in [0,\ldots,N-1]$ is the discrete frequency sampled from the corresponding continuous frequency provided by the Discrete Time Fourier Transform (DTFT) of $x[n]$. In the form given, equation 3.6 samples the frequencies in the interval $[0,\ldots,f_N,\ldots,f_S]$, and because the signal $x[n] \in \mathbb{R}$, there is a complex conjugated symmetry around f_N. The relation of the discrete frequency k and the continuous frequency f (in Hz) is given by

$$f = k\frac{f_s}{N} \tag{3.7}$$

Consequently, given a sampling frequency f_S, which is twice the bit-rate R_b, and a filter length N, the MF FIR coefficients can be obtained from equation 3.6 with the appropriate k values derived from equation 3.7. It should be pointed out than k is an integer positive number, so the filter length N should be carefully chosen to meet this condition for the range of frequencies to be estimated. In addition, the output of the

complex matched filter is a number $o_n \in \mathbb{C}$, so the absolute value is taken. Also, the current detector implementation of equation 3.6, which is implemented as a direct form FIR filter, is computationally inefficient. However, more efficient implementations in terms of chip area and power consumption exist, such as the Goertzel algorithm [Oppenheim et al., 1996, chapter 9].

Once a burst is detected, the BD is disabled to reduce the power consumption and the rest of the system is enabled to recover the burst payload data.

3.1.3 Complete burst preamble description

In the implementation of the burst detector, the MF number of taps N is equal to the number of preamble bits. Because the electrical signal is sampled at two samples-per-bit, this implies that only half of the available preamble bits are used for optical burst detection purposes. The reason for doing that is that the preamble is not only used for burst detection, but also for DC-offset and burst amplitude estimation, and for the initial clock estimation. Figure 3.3 illustrates this. The blue line corresponds with the electrical received signal and the green line with the output of the burst detector MF. It can be seen that the maximum amplitude at the output of the burst detector MF is reached at half of the preamble length.

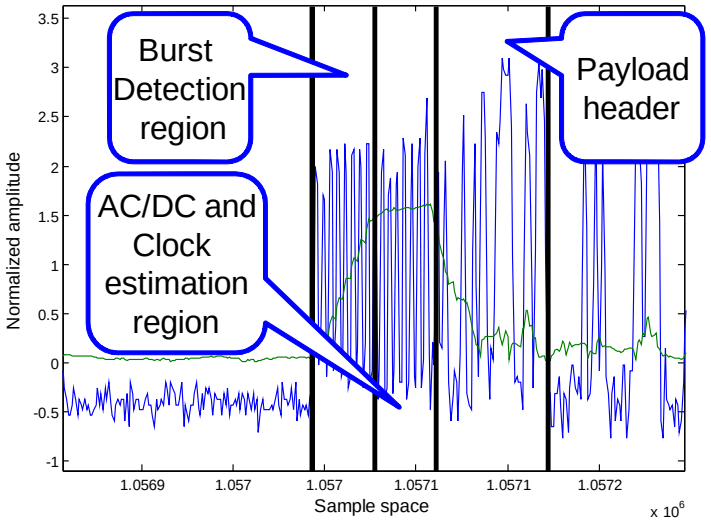

Figure 3.3: Illustration of the optical burst preamble, the payload header, and the output of the burst detector matched filter. The detection regions are also indicated.

Also in this figure three regions are identified: the **burst detection region**, the **parameter estimation region**, and the **payload header region** (which consists of a 32-bit Pseudo-Random Binary Sequence (PRBS)). As pointed out in section 3.1.4, the estimation of the DC-offset and amplitude of the burst should be done rapidly, with a limited number of input samples, and the proposed burst preamble shape allows for

this. In addition, the accuracy of the burst timing estimator is maximised, because the main spectral component of the preamble is precisely the clock component that is being estimated. The optical burst is likely to be detected at the end of the burst detection region or at the beginning of the parameter estimation region and so the first bit coming out of the CDR will belong to the preamble. The digital correlator uses then the payload header to accurately delineate the beginning of the payload.

3.1.4 Clock and data recovery

The CDR subsystem involves several stages: interpolation, DC-offset and amplitude normalisation, BLW correction, equalisation, and bit slicing.

Interpolator

In the proposed digital optical receiver, the analog signal coming from the TIA is digitised at least at two samples-per-bit. The digitiser is governed by a local sampling clock, which can be synchronised to the incoming bit stream or not [Gardner, 1993]. At optical line-rates, building such a synchronisation circuit is not feasible, so it can be considered that all optical digital receivers will take asynchronous samples of the electrical low-pass signal and then perform the interpolation in the digital domain.

The seminal paper [Gardner, 1993] points out that the term *interpolation* does not correctly refer to the digital operation carried out. Indeed, assuming that the symbol transmission is governed by a clock with frequency f_t and phase θ_t and that the sampling clock has a frequency f_s with phase θ_s, if $f_t \neq f_s$ the receiver should perform a digital resampling [Crochiere and Rabiner, 1981]. If f_t and/or f_s vary with time, tracking of this change leads to a Digital Phase-Locked Loop (DPLL), which is the digital equivalent of an analog Phase-Locked Loop (PLL) [Gardner, 2005]. The case of $f_t = f_s$ and $\theta_t = \theta_s$ corresponds to the ideal case when both transmitter and receiver are perfectly synchronised and only occurs in communication theory books.

If $f_t = f_s$ and $\theta_t \neq \theta_s$, the receiver should perform a *digital phase shift* [Crochiere et al., 1975], also called a *delay filter* [Farrow, 1988] or *fractional delay*, because the duration of the delay, μ_k, is less than the sampling period, T_s. The process of interpolation in this context consists, thus, in detecting this fractional delay μ_k using whatever timing detection algorithm and then apply a computationally efficient digital filter in order to obtain the samples of $s[n]$ at the proper time instant for thresholding.

There are many kinds of interpolation filters than can be used [Erup et al., 1993; Farrow, 1988; Crochiere et al., 1975] and there is a compromise between the interpolation FIR filter complexity and the distortion of the output delayed samples. This is because the ideal interpolation filter, the Nyquist filter, is a non-causal filter and thus unrealisable with a finite number of components. Consequently, any interpolation filter

will have a frequency and/or phase response with a main lobe that is not completely flat and with secondary lobes that produce aliasing in the interpolated signal.

Interpolator implementation

The interpolator used here, shown in figure 3.4.A, consists of a fractional detector algorithm that works at two samples-per-bit [Lee, 2002] followed by a Gardner linear interpolator [Erup et al., 1993]. The timing estimator works on a block-by-block basis, updating the estimated value of μ_k every 512 samples of $s[n]$. This allows for timing tracking of the incoming signal and thus the interpolator can compensate a potential sampling clock frequency drift. However, depending of the burst length, in many cases the timing phase can be assumed to be constant over the entire burst length and so the μ_k estimation can be done only once at the beginning of the burst.

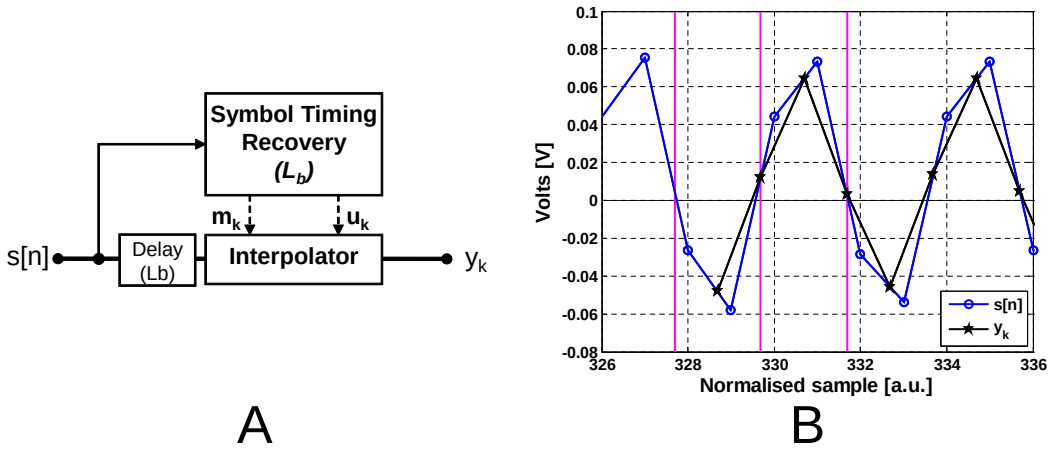

Figure 3.4: (A) Block diagram of the interpolator. (B) Plot of the interpolator input $s[n]$ (in blue) and the interpolator output y_k (in black). The vertical pink lines correspond to the estimated symbol delimiters.

The interpolator follows the linear approach presented in [Erup et al., 1993] and takes two input samples to produce one output sample. Whilst the linear interpolator does not produce optimum results and also has a performance dependence with the value of the phase μ_k [Erup et al., 1993], is the most simple and straightforward solution and thus easy to implement with low hardware footprint and energy consumption. Figure 3.4.B shows an experimental-data example of the interpolator input/output signals. In this example, the input signal (in blue) has an estimated phase of $\mu_k \approx 0.3$. The vertical pink lines correspond to the estimated bit intervals, that is, the eye diagram limits. The output signal (black) samples are located at the optimum sampling points, which are at the start of the bit interval and at half the bit interval, respectively.

Signal normaliser

The purpose of the **signal normaliser** is to estimate the incoming burst amplitude and DC-offset. In a DON, optical bursts coming from different transmitters are likely to have different amplitudes that should be compensated for.

The problem of estimating the amplitude and DC-offset lies in the statistical signal theory field, and so the two well-know estimators for the mean and the variance can be used [Manolakis et al., 2005, p. 136], or efficient but sub-optimal digital implementations [Cheng and Evans, 1997]. However, since the number of available estimation samples N should be small in order to increase the network throughput, an adequate preamble should be chosen in order for these estimators to converge quickly and thus provide accurate values.

Signal normaliser implementation

The signal normaliser, shown in figure 3.5, consists of a DC-offset and amplitude estimators, whose values are subtracted and multiplied to the signal, respectively.

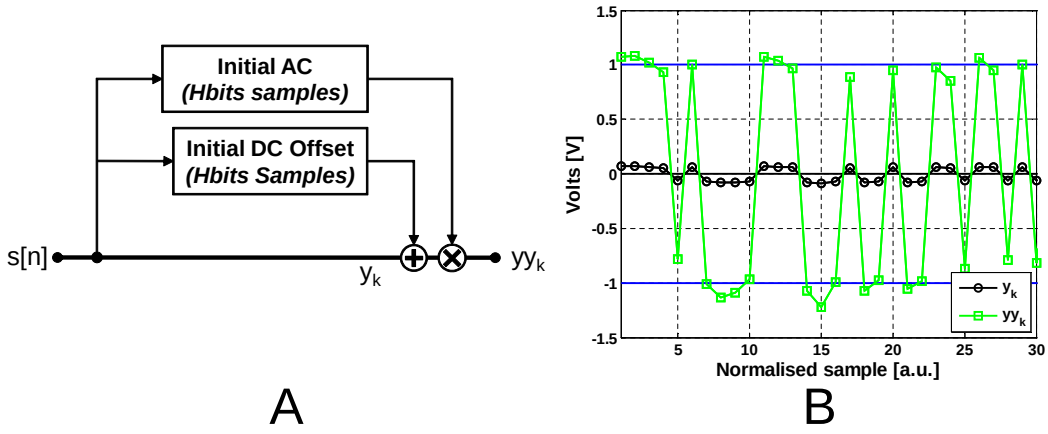

Figure 3.5: (A) Block diagram of the used signal normaliser. (B) Example of the signal normaliser input (black) and output (green) signals. The blue horizontal lines show the ideal normaliser output (either 1 or -1 volts).

The DC-offset estimator consists of the estimator of the mean [Manolakis et al., 2005],

$$\mathrm{DC} = \frac{1}{N}\sum_{n=0}^{N-1} x[n] \tag{3.8}$$

where N is the total number of samples used. The amplitude estimator consists of the estimator for the variance,

$$\mathrm{AC} = \sqrt{\frac{1}{N}\sum_{n=0}^{N-1}(x[n]-\mathrm{DC})^2} \tag{3.9}$$

where N is the number of samples and DC is the estimated DC-offset. The shape of the preamble can be approximated by a sinusoidal function sampled at instants of time $t = kT/4$ with a fractional delay μ_k. If the number of samples N is even, then the Direct Current (DC) estimator has a balanced number of samples and thus the DC estimation is accurate even with a reduced N. Similarly, the amplitude estimator has a balanced signal and thus the estimation is accurate. In this receiver, N equals to the number of preamble bits.

Figure 3.5.B shows an experimental-data example of the normaliser input (black line) and output (green line) signals. The horizontal lines (blue) correspond to the ideal output values. For clarity, in this figure only the even samples (located at the centre of the bit interval) are plotted. The output samples of the normalised signal yy_k are random values with mean 1, -1, or 0, due to noise in the normalised signal.

Base-line wander compensation

The BLW is defined as a variation of the optical burst DC-offset over the burst duration. BLW arises when the transmitted signal traverses a high-pass filter, such as the DC blockers encountered in most AC-coupled optical photo-receivers. Also, BLW can be generated in optical amplifiers due to the gain change by the add-drop process of optical signals [Puttnam et al., 2008a]. The BLW can be characterised by a time constant τ_{BLW}, in a similar way of a first-order RC circuit. Figure 3.6 illustrates the effect of BLW in an AC-coupled photodiode when receiving optical bursts with different optical power. Because in this case the BLW is mainly related to the value of the capacitor used in the AC-coupling of the receiver electronics, the higher the variation of the optical power (which produces a higher variation in the photocurrent) produces a higher BLW.

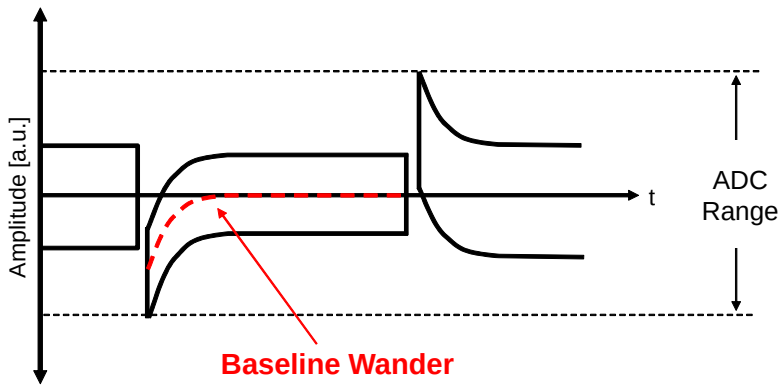

Figure 3.6: Example of the base-line wander impairment.

There are several ways of correcting the BLW [Baek et al., 2004], all of them employed in Ethernet receivers. The BLW can be A) estimated and corrected in the analog domain, or B) being estimated in the digital domain and corrected in the analog domain, or C) being estimated and corrected in the digital domain. Approaches A and B are difficult to implement at optical line-rates due to the required bandwidth of the electrical front-end electronic components. Thus, a fully digital BLW compensation is preferred. The reference [Baek et al., 2004] contains a survey of BLW approaches and proposes a new one that has the advantage of working correctly even if the taps of the digital Inter-Symbol Interference (ISI) mitigation filter are not fully converged.

Base-line wander compensation implementation

After the interpolator, a BLW correction coefficient is added to the samples. The implemented approach, shown in figure 3.7, follows the fully digital algorithm presented in [Baek et al., 2004], which has the advantage of not requiring a converged equaliser to work properly. After the normalisation stage, the samples yy_k, at the baud rate, are in a space $[1, 0, -1]$ plus some random noise around this values. After the slicer, the recovered samples have a binary value. An error signal is generated between the sliced bits and the pre-equalised samples, compensating for the delay of the equaliser (if any). This error signal is averaged over N_{BLW} bits to reduce the noise. Consequently, there is a tradeoff between the noise rejection (large N_{BLW}) and a fast response to BLW changes. In this work, a value of $N_{\text{BLW}} = 256$ bits was found to be a good compromise.

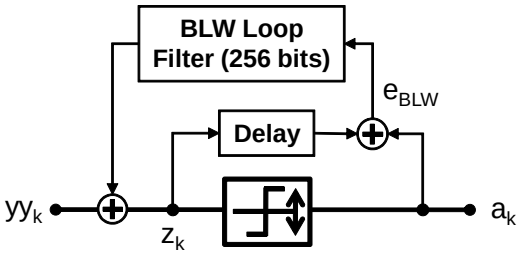

Figure 3.7: Block diagram (extracted from figure 3.2) of the baseline wander compensator.

Digital filtering and dynamic thresholding

Analog optical receivers make use of receiver filters in order to remove out-of-band noise, shape the received signal to compensate for the frequency response of the channel, and compensate for ISI or other impairments like CD.

A Baud Spaced Equaliser (BSE) can be used to compensate for ISI and CD. However, Fractionally Spaced Equalisers (FSEs) equalisers have the advantage that they can combine matched filtering and fractional timing delay into the equalisation process, at a cost of an increased computationally complexity.

If channel conditions are known or could be estimated, a precomputed causal Wiener filter can be used digitally. In dynamic networks, however, conditions such as channel noise are likely to vary and adaptive filters can be implemented digitally. It can be shown that for high SNR, a Least Mean Squares (LMS) filter converges to the optimum Wiener solution. In addition, adaptive fractional filters can compensate for frequency drifts whit in the optical burst.

Another technique that can be used in the digital domain is dynamic thresholding. This technique consists of estimating the eye variances and updates the decision threshold λ accordingly [Kawai et al., 1989].

Digital filter and thresholding implementation

A fractionally spaced 3-bit (6 taps) equaliser is used to remove out of band noise and compensate for any remaining amplitude or phase fluctuation across the burst. The equaliser, shown in figure 3.8.A, is updated using the LMS algorithm [Haykin, 2002]. The equaliser also downsamples the 2 samples-per-bit z_k signal to a baud rate ye_k signal, which is fed into the slicer. The equaliser is initialised by setting the central tap to 1, so the initial equaliser kernel is

$$\mathbf{w}_0 = [\ \underbrace{0\ \ 0}_{\text{bit } n-1}\ \ \underbrace{0\ \overbrace{1}^{\text{central tap}}}_{\text{bit } n}\ \ \underbrace{0\ \ 0}_{\text{bit } n+1}\ ] \tag{3.10}$$

Since the samples at the input of the equaliser are normalised, interpolated, and the timing is known from the burst detector, this allows for a very rapid equaliser convergence.

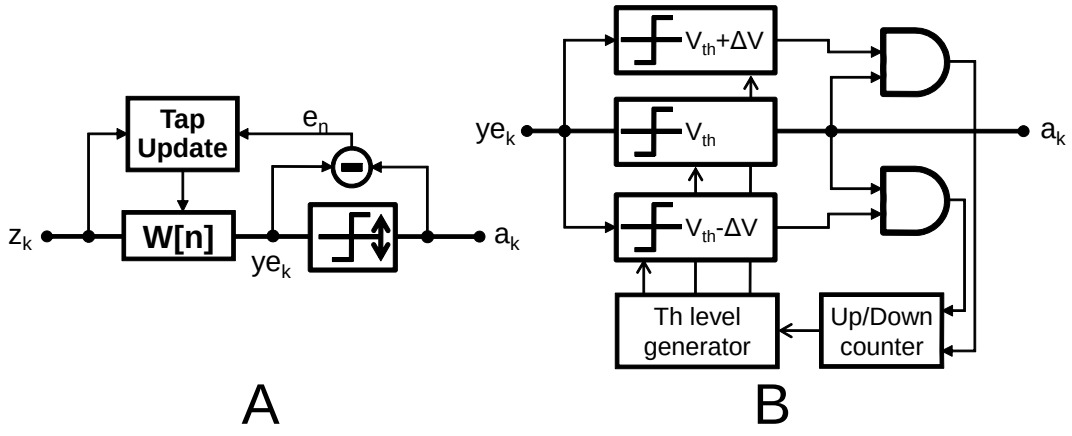

Figure 3.8: (A) Diagram of the LMS equaliser and variable-threshold bit slicer. (B) Detailed diagram of the variable-threshold slicer (from [Kawai et al., 1989]).

Finally, the equalised samples are sliced with a variable threshold slicer in order to recover the data [Kawai et al., 1989], depicted in detail in figure 3.8.B. Since the

samples ye_k after the equaliser are in a space $[1,-1]$, an initial threshold $\lambda = 0$ is used. Because of the large dynamic range the burst-mode receiver has to cope with, this threshold is not optimum as the variances around ± 1 will depend on the input power. The dynamic threshold algorithm updates the threshold value and thus adapts to this changes, increasing the robustness of the receiver. The output of the slicer is a stream of bits a_k into a binary space $[+1,-1]$.

3.1.5 Payload delimitation

Once an optical burst has been detected, the digital receiver starts the CDR subsystem and an output bit stream is produced. The burst detection has some uncertainty of when the actual payload starts. Thus, the start and end of the payload should be determined in order for the receiver to switch between the burst searching state and the CDR state. The easiest way of achieving this is by inserting a marker at the beginning of the payload (header) and at the end (tail), and then apply a digital correlator—which can be viewed as a digital correlator that gives the Hamming distance—and compare the correlator output with a stored version of the marker [Scholtz, 1980]. If the burst payload has variable length, the robustness can be increased by coding the length of the burst after the payload header and thus control the payload timeout in case the tail of the burst is not detected. The election of the frame synchronisation thresholds h_{header} and h_{tail} will have implications in the BER of the system.

Frame delineation implementation

Depending on the exact occurrence of the burst detection triggering event (ideally in the burst-detection region), there are some uncertainty about the exact starting bit of the payload (the first bit output by the CDR). In order to eliminate this uncertainty and accurately delineate the payload beginning, a digital correlator and a payload header of 32-bits are used. The output of this digital correlator is a natural even number between -32 (all bits in the stream are different) and 32 (all bits in the stream are the same). A similar digital correlator with the same threshold value searches for the payload tail. Threshold values of $\lambda_d^{\text{header}} = \lambda_d^{\text{tail}} = 30$ were used, thus allowing one bit error into the 32-bit header/tail marker.

In this work, constant length bursts are assumed and thus a bit timeout is used every time a burst is detected and the CDR section activated. This timeout resets the receiver to the burst searching state in the event that either the payload header or tail are not found, due to errors in the delimiter bits or false burst detection events. For variable-length bursts, after the payload header the burst length can be encoded with some redundant bits for increased robustness, and the currently constant timeout can be made variable.

3.2 Packet-error rate measurement

As mentioned in chapter 2, in OBS networks there are two important performance metrics: a) the BER of the individual packet data payloads, and b) the number of correctly received packets which is quantified, analogously to the BER, with the PER. A number of studies have been done employing probabilistic analysis and simulation techniques for OBS networks [Tintor et al., 2008; Klinkowski et al., 2007; Rodrigues et al., 2007], focusing mainly at the logical but not at the physical level to determine the PER that is produced because lack of network resources to deliver all the network traffic. However, in this section the main concern is the PER that occurs due to limitations and impairments that arise in the physical layer of OBS networks. BER of the data payload can be measured with reasonable confidence intervals capturing only a few bursts [Jeruchim, 1984] as the size of data bursts in OBS networks is in the range from Kb to Mb. However, to measure PER accurately many bursts should be captured and processed. PER is an crucial performance parameter, because if the receiver fails to detect the burst header, the full payload will be lost. The burst processing time required for offline processing makes this method unattractive for the evaluation of the PER arising from physical layer impairments in OBS systems.

Many unofficial MATLAB parallel environments have been developed [Choy and Edelman, 2005], and recently a *Parallel Computing Toolbox* and a *Distributed Computing Server* were officially released [Mat, 2009]. Whilst these toolboxes address *embarrassingly parallel* problems, making them suitable for PER measurement, they do not deal with the data acquisition and task synchronisation that is necessary in this application. Here, a general-purpose cluster processing system is presented that controls the data acquisition and allows offline software-based processing of received burst-data using MATLAB for algorithm development. The advantages of this solution comparing with real-time FPGA are the ease with which the MATLAB DSP code can be changed to test different algorithms and thus the fast development time.

In this section, I report on the results from a distributed offline processing system that enables the determination of both the PER and the BER and therefore to fully characterises the performance of the digital burst-mode receiver, over the entire dynamic range. The minimum required header length and the optimum threshold to ensure an acceptable PER are determined experimentally. Minimising the header length in burst-mode networks is important as the throughput of the system is inversely proportional to the header length.

3.2.1 Cluster processing for packet-error rate measurement

The easiest way of developing and testing new algorithms for burst-mode DSP receivers is to use a fast development and powerful computer language like MATLAB.

However, the execution speed of MATLAB compared with other technical alternatives such as hardware implementation in an FPGA is very slow. In previous work, the performance of the digital burst-mode receiver was simply characterised in terms of the BER of the data payload for a single or a few bursts. The Payload Bit-Error Rate (pBER) could be measured with a small confidence interval by capturing only a small number of packets, as the number of bits per packet is quite large in OBS networks. Consequently, a single Personal Computer (PC) interfaced to the real-time oscilloscope was sufficient to capture and process all the required data. However, to measure the PER a large number of bursts, in the order of thousands, should be processed. Assuming that the probability of transmission for both symbols is equal and that the probability to be measured is α, the required number of bursts is approximately $N = \frac{10}{\alpha}$, which produces an acceptable confidence interval of about $[2\alpha, 0.5\alpha]$ [Jeruchim, 1984]. Thus, a new tool is required in order to fully study all the aspects of the dynamic OBS networks receivers and the impact of other components.

Clearly, the DSP processing of many optical bursts is a so-called **embarrassingly parallel** problem, as the processing is carried out with no communication at all between the parallel-running tasks [Foster, 1995]. However, most of the surveyed MATLAB parallelising tools [Choy and Edelman, 2005] are designed for developing parallel versions of well-known algorithms, such as matrix multiplication or factorisation, and usually require small modifications to the source code and installation of additional software on the central node and on each worker PC. Moreover, it is necessary to install further toolboxes on the central node to communicate with the real time scope to get the received burst data. To overcome these problems, a tailored cluster solution, shown in figure 3.9, was developed. The optical signal from an arbitrary optical network operating at a line-rate of 10 Gb/s is first detected using an Alternating Current (AC) or DC coupled optical receiver. Then, the electrical output of the receiver is sampled at 20 GS/s with a Tektronix TDS6154C real-time oscilloscope. The cluster controller reads through the network, using Virtual Instrument Software Architecture (VISA), one trace of captured data and concurrently sends this to one free processor. When the processor finishes the processing job, it sends back the results to the controller. This computer is marked as free and new acquired data is sent as soon as available.

Figure 3.10 shows in detail the software architecture of both the cluster controller and the worker PC server script. The cluster controller is the software process that gets data from the real-time scope, sends it for processing to the worker PCs, stores and writes the received data, and synchronises the whole system operation. The technologies required to perform all of these tasks are: VISA instrument control, network communication sockets, and multi-threading programming and synchronisation. `C++` was chosen as the main programming language due to the availability of libraries to

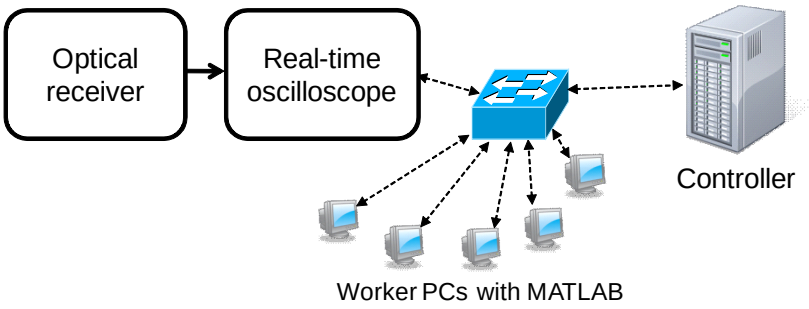

Figure 3.9: High level architecture of the cluster processor for PER measurement.

perform all these tasks efficiently.

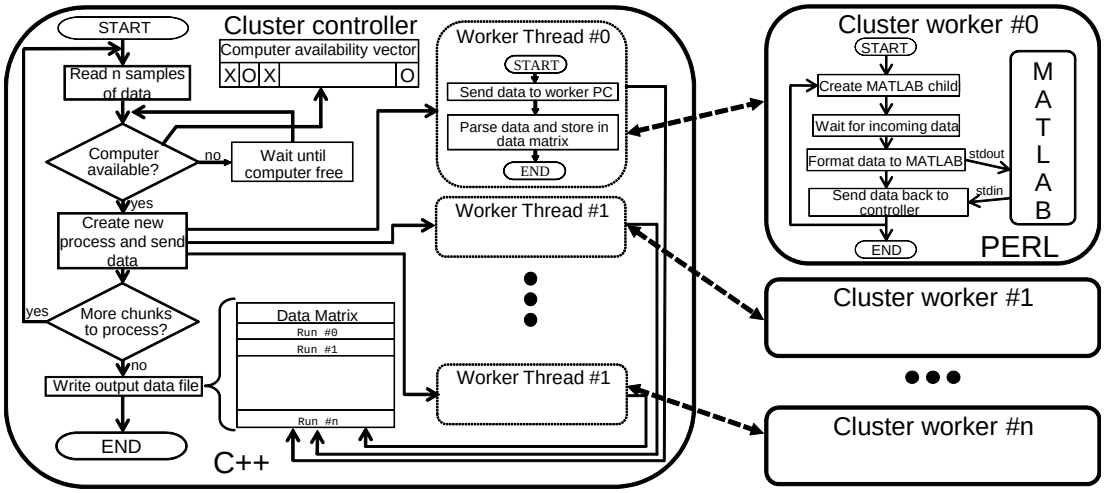

Figure 3.10: Block diagram of the cluster processing solution for packet-error rate measurement. This diagram represents both the cluster controller process (written in `C++`) and the worker processes (written in `PERL`).

Cluster controller process

The cluster controller operates in the following way

1. A configuration file that contains the names of the machines belonging to the cluster is read. This configuration file also contains the experimental variables of the DSP code to be modified as independent variables.

2. A data chunk containing a configurable number of samples is requested from the scope. This chunk of data is then transferred into the controller's memory space over the network.

3. The availability vector, which keeps track of which processors are not in use, is then checked and if there is an available processor a new thread is created. Each thread in the cluster controller is represented in figure 3.10 as a dashed line inside the controller process.

4. The newly created thread, which runs concurrently with the main controller and other worker threads, connects to the worker processor, sends the experimental data, and then waits for the results of the processing.

5. When these results arrive, the thread stores them in the thread-safe data matrix, closes the connection with the worker PC, changes the status of the worker PC in the availability vector, and terminates itself.

6. If the number of data chunks reaches a predefined limit, the controller waits for all the threads to finish and then writes the results in a convenient MATLAB file format for easy post-processing.

Cluster worker process

The cluster contains an arbitrary number of working processors, each of them running the Linux operating system. Each worker PC runs a small server script that waits for an incoming connection from the controller. A light-weight network protocol was designed for transferring both data and results between the cluster controller and the worker processors. The selected programming language for the worker PCs was `PERL` because it offers great network sockets support, text manipulation capabilities, and child process management.

The worker PC script operates in this way

1. At the beginning, it creates a MATLAB child process and communicates with it using the standard input/output. This reduces the overhead of creating a new MATLAB instance for each job.

2. The script waits for incoming jobs. When one job arrives, it sends the data to MATLAB for processing, and when the data processing is completed, sends back the results to the controller.

3. The network connection is closed and the script waits for the next incoming connection.

In addition to the cluster controller process and the worker PC script, some utilities for starting up the cluster and check the status of the cluster processors were developed as well. The DSP algorithm for the digital receiver is written in MATLAB and the code could be easily changed without modifying the cluster software. However, if the data format of the results change, the network data parser on both the cluster controller and the worker script should be modified.

We have tested this architecture with 45 computers and discovered that for the DSP algorithm presented in this work the limitation is the processing power of the

cluster. However, for faster algorithms the data transfer rate of the network between the oscilloscope and the cluster controller and the controller and the cluster processors became the limiting factor.

3.2.2 Experimental setup

The experimental set-up comprising an optical burst transmitter and a digital burst-mode receiver is shown in figure 3.11. A single external modulator was used to ensure that the transmitter performance was identical for the strong and weak bursts. Four attenuators allow to set an arbitrary optical power and noise loading for the weak and the strong bursts. A gain-clamped EDFA was used to amplify the optical signal. The feedback cavity attenuation was set to 24 dB, which minimises the optical gain but also the unwanted gain transients. The optical receiver consists of a 37.5 GHz Lorentzian optical filter, a standard AC-coupled PIN photodiode with integrated TIA, and followed by an anti-aliasing and shaping 4^{th} order Bessel filter. Digital sampling at just over twice the bit-rate (25 GS/s) with an effective resolution of 5 bits was performed with a Tektronix TDS 72004 real-time oscilloscope.

The digital signal processing was carried out offline in MATLAB using a cluster of PCs to increase the number of bursts that could be processed, as described in section 3.2.1. The digital burst-mode receiver used in this work was described in section 3.1.

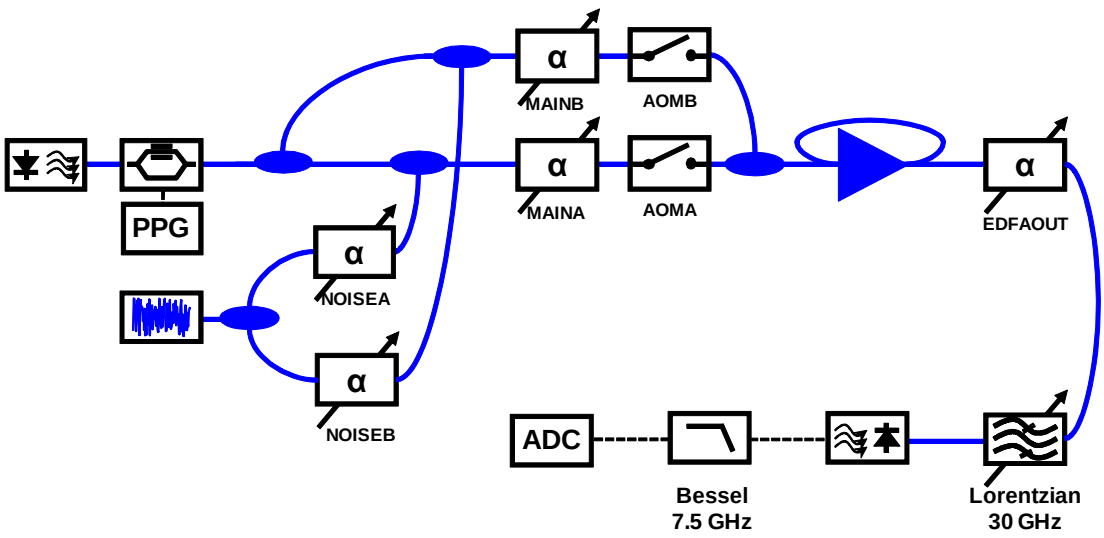

Figure 3.11: Experimental burst transmitter and digital burst-mode receiver for PER measurement.

The optical bursts, shown in figure 3.12 and at a bit-rate of 10.709225 Gb/s (ITU-T G.709), consist of a variable length preamble of alternating ones and zeros, and an arbitrary length data payload. A burst tail is used to delineate the end of the burst, which allows for variable length bursts. However, errors in the detection of the burst tail will propagate to subsequent bursts. In order to limit the range over which such

errors can propagate a timeout is also used. However, this limits the maximum burst duration to less than the timeout which was set to ≈ 200 μs (the payload duration) in this work.

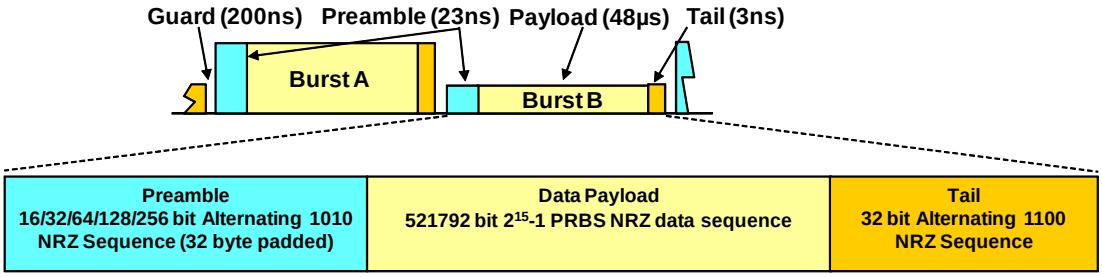

Figure 3.12: Detailed diagram of the generated optical bursts for the characterisation of the digital burst-mode receiver.

3.2.3 Experimental results and discussion

The PER measurement was carried out following a three-step approach. Firstly, a continuous-mode assessment of the receiver performance was done in order to determine the pBER as a function of the OSNR and, thus, to determine the ROSNR. Secondly, the burst detector threshold λ was optimised. Finally, using this optimised threshold, the PER measurement was carried out for a number of preamble lengths.

Required OSNR

The dynamic range of the digital receiver with respect to burst-to-burst power difference was determined in terms of the ROSNR, to ensure that the data payload had a BER of 10^{-3}. It is assumed that FEC will be employed in this system so a pre-FEC bit error rate of 10^{-3} was used as the performance metric in this work, which approximately leads to a BER better than 10^{-12} after FEC. The optical power incident on the receiver from burst A was fixed at -6 dBm and the power of burst B was varied from -6 dBm to -16 dBm. Independent noise loading stages were used to set the OSNR of each burst to be the same, independently of the burst power difference.

As shown in figure 3.13, the dynamic range of the receiver is 7 dB for an ROSNR penalty of less than 1 dB. The dynamic range of the digital burst mode receiver is mainly limited by the electrical and quantisation noise generated at the ADC.

Threshold optimisation

The burst detection threshold λ was then optimised to minimise the PER at the point corresponding to the maximum dynamic range, i.e. for the burst-to-burst power variation of 7 dB and an OSNR of 10.85 dB, for header lengths ranging from 16 to 256

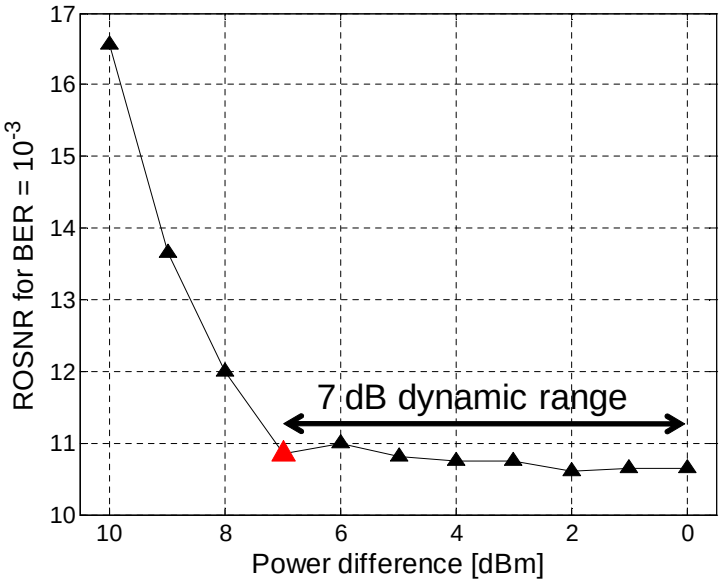

Figure 3.13: The required OSNR for a payload BER of 10^{-3} and the threshold detector optimisation point (red triangle).

bits. Note that the burst header detector utilises only half the number of bits in the header for the detection, as the remaining bits are used to estimate the burst DC-offset and initial amplitude, as illustrated in figure 3.3.

Figure 3.14 shows the PER calculated from 200 bursts as a results of sweeping the burst detector threshold λ for preamble lengths of 16 (★), 32 (◯), 64 (×), 128 (♦), and 256 (▲) bits. By inspecting this figure, three regions can be identified. The first region is where the optimum threshold is found. For all preamble lengths, the optimum thresholds lies in the interval $0.2 \leq \lambda \leq 0.25$. Also, as the number of preamble bit increases, the optimum threshold lowers. This can be explained because a longer correlator filters out more noise, increasing the SNR, and consequently the threshold can be lowered and still detect optical bursts reliably. The region $\lambda < 0.2$ corresponds to the case when the burst detector is triggered by noise rather than the burst preamble, for both strong and weak bursts, and thus all bursts fail detection and the PER approaches 1. Finally, the region $\lambda > 0.25$ corresponds to the case where the threshold is too high to detect weak bursts, because the MF output is very low due to the low optical received power even when the MF is matched, and only the strong bursts are correctly detected. Although not shown in this graph because of long processing times—even for the computer cluster—if the threshold λ increases beyond 0.4 errors will also grow as high power bursts, like weak bursts, will not be detected at all.

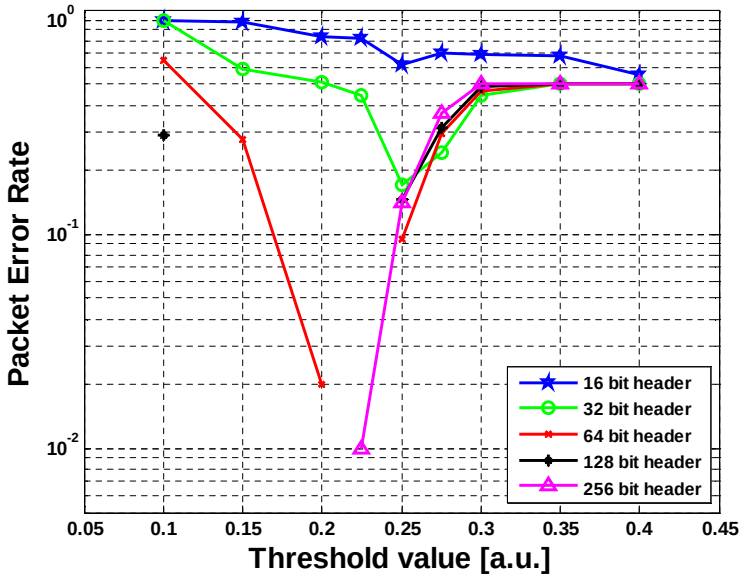

Figure 3.14: PER for different preamble lengths as a function of the threshold λ, showing the optimum threshold value which minimises the PER.

Packet error rate measurement

The packet error was then characterised as a function of the burst-to-burst power difference for preamble lengths of 32, 64, and 128 bits—the MF number of taps equals this number because the MF works at 2 samples-per-bit, however only half the preamble bits are used for burst detection purposes—using the optimum burst detection threshold λ as determined from figure 3.14 in the previous section. Figure 3.15 shows that the PER sharply reduces as the power difference between bursts diminishes. This is expected, because if the power of the weak burst increases, that produces and increasing in the SNR at the output of the MF for weak bursts, which leads to a decreasing of the PER, which is dominated by weak burst missed and MF noise triggering errors.

For the 128 bit header at a weak-burst power of -12 dBm (burst power difference of 6 dB), no packet loss was measured in $20,000$ bursts, thus the PER is better than 5×10^{-5}. It was found that it is necessary for the burst preamble to be greater than 64 bits to ensure that the PER is better than 10^{-2} over the 7 dB dynamic range of this digital burst-mode receiver.

3.3 Digital receiver chain modelling

In this section, a simulation model of a digital burst-mode receiver—which combines experimental data gathering with model parameter fitting—is carried out. The purpose of this model is to have a better understanding of the impact of all the elements in the receiver chain front-end that affect the performance of the digital receiver described in

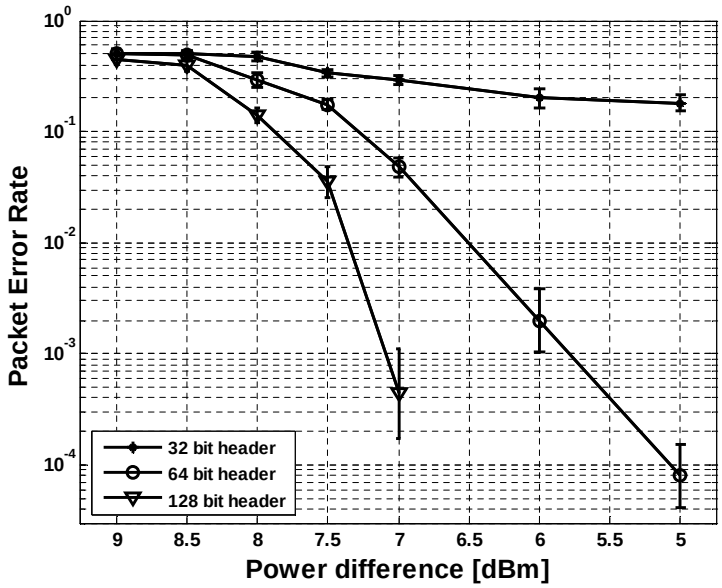

Figure 3.15: Experimental PER measurement, for preamble lengths of 32, 64, and 128 bits. Note that only half of the preamble bits are used for burst detection purposes.

section 3.1 and characterised in section 3.2.

3.3.1 Experimental setup and system model

Figure 3.16 shows the experimental setup used for the development of the digital receiver model. A DFB is externally modulated at 10.709225 Gb/s (ITU-T G.709), and then optical noise is loaded to arbitrarily set the OSNR. The receiver optical filter is 30 GHz Full Width at Half Maximum (FWHM) 3rd order Lorentzian and the optical receiver is a standard PIN AC-coupled photodiode and TIA (Hamamatsu G8925-21) with minimum and typical responsivity values of 0.75 and 0.9 A/W, respectively. An electrical 4th order Bessel filter is used both to remove electrical noise and as a shaping filter. The electrical signal is then digitised with a Tektronix Digital Phosphor Oscilloscope (DPO) and processed offline with DSP software written in MATLAB.

Processing speed is critical at optical line rates, so two samples-per-bit were used for all the DSP in the receiver. However, the digitiser does not allow arbitrary sampling rates to be selected. Thus, 25 GS/s was chosen to be a close upper approximation to the Nyquist frequency, and the experimental signal was resampled using a linear-phase 10th order Kaiser filter and then ideally requantised with 8 bits resolution to obtain a 2 samples-per-bit output signal. In contrast, the simulator uses 16 samples per bit to represent the optical/electrical signal before the ADC stage. The simulated signal is then quantised, Kaiser-antialiasing filtered, and downsampled to 2 samples-per-bit using the same procedure as for the experimental data.

The DSP receiver software is identical for both experimental and simulated traces.

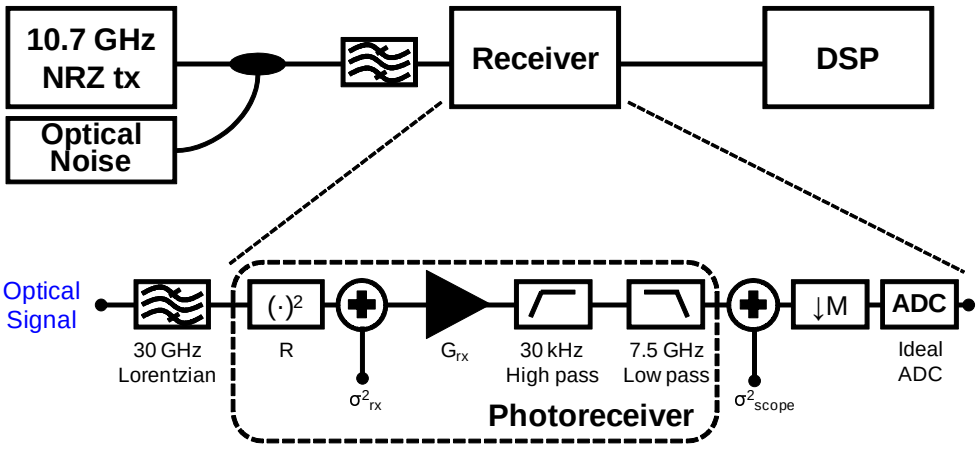

Figure 3.16: Experimental setup for the characterisation of the digital optical receiver.

The purpose of this section is to characterise the impact of noise and quantisation on the digital receiver chain and, thus, a simple DSP receiver architecture was chosen. Firstly, the incoming samples are upsampled to 16 samples-per-bit and the optimum sampling point is determined with a digital squaring technique [Oerder and Meyr, 1988]. Secondly, the optimum threshold is calculated with the estimation of the Q-factor and then samples of the signal are sliced to obtain the output bits.

The digital receiver chain model used in the simulator is shown in figure 3.16. AWGN is first added to the optical signal to give the required OSNR and then it is band-pass filtered with a Lorentzian optical filter as described above. The AC-coupled photodiode is modelled as an ideal square-law detector with responsivity R, and includes AWGN of variance σ^2_{rx}, followed by an ideal TIA of gain G_{rx} V/A. The AC-coupling is simulated with a 1$^{\text{st}}$ order high-pass filter with $F_c = 30$ kHz, followed by the Bessel filter as described above. The digitiser thermal noise is modelled as an AWGN of variance σ^2_{scope}, and this is followed by an anti-aliasing Kaiser filter and a decimator. Finally, the simulated trace is ideally quantised with 8 bit of resolution to output a 2 samples-per-bit discrete-amplitude signal.

3.3.2 Digital receiver chain model characterisation

The receiver chain was experimentally characterised to estimate the model parameters (responsivity, photodiode and TIA noise, transimpedance gain, and digitiser noise).

The first model parameter investigated was the intrinsic electrical noise of the digitiser, σ^2_{scope}, due to the electrical digitiser front-end. We called this parameter the **noise floor**, defined as the noise present at the output of the digitiser when no electrical signal is present at the input. To estimate the noise floor, a short was connected to the digitiser input and five traces of 10 mega-samples were acquired and conditioned as described in the previous section. Then, the normalised histogram of the noise floor—which

corresponds to the Probability Mass Function (PMF)[1]—was computed.

Figure 3.17 shows the estimated standard deviation as a function of the oscilloscope vertical scale using the quantiser step [Marco and Neuhoff, 2005] as the reference unit. The arrow indicates the vertical scale used for subsequent characterisations of the digitiser, which corresponds to 50 mV/div. This vertical scale is sufficient to capture an optical signal of power −6 dBm using half the digitiser range and, thus, to reserve some digitiser dynamic range for potential BLW that may arise in burst-mode operation of the receiver. We note the large degradation in noise as the scale is switched from 90 to 100 mV/div, which we believe arises from the change in the internal digitiser front-end amplifier.

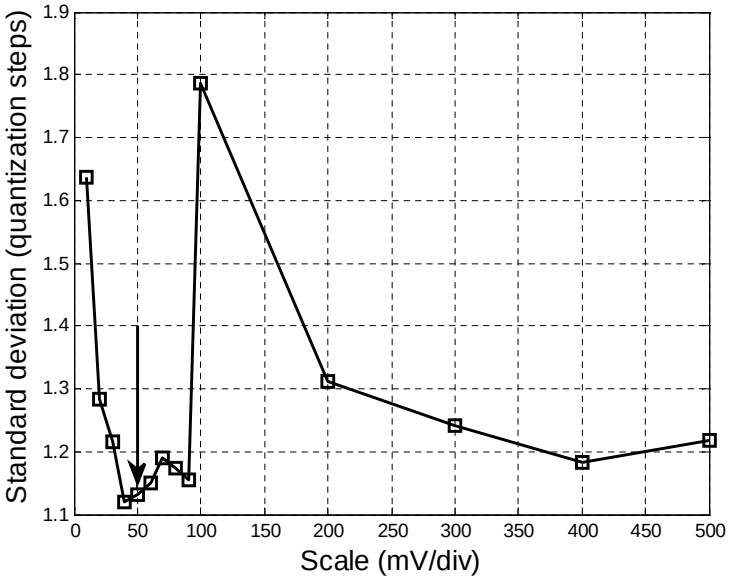

Figure 3.17: Standard deviation of the digitiser noise floor as a function of the digitiser vertical scale. The arrow indicates the scale used for the digital NRZ receiver in subsequent measurements.

The noise floor parameter σ^2_{scope} for the simulation was determined by minimising the logarithmic likelihood function between the experimental and the simulated PMFs. Before computing the log likelihood error function, simulated histogram points with confidence intervals less than 10% in relative size were removed. The estimated value of σ^2_{scope} was 4.8385×10^{-5} W.

The second step was to estimate the gain and electrical noise power due to the photodiode and TIA. The photodiode responsivity chosen was the typical value provided by the manufacturer, 0.9 A/W. The received-power dependant shot-noise was neglected because the calculated shot-noise variance was on average an order of magnitude less than thermal noise variance over the received power range. In consequence, both the

[1] the PMF corresponds to the discrete version of a probability density function

photodiode and TIA noises were modelled as an AWGN of variance σ^2_{rx}. The methodology employed was to compute three error functions of the PMFs for optical noise powers of -6 and -14 dBm and for **dark noise** (defined as the photodiode noise when no optical signal is present at the input) and their simulated counterparts. Both the photo-receiver noise and the transimpedance gain were estimated by minimising the Euclidean norm of the three log likelihood error functions, given by

$$\varepsilon = \frac{\sqrt{3}}{N}\left[\underbrace{\left(\sum^{N}|\log E_{-6}-\log S_{-6}|\right)^2}_{-6\text{ dBm}} + \underbrace{\left(\sum^{N}|\log E_{-14}-\log S_{-14}|\right)^2}_{-14\text{ dBm}} + \underbrace{\left(\sum^{N}|\log E_{d}-\log S_{d}|\right)^2}_{\text{Dark noise}}\right]^{\frac{1}{2}} \tag{3.11}$$

where ε is the error magnitude, $E_{\{-6,-14,d\}}$ are the experimental samples, $S_{\{-6,-14,d\}}$ are the simulated samples, and N is the total number of samples. Figure 3.18 shows a two dimensional plot of ε against G_{rx} and σ^2_{rx}, showing the optimum region (dark blue). The estimated values for the photo-receiver noise σ^2_{rx} and photo-receiver transimpedance gain G_{rx} were 2.5×10^{-11} W and 325.46 Ω, respectively.

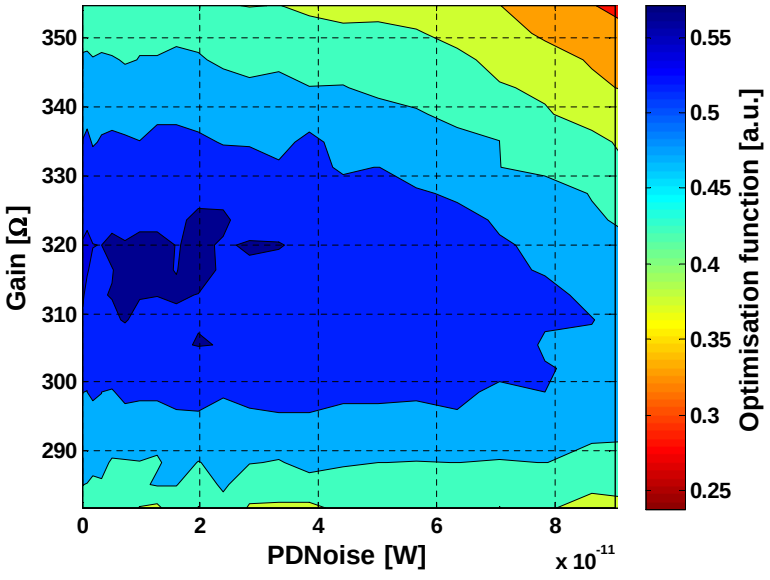

Figure 3.18: Logarithmic error function fitting, showing the optimum region for the gain and photodiode noise parameters.

Table 3.1 summarises the estimated parameters for the digital optical receiver model of figure 3.16. Here, the photo-receiver and digitiser noise values are given in terms of PSDs such that they are independent of the particular experimental or sim-

ulation bandwidths.

Table 3.1: Estimated model parameters of the digital receiver.

Symbol	Value	Units	Description
R	0.9	A/W	Photodiode responsivity
N_{rx}	2.92×10^{-13}	W/GHz	Photo-receiver noise PSD
G_{rx}	325.46	Ω	Photo-receiver transimpedance
N_{scope}	5.6492×10^{-7}	W/GHz	Digitiser electrical noise PSD

To conclude this section, figure 3.19 shows a comparison of the experimental and simulated PMFs for optical noises of power −6, −11, and −14 dBm, using the estimated values. We note that there is a small variation in the wings of the PMFs between the experimental and simulated −6 dBm noise traces, which we believe is due to nonlinearities in the digitiser partition which are not present in the ideal simulated quantiser.

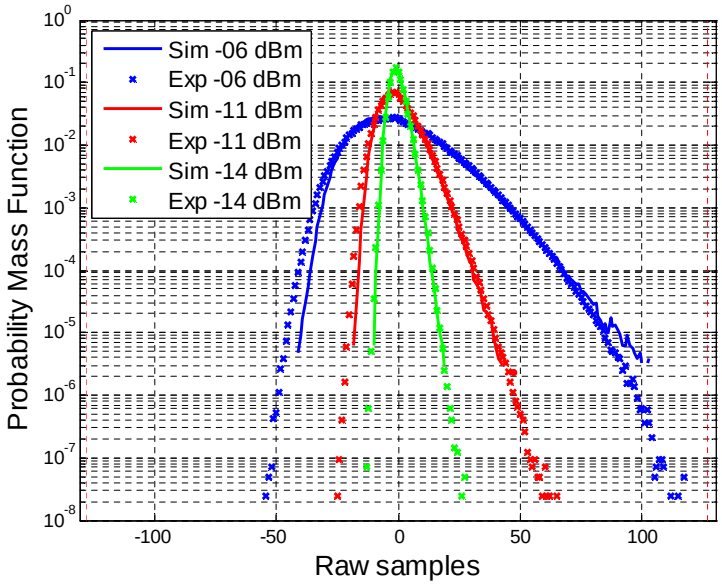

Figure 3.19: Experimental and simulated probability mass functions for −6 dBm, −11 dBm, and −14 dBm optical noise.

3.3.3 Experimental and simulated digital receiver performance

In order to test the validity of the model described in the previous section, the experimental setup of 3.16 and the simulator was used to study the performance and dynamic range of a digital Non-Return to Zero (NRZ) receiver. A set of traces with 800 kilosamples each were experimentally captured with signal power and OSNR varying from −6 dBm to −18 dBm and 8 dB to 16 dB (in increments of 1 dB), respectively. A similar number of synthetic traces were generated with the simulator using the estimated

parameters of table 3.1. Experimental and synthetic traces were processed offline with the same DSP receiver code as described in section 3.1. The methodology used to compare experimental and simulated data was as follows: first, the BER was computed by error counting as a function of the OSNR and BER values with a relative confidence interval less than 10% were discarded. Then, the ROSNR for a BER equal to 10^{-3} was interpolated from the discrete OSNR sweep for each input power level.

The ROSNR for both experimental and simulated traces is shown in figure 3.20. Good agreement between the proposed simulation model and experimental data is seen over the full dynamic range of received optical powers. For this receiver the dynamic range is -6 dB, defined for a 1 dB penalty in ROSNR, and the best performance is ROSNR 11 dB for -6 dBm received power.

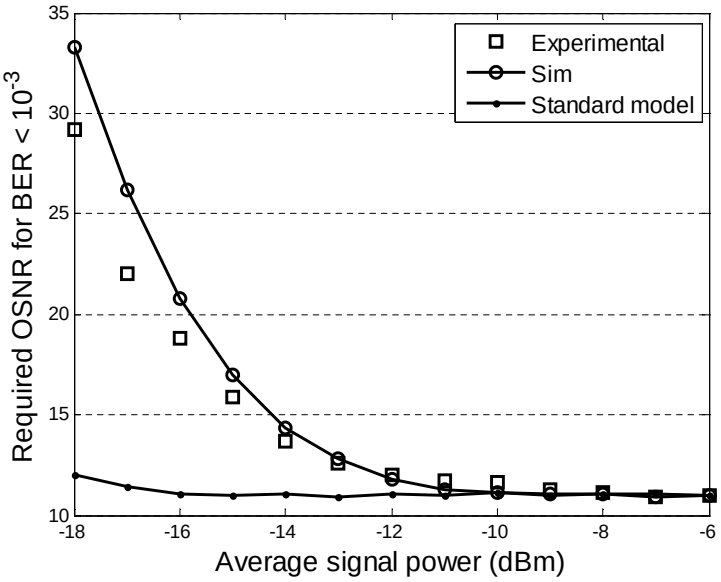

Figure 3.20: Required OSNR for a BER of 10^{-3} for both experimental (squares) and simulated data (circles for this work model and points for the digitiser additive uniform noise model).

For comparison, figure 3.20 also shows the results of a simulation where the standard quantiser noise model, which consists of substituting the quantiser with an additive uniform distributed noise [Marco and Neuhoff, 2005], is used. This model gives good agreement in the high input power region where the performance is limited by the photo-receiver noise but deviates markedly in the low power region where the digitiser thermal and quantisation noises dominate.

3.4 Influence of the network traffic model on packet-error rate

The use of optical burst switching requires components that are tolerant to variations in both power and network load. Moreover, the optical bit-stream could be completely interrupted for a long period of time in order to save energy. In section 3.2, a Digital Burst-Mode Receiver (DBMRx) was demonstrated and the packet error rate as a function of the header length and burst-to-burst power variations was measured. In this section, the impact that the network traffic pattern sparsity and the network load ρ have on the PER is investigated.

3.4.1 Experimental setup

The experimental set-up is shown in figure 3.21. The transmitter is composed of a laser with wavelength of 1551.7 nm and a standard Mach-Zehnder modulator. The bit rate is 10.709225 Gb/s, which corresponds to the ITU-T G.709 standard. A noise generator to control the OSNR before the receiver allows for the characterisation of the system by noise loading and direct error counting.

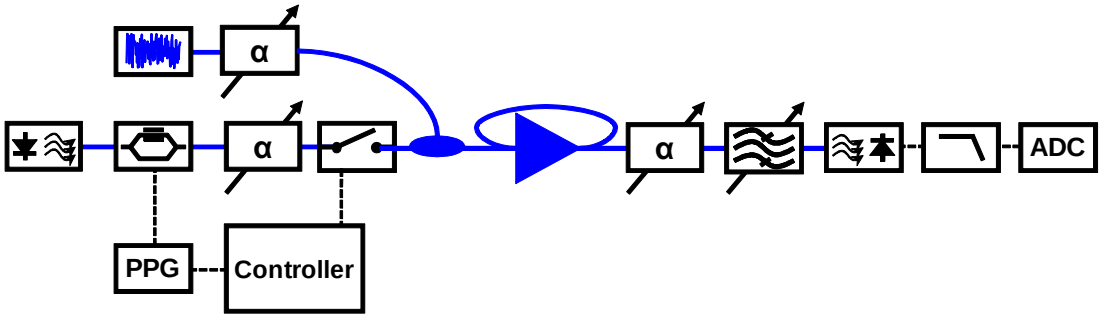

Figure 3.21: Experimental set-up for the generation of optical bursts and different network loads.

The Pulsed Pattern Generator (PPG) pattern consists of 8 burst frames and each of these frames can be independently turned ON or OFF with and Acousto-Optical Modulator (AOM) switch, enabling the independent generation of 8 different traffic loads with bursts of equal size. The AOM is controlled by a data generator, which has a different program for every traffic pattern under test. Figure 3.22 shows the structure of one burst frame. Each burst consists of a guard band of 272 bytes, a burst preamble slot of 32 bytes that can accommodate arbitrary size preambles ranging from 2 to 256 bits, a payload header of 4 bytes, 16072 payload bytes, and a 4 byte payload tail used to delineate the end of the burst. The guard band between frames allows for the much slower switching speed of the AOM and emulates the kind of switching speeds that might be expected with tunable laser based burst transmitters.

Figure 3.22: Burst frame composition.

In order to overcome the attenuation of the various optical components, a gain-clamped EDFA amplifier was used [Puttnam et al., 2008a]. The gain clamping was adjusted to minimise the transient effects. The receiver has a 30 GHz 3rd order Lorentzian optical filter, and a standard AC-coupled photodiode and TIA, followed by a 4th order low-pass Bessel electrical filter. Bursts are then asynchronously sampled with a Tektronix scope at 25 GS/s and an effective resolution of 6 bits.

The digital signal processing required in the DBMRx is currently implemented offline in MATLAB. In order to reliably determine the PER it is necessary to capture a large number of bursts so the data acquisition process is fully automated and each captured trace containing 16 burst slots is processed using a custom computer cluster solution—described in section 3.2—to analyse all the traces in an affordable time.

For a detailed description of the DBMRx implementation used in this experiment please refer to section 3.1.

3.4.2 Measurement methodology

In section 3.2, the impact of burst-to-burst power variations was studied with a set of continuous bursts, which is equivalent to a normalised network load of $\rho = 1$. In this section, all the bursts have a constant power of -6 dBm after the optical filter and the OSNR is kept constant to 11 dB to ensure a pBER that is better than 10^{-3}. Then, it is considered the more realistic scenario of varying the network load so that the gap band between bursts can be orders of magnitude longer than the guard band. An impact on the PER of the burst detector is therefore expected.

Figure 3.23 shows the two network traffic scenarios investigated. For both scenarios the network load in each case is exactly the same, and equal to the number of bursts divided by eight (not taking into account the effect on the network load of the burst frame guard band, which is negligible). However, the traffic sparsity is maximum for traffic scenario **A** and minimum for traffic scenario **B**. We used these two cases as the worst case scenarios for both approaches, the first minimising the base line wander effects arising from the 10 Gb/s AC-coupled receiver while the second maximises it.

For every traffic scenario [A1, A2, ..., A8, B1, ..., B8], 100 traces containing 2 full patterns each were acquired and processed. The threshold of the burst detector, which uses a correlator to detect the burst preamble and is the first stage of the DBMRx, was swept as the independent variable. The burst detector was implemented as a digital complex, phase agnostic correlator as detailed in section 3.1.2. The DBMRx

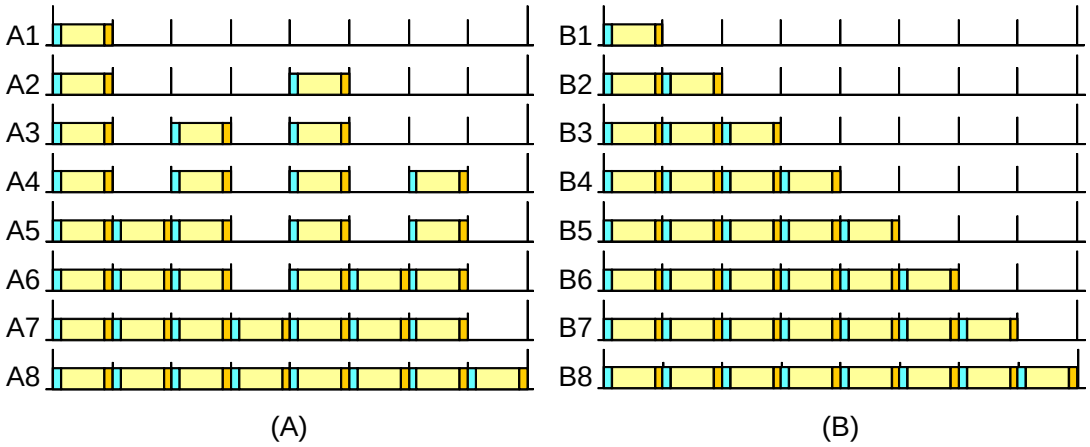

Figure 3.23: Experimental optical burst patterns used. (A) Eight network loads with maximum burst sparsity. (B) Eight network loads with minimum burst sparsity.

implementation complies with the following protocol

1. A burst is considered correctly received for PER statistics if **both** the complex, phase-agnostic correlator and the digital payload header correlator are triggered.

2. If the complex correlator is triggered but the payload header is not found in the next $1,000$ bit period, then the receiver resets.

3. If the payload header is found, the burst detector is reseted after a timeout equal to the payload length and tail length in bits.

After the offline cluster processing of the experimental data, standard statistics by error counting were applied to get the PER probability [Jeruchim, 1984]. An average of 30 computers completed the job in about 22 hours.

3.4.3 Results and discussion

This section reports the measured PER for every traffic scenario analysed. Figure 3.24 shows a plot for every traffic load with equal traffic load but different sparsity as a function of the burst detector threshold. Points not shown in this graph indicate that no burst errors were counted over the measurement period.

If the normalised threshold is greater than 0.015, such that the burst detector is not continuously triggered by noise floor, then the PER in each scenario is very similar indicating that there is almost no impact due to traffic model sparsity on PER. In addition, for traffic scenarios A1, B1, and A2 no burst detection errors were counted in almost the entire threshold range. Interestingly, for the analysed conditions described in the previous section, reducing the network load does not degrade the packet detection performance and that the fully loaded network scenario provides the lower bound on network performance in terms of PER.

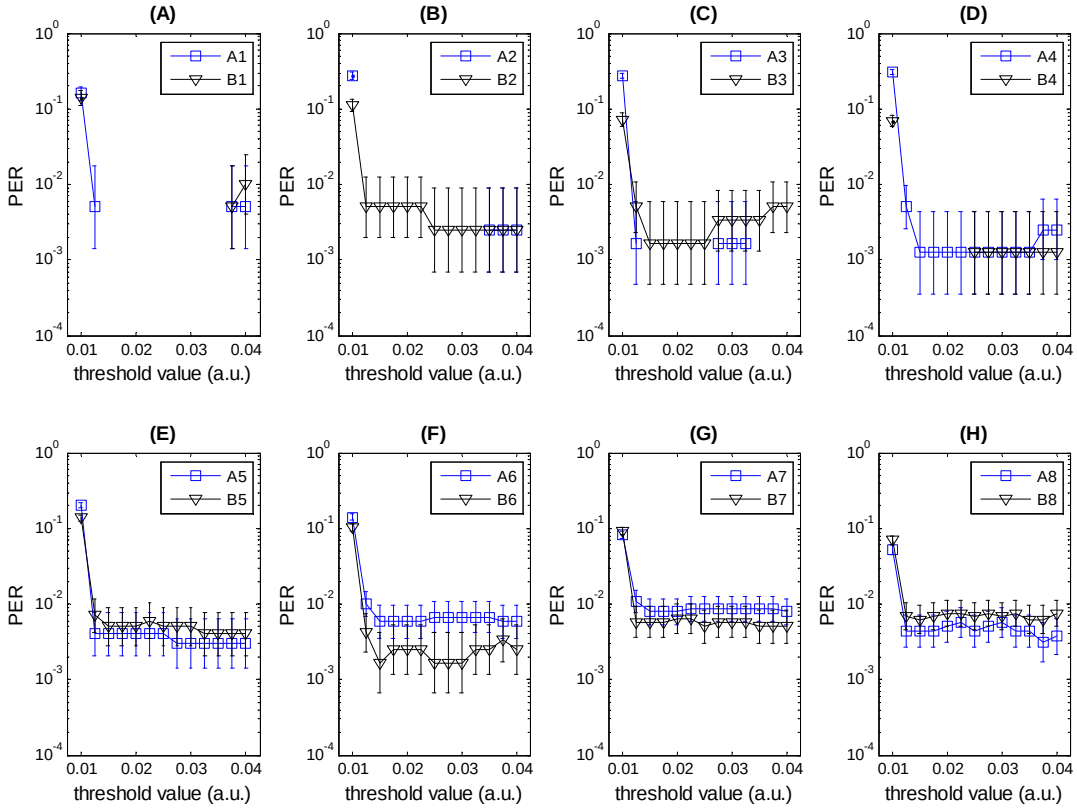

Figure 3.24: Packet Error Rate against complex correlator threshold for every of the 8 different traffic loads. (A) Traffic Models (TM) A1 and B1, (B) TM A2 and B2, (C) TM A3 and B3, (D) TM A4 and B4, (E) TM A5 and B5, (F) TM A6 and B6, (G) TM A7 and B7, (H) TM A8 and B8.

3.5 Chapter summary

This chapter investigated the performance of a digital burst-mode receiver, suitable for OBS and PON applications.

The performance of digital signal processing in a 10.705 Gb/s burst-mode receiver to both detect the burst and to recover the signal timing and data from bursts that exhibit burst-to-burst power variations was analysed in terms of both PER and pBER. It was found that over the 7 dB dynamic range defined by a 1 dB penalty in the ROSNR for a FEC "error-free" data pBER of 10^{-3}, the PER arising from failure to detect an incoming burst could be easily tuned by increasing the number of bits in the burst header, in a receiver configuration dominated by noise arising from optical amplification. To ensure that this does not have an adverse impact on the upper layers in and OBS system this PER should be less than the packet loss arising from contention which ranges from 10^{-1} to 10^{-5}. In this receiver, a preamble length of 64 bits, of which 32 are used for burst detection purposes, was enough to ensure that the PER is below 10^{-2}.

Section 3.3 investigated a high speed ADC that is typically used in current state-of-the-art high bit-rate lightwave communication receiver experiments, and the main

parameters of the receiver chain were extracted to develop a realistic model for simulation purposes. For this particular digitiser, the electrical noise ($N_{\text{scope}} = 5.6492 \times 10^{-7}$ W/GHz) of the digitiser front-end is the main source of signal degradation, particularly for low power signals. It is also important to operate with the optimum vertical scale to obtain the best performance. The model was further verified for a complete NRZ receiver, and comparison between both experiment and the developed model shows good agreement. Including the often neglected noise contribution of the digitiser will be particularly important when developing systems that require a large dynamic range such as burst-mode receivers.

Finally, section 3.4 reported the performance of a digital burst-mode receiver under several network load conditions. For every network load, the burst sparsity was also considered. The results show that the sparsity has negligible effects on the receiver performance in terms of PER. In addition, and contrarily to what might be expected, it is found that reducing the network load ρ does not reduce the packet detector performance.

4

Digital multi line-rate burst-mode receivers for optical access networks

THIS CHAPTER FOCUSES on optical access networks, i.e., optical networks intended to be deployed locally from the Internet provider office to the customer premises. In order to keep costs low, optical access networks are passive and do not have optical amplification. Therefore, they are referred as PONs. It is clear that reach in PONs is mainly limited by electrical noise arising at the receiver, splitting losses (and less significantly fibre losses), and fibre chromatic dispersion.

One kind of PON already deployed is Ethernet Passive Optical Network (EPON), at a line-rate of 1 Gb/s. However, to tackle the increasing bandwidth demand of access networks, 10G-EPON, with a line-rate of 10 Gb/s, has been recently standardised [Tanaka et al., 2010]. From an upgrade and cost point of view, such networks will need to support 10 Gb/s and lower line-rates concurrently. This can be achieved in the downstream direction by using separated wavelength bands. However, in the upstream direction a burst-mode receiver capable of receiving multiple line-rates will be essential to terminate both 10 Gb/s and legacy users at the central office. In current PONs, analog burst-mode receivers are typically used [Ossieur et al., 2009; Sugawa et al., 2010], however, these do not readily lend themselves to multi-rate operation. [Nakagawa et al., 2010a] recently demonstrated a multi-rate receiver that uses two separate electrical front-ends for 10 and 1.25 Gb/s and employs 8× oversampling for burst-mode clock recovery.

In this chapter, a complete digital dual-rate burst-mode receiver is designed and experimentally demonstrated. This receiver uses a DC-coupled PIN front-end, followed by a digitiser that samples the signal at the Nyquist rate for 10 Gb/s, and performs all the burst-mode clock and data recovery in the digital domain. This architecture has the advantage that the required sampling rate of the ADC is only 20 GS/s rather than the 80 GS/s required in [Nakagawa et al., 2010a]. Additionally, the receiver employs clipping of the signal in the high power operating regime to increase the dynamic range of the receiver.

This chapter is organised as follows. Section 4.1 introduces the reader to PONs and its principal standards, and defines the physical layer requirements of burst-mode receivers for such networks. Then, section 4.2 briefly outlines the architecture of the digital receiver investigated in this chapter. The multi-rate packet and line-rate detector operation principle is described in detail in section 4.3. The following two sections investigate two algorithms for CDR and validate their performance with simulation modelling and experimentally. The full design of the dual-rate burst-mode receiver is then presented in detail in section 4.6 and it is experimentally characterised in terms of both pBER and PER in the next section. Finally, this chapter has a brief conclusion in section 4.8.

4.1 Optical access networks

This section briefly introduces the concept of optical fibre access networks, introduces some terminology associated with them, describes the physical layer impairments of this kind of networks, and outlines the standardised physical layer requirements.

4.1.1 Optical access networks standards and architecture

Optical access technologies are referred in the literature as Fibre to the Node, Curb, Building, or Home (FTTX). The several words that stand for the **X** in this acronym refer to the place or device where the optical signal in the access network is converted to the electrical domain. Another characteristic of optical access networks is the use or lack of optical amplification. The former case is known as Active Optical Network (AON) and the latter case as PON. In addition, considering the topology, optical access networks can be categorised into two kinds: point-to-point topology and point-to-multipoint topology [Effenberger and El-Bawab, 2009]. Figure 4.1 shows and illustration of both topologies.

There are two principal PON family of standards. The first one, standardised by the International Telecommunication Union (ITU), define the standards B-PON and G-PON. B-PON uses fixed-size ATM cells as data-link layer protocol. G-PON,

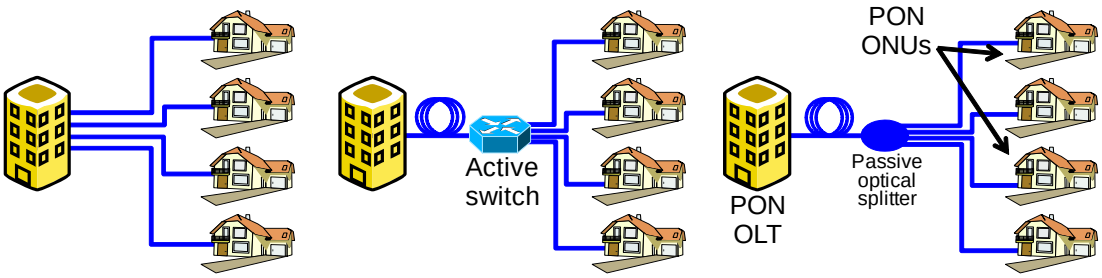

Figure 4.1: An illustration of the FTTX more common network topologies [Tanaka et al., 2010]. From left to right: (A) point-to-point, (B) point-to-multipoint curb-switched, and (C) point-to-multipoint PON.

which is an evolution of B-PON, increases the line-rate and uses G-PON Encapsulation Method (GEM) as data-link layer protocol, which allows the encapsulation of protocols such as Ethernet, IP, or Point-to-Point Protocol (PPP). The second family has been standardised by the Institute of Electrical and Electronics Engineers (IEEE), defining the standard EPON and 10G-EPON, and their main characteristic is the use of Ethernet as data-link protocol. Aside from this difference, both standards use the same wavelength allocation: 1490 nm for downstream binary data, 1550 nm for downstream analog video, and 1310 nm for upstream data, voice, or video [Green, 2006]. Table 4.1 summarises the downstream and upstream rates and MAC protocol of the most currently deployed PON standards [Green, 2006; Effenberger and El-Bawab, 2009; Tanaka et al., 2010].

Table 4.1: Common FTTX standards main characteristics.

	B-PON	G-PON	1G-EPON	10G-EPON
Standard	G.983	G.984	802.3AH	802.3AV
Down rate	155.52 Mb/s 622.08 Mb/s	1.244 Gb/s 2.488 Gb/s	1.25 Gb/s	10 Gb/s
Up rate	155.52 Mb/s	0.155 Gb/s 0.622 Gb/s 1.244 Gb/s 2.488 Gb/s	1.25 Gb/s	10 Gb.s 1.25 Gb/s
MAC protocol	ATM	GEM	Ethernet	Ethernet

All of the standards of table 4.1 correspond to passive networks. The two main traits of a PON are the shared optical channel, implemented with a passive combiner/splitter, and the absence of optical amplification. Thus, these networks are cost affordable and also power efficient. In addition, due to the lack of optical amplification, it is clear that the most important physical layer impairments that dominate PONs are, namely, **splitting losses** and **dispersion**. Thus, the OSNR of the system will be high and the receiver thermal noise or shot noise is the main issue depending if a PIN

photodiode or APD is used at the receiver, respectively.

Although not stated in table 4.1, all current PON standards make use of NRZ modulation. Optical transmitters need to be cheap, and so direct modulation is preferred—particularly for transmitters located at the customer's premises. Consequently, modulation formats are limited to amplitude modulated formats. Whilst in principle multiple amplitude levels could be used, the cheap transmitter drive electronics are digital which limits the modulation to two level OOK formats.

Technical terms associated with PONs

The optical transceiver located at the service provider premises is known as OLT, and its counterpart located at the customer premises is named ONU. **Downstream traffic** is defined as the network traffic from the service provider to the customer, and **upstream traffic** is the traffic originated in the customer to the service provider. In the context of access optical networks, the term "packet" if preferred over "burst". However, the term burst is used to refer to burst-mode receivers.

4.1.2 Optical access networks standards and physical layer

The PON standards, cited in table 4.1, define a series of physical layer requirements that transmitters and receivers must comply with. Table 4.2 summarises the main physical layer requirements and table 4.3 summarises the upstream/downstream line-rate, launch power, sensitivity, and receiver maximum allowed power (also referred as overload or overshoot point) [Green, 2006; Tanaka et al., 2010].

Table 4.2: Physical layer requirements of the most common FTTX standards.

	B-PON B	B-PON C	G-PON A	G-PON B	G-PON C	1G-EPON	10G-EPON
Fibre splits	≤ 32	≤ 32	≤ 64	≤ 64	≤ 64	≤ 16	≤ 16 (PR10, PR20) ≤ 32 (PR20, PR30)
Max. distance	20 km	20 km	20 km (DFB) 10 km (FP)	20 km (DFB) 20 km (FP)	20 km (DFB) 20 km (FP)	10 km (PR10) 20 km (PR20)	10 km (PR10) 20 km (PR20) 30 km (PR30)
Attenuation Up	10 to 25 dB	15 to 30 dB	5 to 20 dB	10 to 25 dB	15 to 30 dB	5 to 20 dB (10 km) 10 to 24 dB (20 km)	5 to 20 dB (PR10) 10 to 24 dB (PR20) 15 to 29 dB (PR30)
Attenuation Down	10 to 25 dB	15 to 30 dB	5 to 20 dB	10 to 25 dB	15 to 30 dB	5 to 20 dB (10 km) 10 to 23.5 dB (20 km)	5 to 20 dB (PR10) 10 to 24 dB (PR20) 15 to 29 dB (PR30)
BER Ex. ratio	$< 10^{-10}$ > 10 dB	$< 10^{-10}$ > 10 dB	$< 10^{-10}$ > 10 dB	$< 10^{-10}$ > 10 dB	$< 10^{-10}$ > 10 dB	$< 10^{-12}$ > 6 dB	$< 10^{-3}$ > 9 dB

The need for an upstream burst-mode transmission channel

The transmission from the OLT to the ONU is point-to-multipoint (multicast) and, thus, a continuous-mode bit stream is employed to simplify the design of the optical receiver. The burst-mode receiver requirement arises in the upstream channel. Although the

Table 4.3: Physical layer upstream/downstream line-rate, launch power, sensitivity, and receiver overshoot requirements of the most common FTTX standards.

	Down	Up	Down L_p	Down sens	Down over	Up L_p	Up sens	Up over
B-PON B	622 Mb/s	622 Mb/s	−2 to +4 dBm	−28 dBm	−6 dBm	—	−30 dBm	−8 dBm
B-PON C	622 Mb/s	622 Mb/s	−2 to +4 dBm	−33 dBm	−11 dBm	—	−33 dBm	−11 dBm
G-PON A	1.244 Gb/s	1.244 Gb/s	−4 to +1 dBm	−25 dBm	−4 dBm	−3 to +2	−24 dBm	−3 dBm
G-PON A	2.488 Gb/s	1.244 Gb/s	0 to +4 dBm	−21 dBm	−1 dBm	−3 to +2	−24 dBm	−3 dBm
G-PON B	1.244 Gb/s	1.244 Gb/s	+1 to +6 dBm	−25 dBm	−4 dBm	−3 to +3	−28 dBm	−7 dBm
G-PON B	2.488 Gb/s	1.244 Gb/s	+5 to +9 dBm	−21 dBm	−1 dBm	−3 to +3	−28 dBm	−7 dBm
G-PON C	1.244 Gb/s	1.244 Gb/s	+5 to +9 dBm	−26 dBm	−4 dBm	+2 to +7	−29 dBm	−8 dBm
G-PON C	2.488 Gb/s	1.244 Gb/s	+3 to +7 dBm	−28 dBm	−8 dBm	+2 to +7	−29 dBm	−8 dBm
1G-EPON PX10	1.25 Gb/s	1.25 Gb/s	−3 to +2 dBm	−24 dBm	+4 dBm	−1 to +4	−24 dBm	+2 dBm
1G-EPON PX20	1.25 Gb/s	1.25 Gb/s	+2 to +7 dBm	−27 dBm	+4 dBm	−1 to +4	−24 dBm	+7 dBm
10G-EPON PR10	10 Gb/s	10 Gb/s	+2 to +5 dBm	−20.5 dBm	+1 dBm	−1 to +4	−24 dBm	0 dBm
10G-EPON PR20	10 Gb/s	10 Gb/s	+5 to +9 dBm	−20.5 dBm	+1 dBm	−1 to +4	−28 dBm	−5 dBm
10G-EPON PR30	10 Gb/s	10 Gb/s	+2 to +5 dBm	−28.5 dBm	−9 dBm	+4 to +9	−28 dBm	−5 dBm

optical transmission path from the ONU to the OLT is point-to-point, the presence of the passive optical splitter makes this path shared among all the ONUs, and optical packet collisions will happen at the OLT unless a TDMA protocol is used [Tanaka et al., 2010]. As a consequence, a burst-mode receiver is required in the OLT premises for the upstream, which is a cost-effective solution because the number of OLTs is smaller than the number of ONUs and also the OLT cost is shared among all the passive optical network segment subscribers.

The transmission characteristics and wavelengths for the PON standards are as follows: G-PON has a continuous-mode downlink channel in the band from 1480 to 1500 nm, which carries Time Division Multiplexing (TDM) data, and a burst-mode transmission in the 1310 nm range for the upstream [Qiu et al., 2004]. 10G-EPON (in coexistence mode) uses a continuous-mode downstream link in the range 1490 nm for 1 Gb/s and the 1580 nm for 10 Gb/s, and a upstream burst-mode link in 1310 nm and 1270 nm for 1 Gb/s and 10 Gb/s, respectively [Tanaka et al., 2010].

Upstream burst-mode physical layer requirements for EPON

For 10G-EPON, the power budget of the system can be calculated using table 4.3 and the following equation

$$P_b = L_p^{\min} - S + M \tag{4.1}$$

where P_b is the power budget in dB, $L_p^{\min}$ is the minimum launch power in dBm, S is the receiver sensitivity in dBm, and M is a transmitter and dispersion penalty which equals to 3 dB in the upstream and 2.5, 1.5, and 1.5 in the downstream for PR10, PR20, and PR30 transmission classes, respectively [Tanaka et al., 2010]. The burst-to-burst maximum dynamic range is thus equal to the power budget P_b, and corresponds to 23, 27, and 32 dB with receiver sensitivities of −24 dBm, −28 dBm, and −28 dBm, for

upstream PR10, PR20, and PR30 classes, respectively [Tanaka et al., 2010].

4.2 Digital multi line-rate burst-mode receiver outline

This section deals with the design of a digital, multi line-rate capable, burst-mode receiver suitable for multiple line-rate coexistence in optical access networks. Such burst-mode receiver must tackle the following problems:

1. **Burst detection**: the ability to detect an incoming packet when it arrives.
2. **Line-rate detection**: the ability to detect the line-rate of an incoming packet.
3. **Amplitude equalisation**: because of the different distance and splitting losses of the transmitters, every optical packet is of an unknown amplitude. The receiver should estimate this amplitude and compensate it among different packets.
4. **Clock recovery**: every packet is generated at a different transmitter with an unknown reference clock. The burst-mode receiver should lock to the incoming optical packet clock rapidly on a packet-by-packet basis.
5. **Data recovery**: binary symbols should be extracted from the received electrical signal, comparing this signal against a threshold.

Burst-mode receivers can be realised in the analog domain, that is, using analog electronic components, or in the digital domain. Owing to the advent of fast ADCs, capable of sampling signals at a rate suitable for optical line-rates, all the enumerated functions above can be carried out in the digital domain. In this thesis, the focus is on the digital approach.

Figure 4.2 shows a diagram of a generic multi-rate burst-mode receiver, located in the OLT at the central office. The diagram depicts a PON network with clients transmitting upstream traffic at 10 and 1 Gb/s. An optical passive splitter distributes the optical signal in the downstream direction (from OLT to ONU) and combines it in the upstream direction (from ONU to OLT). The optical fibre before/after the splitter can have an arbitrary length, providing that the standard power budget is met.

The generic multi-rate burst-mode receiver is composed of two mains subsystems:

- **An optical/electrical front-end**. The digital receiver optical front-end consists of a DC-coupled PIN photodiode with integrated TIA and is followed by a digitiser. There is no electrical filtering between the TIA and the digitiser to maintain the maximum signal bandwidth and so to minimise the penalty introduced by signal clipping at high input powers.

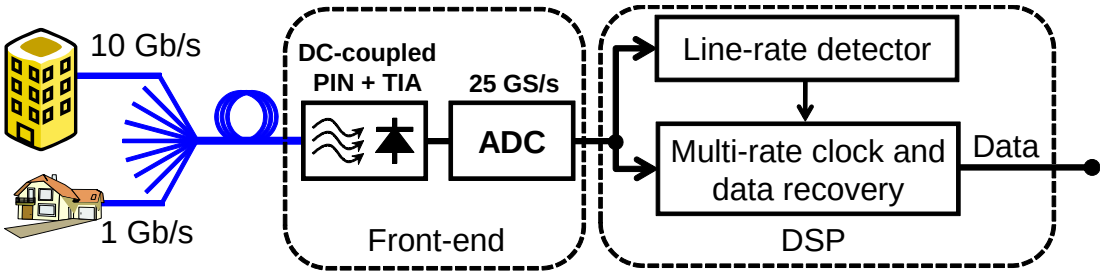

Figure 4.2: General diagram of a digital multi line-rate burst-mode receiver.

- **DSP line-rate detection and multi-rate CDR**. The two principal functions a digital multi-rate receiver must carry out are, firstly, detect both the presence and the line-rate of incoming optical packets, and secondly, perform clock and data recovery (and possibly other impairment mitigation such as correcting for BLW).

In this work, the digitiser used was a Tektronix DPO 72004 real-time sampling oscilloscope. This digitiser provides an 8-bit output with an effective number of bits between 4 and 5. The first DSP step was to precondition the captured signal by ideally resampling from the scope imposed sampling rate of 25 GS/s to 20 GS/s (the Nyquist rate at 10 Gb/s). However, in an actual hardware implementation the ADC will sample the electrical signal from the photodiode asynchronously at 20 GS/s.

4.3 Packet and line-rate detection operating principle

It was shown in chapter 3 that optical bursts can be detected, for a given line-rate, with a MF and an appropriate burst preamble. The matched filter output is compared against a threshold λ and a burst is detected if the output of the MF is bigger than this threshold value. In this section, the problem at hand is to reliably detect both the presence and the line-rate (belonging to a set of predefined line-rates) of the incoming optical bursts in the context of a packetised passive optical access network. In other words, given an available number of burst preamble bits, N, which should be minimised, and a set of line-rates, $R = \{R_1, R_2, \ldots, R_K\}$, the problem is to find $K = \text{card}(R)$ different bit preambles which maximise the MF output for the matched line-rate and minimise the matched filter output of the non-matched line-rates. For simplicity, only three line-rates will be considered here: 10, 2.5, and 1.25 Gb/s, and will be denoted R_{10}, $R_{2.5}$, and $R_{1.25}$, respectively.

From a signal-energy point of view, if the spectrum of every of the K preambles is orthogonal to each other—that is, the spectra of the different R_n preambles does not overlap in the frequency domain—then the orthogonality condition at the output of the MF stated in the previous paragraph is met. Thus, the most straightforward solution is

to choose the set of preambles R_n such that every single preamble generates one and only one spectral tone, and also every tone frequency is different for every preamble in the set R_n. This approach has the advantage that, for every given preamble belonging to R_n, all the signal energy is concentrated into a single frequency, and so the MF becomes a narrow filter that can eliminate the noise in all other non-interesting frequencies and, thus, improve the accuracy of the detector in the presence of uncorrelated additive noise. The reader is referred to section 3.1.2 for more theoretical background about this subject.

It is well known that in NRZ modulation, a `1010 ...` preamble has a spectrum that approximates that of a single tone at half the line-rate. This can be combined with the property that line-rates typically increase in a power of two basis. Consequently, a preamble of the form `1010 ...`, independently of the line-rate and providing that the line-rates are integer multiples of each other, meets the orthogonality condition stated above. To illustrate this condition, figure 4.3 shows the simulated electrical trace of three preambles, each having the same energy and 32, 8, and 4 bits at 10, 2.5, and 1.25 Gb/s, respectively. On the right is a plot the electrical spectrum of these signals. We observe from this spectral plot that the orthogonality condition is met, as pointed by the vertical pink lines that indicate a frequency of half the line-rate.

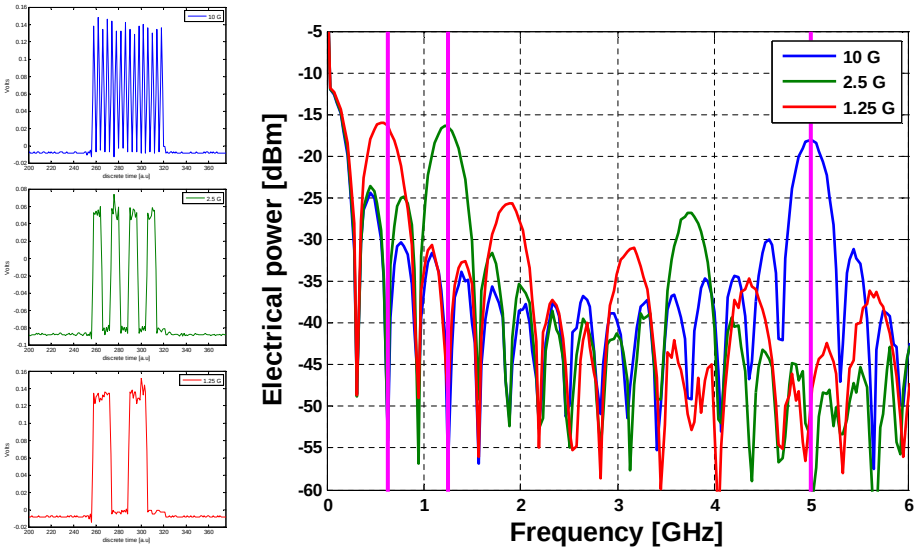

Figure 4.3: Simulation of the electrical spectrum of the packet preamble for 10, 2.5, and 1.25 Gb/s line-rates.

4.3.1 Line-rate detector description

In the previous section it was shown that with a `1010 ...` preamble of equal temporal duration, a number K of NRZ modulated signals whose line-rates are a sequence of multiple integer numbers can be detected with an appropriate bank of MFs, each matched

to a frequency equal to half of the line-rate. This section proposes a digital implementation based on the aforementioned operating principle.

Matched filter array

The block diagram of the proposed multi-rate packet and line-rate detector is depicted in figure 4.4. The signal $s[n]$ is the discrete sampled version of the electrical continuous signal at the output of the TIA, $s(t)$, and it is fed to a bank of complex, discrete MFs. It is assumed that $s(t)$ is sampled at twice the Nyquist rate of the highest line-rate to be detected. For example, if $R_1 = 10$ Gb/s, $R_2 = 5$ Gb/s, $R_3 = 2.5$ Gb/s, ..., then $s(t)$ is sampled at a frequency $f_N = 2 \times R_1$, in this particular case $f_N = 20$ GS/s. Thus, the spectrum of $s[n]$ contains frequencies in the range from 0 to 10 GHz (one-sided bandwidth), independently of the line-rate of the optical received signal. The outputs of this array of matched filters consists of K signals which are fed into an array of thresholders.

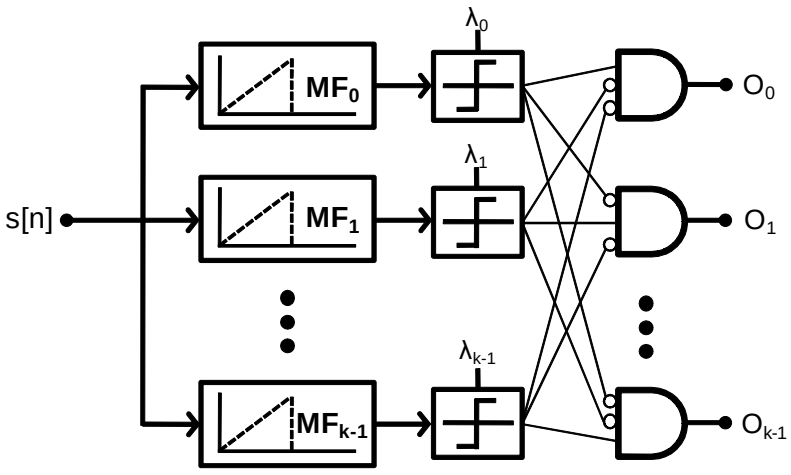

Figure 4.4: Generic structure of a packet presence and line-rate detector.

Every matched filter MF_n in figure 4.4 is a complex correlator tuned to half the line-rate targeted by that MF. As stated in section 3.1.2, the tap coefficients for every matched filter are given by equation 3.6, where the discrete frequency index k can be obtained from equation 3.7 for a given number of preamble bits N.

Figure 4.5 shows the MF output statistics of the 10 Gb/s matched filter when 10, 5, and 1.25 Gb/s optical packets are input, with -19 dBm, -4 dBm, and -4 dBm received power, respectively. The orthogonality property (output maximisation for the matched packet and output minimisation for unmatched packets) is shown there and pointed by the yellow arrow, and allows for some threshold margin (the optimum threshold for this MF lies in the space pointed by the arrow). This margin enables increasing the dynamic range of operation of the line-rate detector, which is one of the core requirements of a multi-rate burst-mode receiver.

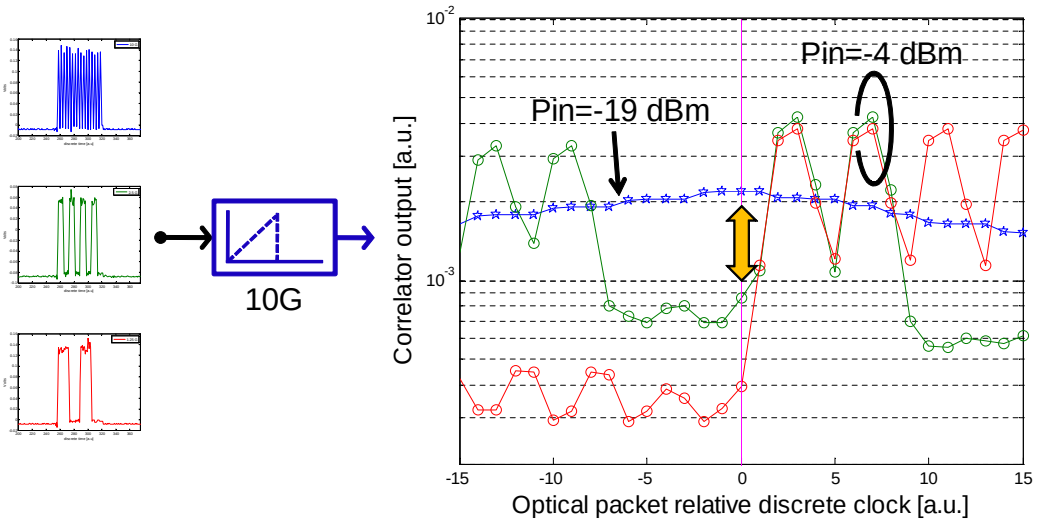

Figure 4.5: 10 Gb/s matched filter output statistics in the presence of 10, 5 and 1.25 Gb/s packets, for received optical powers of −4 dBm (5 and 1.25 Gb/s) and −19 dBm (10 Gb/s).

Threshold comparison and combinational logic

The K matched filter output signals are fed into an array of comparators. The output of each comparator is a digital signal, with values either `1` or `0`. An array of K thresholds, denoted $\lambda_0, \ldots, \lambda_{K-1}$, is thus required for the this bank of comparators. The problem of finding an optimum value for this set of thresholds will be tackled experimentally in section 4.7.

The array of digital signals after the comparators is fed into a combinational logic block, composed of a set of K K-input `AND` gates. A generic output of one of this `AND` gates, O_n, has a logical function of the form,

$$O_n = \overline{\mathrm{MF}_0} \cap \ldots \cap \mathrm{MF}_n \cap \ldots \cap \overline{\mathrm{MF}_{K-1}} \tag{4.2}$$

and so, output O_n is high if, and only if, the MF number n is over the corresponding threshold λ_n value, and all of the other MFs are below their respective thresholds values. This approach has the advantage that only one of the outputs can be in a `1` state at any instant of time, and also exploits the orthogonality property of the `1010` ... preamble described above. This is illustrated in figure 4.6, which shows the output of the 10, 5 and 1.25 Gb/s MFs when a 10 Gb/s packet is input, for received powers of −4 and −19 dBm. The yellow arrow points to the location where the optimum thresholds should lie, and clearly the orthogonality principle—exploited by the combinational logic—holds for a broad dynamic range of input powers.

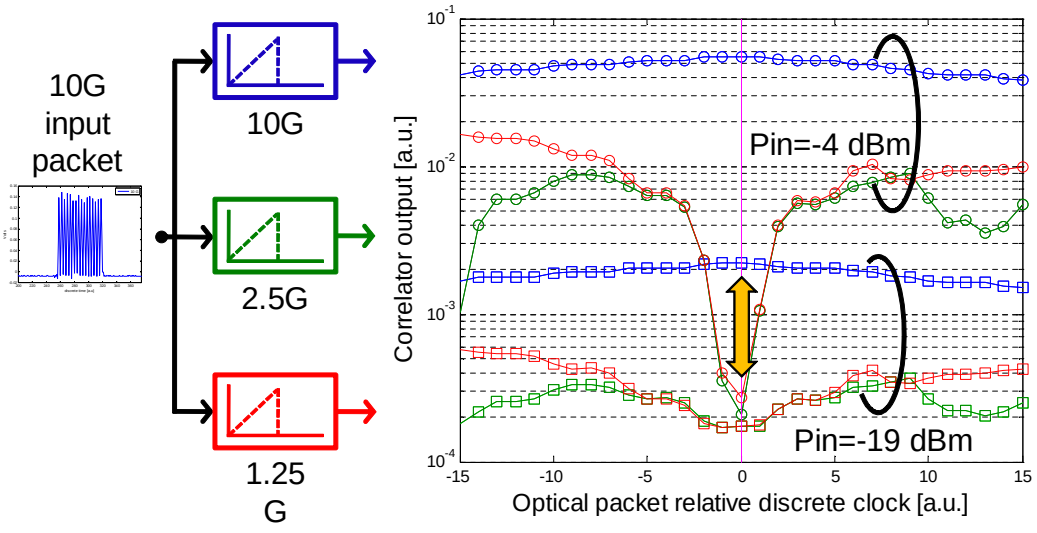

Figure 4.6: Matched filter output statistics in the presence of a 10 Gb/s packet, for received optical powers of -4 dBm and -19 dBm.

4.4 Multi-rate clock-and-data recovery algorithms

In this section, two multi-rate CDR algorithms are presented and described in detail. The performance of these two algorithms will be analysed in the next section.

4.4.1 Multi-fractional equaliser

The first algorithm considered for multi-rate CDR realisation was a decision-directed, feed-backward, variable-length, LMS equaliser. The idea behind this algorithm is to use a fractionally-spaced equaliser that works at 2 samples-per-bit for the highest line-rate, R_1, 4 samples-per-bit for R_2, 8 samples-per-bit for R_3, and so on, under the assumption that the received signal $s(t)$ is sampled at a rate $f_s = 2 \times R_1$, and also the line-rates are such that $R_1 = 2 \times R_2 = 4 \times R_3 = \ldots = 2^{K-1} R_K$

A complete multi-fractional CDR is depicted in figure 4.7. This CDR approach first filters the incoming signal $s[n]$ with an adaptive filter whose response is $h[n]$. An initialisation algorithm initialises the filter response after a packet is detected to a sensible value to ensure fast LMS convergence. The output of the filter is then sliced, and the sliced value is used as the *desired value* to update the $h[n]$ taps using the LMS algorithm. Each of these blocks will be explained with more detail next.

LMS fractional equaliser description

The incoming signal $s[n]$ is processed with a fractionally-spaced equaliser with discrete impulse response $h[n]$. As mentioned in the introduction, the length of the filter $h[n]$ is varied according to the detected line-rate of the incoming optical packet. Let's define

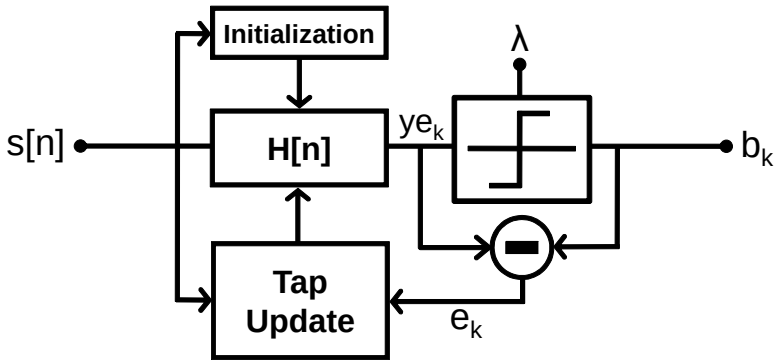

Figure 4.7: Diagram of a multi-fractional clock and data recovery, consisting of a variable-length LMS equaliser followed by a slicer.

the **decimation factor** d_F as the quotient of the number of samples per bit at the current line-rate over the number of samples per bit at the highest line-rate, to which the sampling frequency is related. Since the highest line-rate has 2 samples-per-bit, the decimation factor is $d_F = 4$ for 2.5 Gb/s and $d_F = 8$ for 1.25 Gb/s. Let's also define the number of equalised bits, L, as the total number of filtered bits, independently of the line-rate. In the equaliser analysed in this chapter I chose $L = 3$. The total number of taps of the filter $h[n]$ is thus $L_T = L \times d_F$, and corresponds to 6, 24, and 48 taps for 10, 2.5, and 1.25 Gb/s line-rates, respectively. The linear filter $h[n]$ is executed every d_F incoming samples. In consequence, the output of the filter is at the baud rate.

If the equaliser is properly initialised and the signal $s[n]$ is DC-offset and amplitude normalised before filtering—using the algorithm described in section 3.1.4, for example—it is expected that the output is roughly in a $[1,-1]$ binary space. However, because of signal noise, the output at instant k, that is, y_k, will be a random variable with mean $\mu_k = \pm 1$ and variance σ_k^2. Thus, the slicer has an optimum threshold $\lambda = 0$, and the output will be a deterministic number with value $a_k = \pm 1$. In order to apply the theory of LMS filtering, a *desired value* of the filtered signal is required. Here, the desired value is the output of the bit slicer. Thus, the error signal $e_k = a_k - ye_k$ is computed and the LMS algorithm, defined as the recursive equation [Haykin, 2002, p. 236],

$$\mathbf{h}[k+1] = \mathbf{h}[k] + \mu \mathbf{s}[k] e[k] \tag{4.3}$$

where μ is known as the **step-size** parameter, applied to update the filter taps.

Equaliser initial value

Burst-mode receivers should be able to cope with optical packets coming from different sources, each packet having a different transmitter clock. Moreover, sampling is done asynchronously with respect to the $s(t)$ signal clock. In order for the multi-fractional

CDR algorithm to work properly and converge quickly, it is of paramount importance to correctly initialise the filter first value, h_0, so that the filter/equaliser compensates for the optical packet fractional delay and converges quickly to the optimum solution.

The algorithm used for the filter initialisation, for $L = 3$ bits and 10 Gb/s, is as follows

1. Compute the fractional delay μ_k of the optical packet, using a 2 samples-per-bit algorithm [Lee, 2002; Wang et al., 2003; Zhu et al., 2005]. Let's assume that μ_k is normalised into a $[-1,1]$ space, corresponding -1 to a timing delay of -2π rad and 1 to a timing delay of 2π rad.

2. The fractionally spaced equaliser can be considered as a 2 samples-per-bit linear Gardner interpolator for the central bit of the 6-tap equaliser. Thus, the interpolation coefficients can be calculated as indicated in [Gardner, 1993].

The following equation shows the initialisation explained above,

$$\mathbf{h}_0 = [\ \underbrace{0\quad 0}_{\text{bit } n-1}\quad \overbrace{\mu_k\quad (1-\mu_k)}^{\text{bit } n}\quad \underbrace{0\quad 0}_{\text{bit } n+1}\ ] \tag{4.4}$$

For line-rates where the number of taps per bit is ≥ 4, an approximation is used. With the knowledge of the fractional delay μ_k, the tap closer to the bit center is set to 1, and all the other initial taps of the filter are set to 0.

In this work it is assumed—and verified experimentally—that the frequency drift between the transmitter clock and the sampling clock is small enough to consider that the time delay μ_k across the entire optical packet is constant or it varies very slowly, not deviating more than 10% from its initial value during the optical packet. This approximately corresponds to a beat frequency[1] of 124.5 KHz, or $80,320$ bits (referred to 10 Gb/s). However, the 10 GE-PON standard defines a bit-rate variation of ± 100 ppm [Terada et al., 2008], which corresponds with a beating frequency of 2 MHz. Theoretically, the LMS equaliser is able to adapt to a varying μ_k, providing that the equaliser length N is long enough to accommodate the clock deviations, although this was not investigated in this thesis. Consequently, the equaliser needs 2 taps (which represent one bit) for every $5,000$ payload bits in order to accommodate the worst-case scenario frequency drift defined by the 10 GE-PON standard.

4.4.2 Polyphase equaliser/interpolator

The second multi-rate CDR algorithm considered works at two samples-per-bit independently of the received signal line-rate.

[1] the beat frequency is the absolute value of the difference of the frequency of the transmitter and the sampling frequency of the receiver digitiser

A complete CDR implementation of the polyphase algorithm is shown in figure 4.8. Once the line-rate of the signal is known, the discrete signal $s[n]$ is decimated by means of a low-pass anti-aliasing filter followed by a decimator [Oppenheim et al., 1996]. Then, the signal is interpolated to compensate for the random optical burst fractional delay μ_k. The interpolator can also be used to compensate for the frequency offset between the transmitter clock and the digitiser clock, using a DPLL as described in [Gardner, 1993]. However, in this work this frequency drift is much less than the packet duration and thus the packet clock offset can be estimated only once at the beginning of the packet, which leads to a much simpler DSP algorithm. Then, the DC-offset and amplitude are estimated to normalise the interpolated signal into a $[1,-1]$ space. Finally, a slicer (with threshold $\lambda = 0$) obtains the bit symbols. Additionally, a BLW compensator filter and/or a variable thresholder can be used in this approach, as described in section 3.1.4.

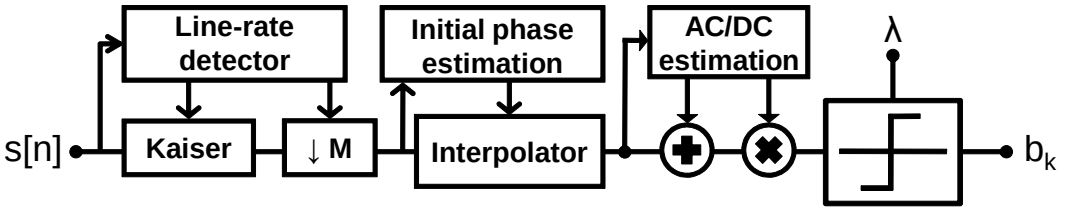

Figure 4.8: Architectural components of a multi-rate polyphase clock and data recovery system, consisting of a programmable decimator, interpolator, normaliser, and slicer.

Because this approach is similar to the one explained in chapter 3 (section 3.1 therein) of this thesis, attention will be devoted only to the decimation and filtering process, which converts the incoming signal into a constant 2 samples-per-bit signal to be fed into the CDR.

Filtering and decimation

The filtering and decimation subsystem purpose is to convert an oversampled signal $s[n]$ to a 2 samples-per-bit output signal that has a sampling frequency equal to twice the detected line-rate. The theoretical foundation of this is the **decimation** process, also known as **sample-rate conversion** [Oppenheim et al., 1996].

The decimation process consists of taking one sample out of every k samples of the discrete input signal $s[n]$ to produce an output signal $y[n]$. If the input signal was sampled at a frequency f_s, clearly the decimated signal sampling frequency will be $f'_s = f_s/k$. Thus, the spectrum of the signal $y[n]$ will be expanded by a factor k with respect to the spectrum of $s[n]$, and because the spectrum of $s[n]$ is periodic with period equal to f_s, the signal $y[n]$ will have undesirable aliased components unless the maximum normalised frequency component of $s(t)$ is equal or less than $f_s/2k$ [Oppenheim et al., 1996]. In order to avoid the aliasing due to signal decimation, and anti-aliasing digital

filter is placed before the decimation process takes place. Moreover, this anti-aliasing filter also removes out-of-band noise present in oversampled line-rate signals and, thus, leads to a sensitivity improvement.

The described filtering-and-decimation process is illustrated in figure 4.9, where a oversampled 1.25 Gb/s signal (in pink) is first filtered (green curve), and then 1 in 8 samples are taken (in blue). The decimation factor is $d_F = 8$ in this case.

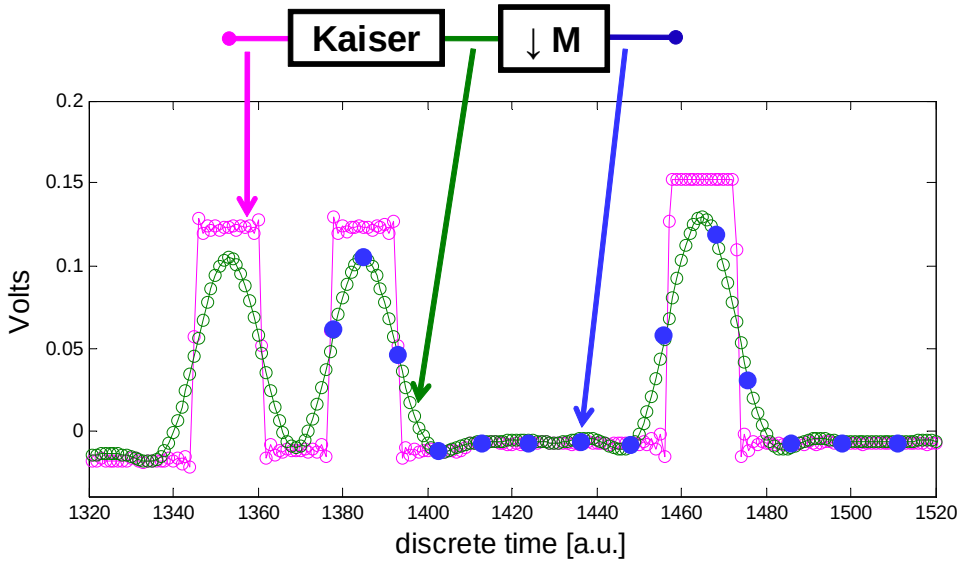

Figure 4.9: Illustration of the decimation process. The incoming signal (pink) is anti-aliasing filtered (green) and then decimated (blue dots) to a 2 samples-per-bit output signal.

The use of a Kaiser filter for the filtering process is justified because Kaiser-window filters allow for the optimisation of the amplitude of the secondary lobes versus the width of the primary lobe [Kaiser and Schafer, 1980]. In this work, a sensible roll-off value of $\beta = 0.5$ was used.

Polyphase implementation

In figure 4.9, it is shown that after the digital Kaiser filter, only 1 in d_F filtered samples is used and passed forward to the CDR section. Thus, a standard, direct form implementation of the anti-aliasing filter [Rabiner et al., 1972] is clearly inefficient and resource wasteful. However, the Kaiser noise-removal, anti-aliasing filter, with frequency response $K(z)$, can be decomposed using the polyphase decomposition,

$$K(z) = \sum_{i=0}^{d_F-1} K_i(z^{d_F})\, z^{-i} \tag{4.5}$$

and then the decimation identity (which allows to exchange the order of the decimation and the filtering) applied to every sub-filter $K_i(z^{d_F})$ [Oppenheim et al., 1996]. Thus, the direct form of the filter $K(z)$, that works at a clock frequency defined by f_s, can be substituted by d_F parallel filters working at a clock rate of f_s/d_F, which can

lead to significant computational improvements depending on the values of d_F and the number of the $K(z)$ filter taps, N.

4.5 Multi-rate clock and data recovery algorithms performance analysis

Two CDR algorithms, named multi-fractional LMS equaliser and polyphase receiver, were described in section 4.4. Here, a modelling study compares the performance and the sensitivity gain due to digital filtering of out of band noise. It will be shown that the polyphase 2 samples-per-bit solution is preferred over the multi-fractional approach. Thus, after this section only the polyphase approach will be used for the dual-rate receiver development.

4.5.1 Performance modelling

A simulation modelling was carried out in order to investigate the performance of the multi-fractional (MLF) equaliser and the polyphase receiver (PPh), discussed in sections 4.4.1 and 4.4.2, respectively. The simulation used the model developed in section 3.3. Every simulation trace contains $65,536$ samples (referred to a sampling frequency of $f_s = 20$ GHz), and for every simulated received power, 32 traces were generated, each having a uniformly distributed fractional delay $\mu_k \in (-2\pi, 2\pi)$. This is because the polyphase receiver performance has a dependence on the relative clock phase of the incoming trace, as described in [Erup et al., 1993]. In order to obtain accurate simulation results, for every received power all these results were averaged to obtain the mean BER performance. Also, in this simulation, a two-pass approach is used for the MLF receiver—the first-pass intended for the LMS to converge and the second-pass to count bit errors, having as initial equaliser kernel the last value of the first-pass—which is unrealistic for a burst-mode receiver and unfair for comparison with the one-pass of the PPh receiver. However, this was necessary for the LMS equaliser to blindly converge.

Figure 4.10 shows the BER performance of both digital receivers as a function of the OSNR, for 10, 5, 2.5, and 1.25 Gb/s line-rates. As expected, due to noise removal by digital filtering in the case of the PPh receiver and by the LMS equaliser in the case of the MLF receiver, there is a sensitivity improvement as the line-rate decreases. If an ideal Gaussian-noise receiver with infinite extinction ratio is assumed, it is easy to prove that the sensitivity improvement is given by,

$$P_{\mathrm{A}} - P_{\mathrm{B}} = 5\log_{10}\left(\frac{B_{\mathrm{A}}}{B_{\mathrm{B}}}\right) \tag{4.6}$$

where B_{x} is the electrical bandwidth and P_{x} is the received optical power in dBm.

Equation 4.6 establishes a theoretical 1.505 dB worsening in sensitivity if the electrical bandwidth is doubled. This is observed for the PPh receiver, for which the sensitivities are -20.78, -19.31, -17.58, -15.98 dBm, for 1.25, 2.5, 5, and 10 Gb/s, respectively. The differential sensitivities are thus $S_{2.5} - S_{1.25} = 1.47$, $S_5 - S_{2.5} = 1.73$, and $S_{10} - S_5 = 1.6$ dB, which closely follow the aforementioned 1.505 dB figure established by equation 4.6.

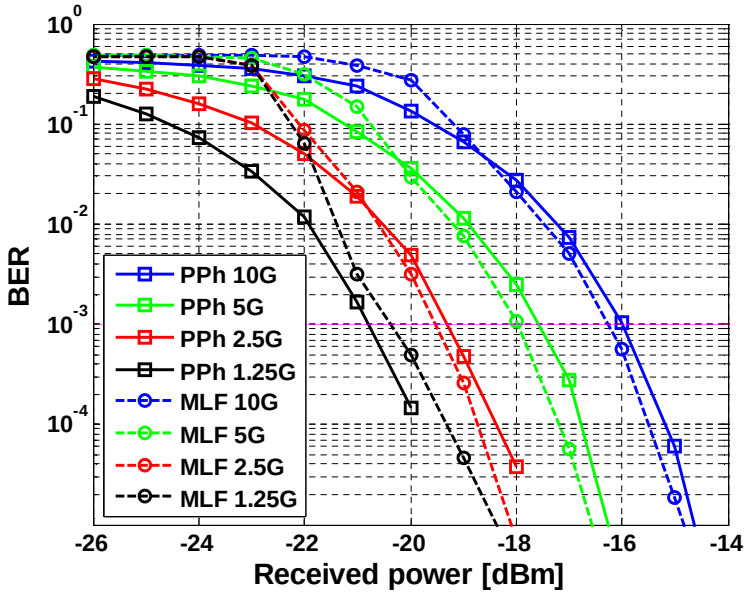

Figure 4.10: Continuous-mode simulation of a multi-fractional equaliser receiver and a polyphase 2 samples-per-bit receiver receiver, for 10, 5, 2.5, and 1.25 Gb/s line-rates, as a function of the received optical power. PPh: polyphase receiver. MLF: multi-fractional receiver.

The MLF receiver improves the performance of the PPh receiver for 10, 5, and 2.5 Gb/s line-rates. The reason for this is that the LMS equaliser converges to the optimum Wiener solution [Widrow et al., 1975] and, thus, this filter not only removes noise but also shapes the received signal. In addition, the digital Kaiser filter cut-off frequency is R_b GHz (where R_b is the line-rate), which is broader than the required bandwidth for optimal balance between inter-symbol interference and noise removal [Personick, 1973a,b].

The MLF receiver performs worse than the PPh receiver for low received powers, because the SNR should be relative high in order for the LMS algorithm to converge to the optimum Wiener solution [Zeidler, 1990]. This point is, however, well beyond the FEC limit, which is approximately BER$= 10^{-3}$.

In conclusion, the MLF approach slightly outperforms the PPh approach. However, fast equaliser convergence is an essential requirement in a digital burst-mode receiver and so the PPh is the only considered solution that allows for that. Also, the computational requirements of the MLF are much higher compared to the PPh approach (for example, 48 taps running every $1/f_s$ seconds compared to 8 filters of $N_k/8$ taps running

every $8/f_s$ seconds, where N_k is the order of the Kaiser filter, for 1.25 Gb/s line-rate), and this is not justified for the little sensitivity improvement gained. In consequence, the polyphase receiver will be used in the rest of this chapter for the realisation of the digital dual-rate receiver.

4.5.2 Experimental verification

This section experimentally assesses the performance of the polyphase 2 samples-per-bit receiver, as the implementation chosen for the digital dual-rate receiver.

Experimental setup

The experimental setup for the generation of optical packets at 10, 2.5, and 1.25 Gb/s is shown in figure 4.11. The setup is quite straightforward, consisting of an externally modulated DFB laser followed by an optical attenuator that allows setting the optical power to an arbitrary level and thus simulate the splitting losses of a PON network. The receiver electrical front-end consists of a standard AC-coupled PIN photodiode and integrated TIA, followed by a 4^{th} order electrical Bessel filter of bandwidth 7.5 GHz. The electrical signal is then digitised using a Tektronix DPO 72004 oscilloscope with a 20 mV/div vertical scale. The digitiser does not allow setting an arbitrary sampling rate and so the electrical signal was digitised at a rate of $f_S = 25$ GS/s, which is the closest possible rate to the 10 Gb/s Nyquist frequency of $f_N = 20$ GS/s required by the digital receiver. Consequently, before processing, the captured signal is ideally resampled to 20 GS/s to give the required $2x$ oversampling.

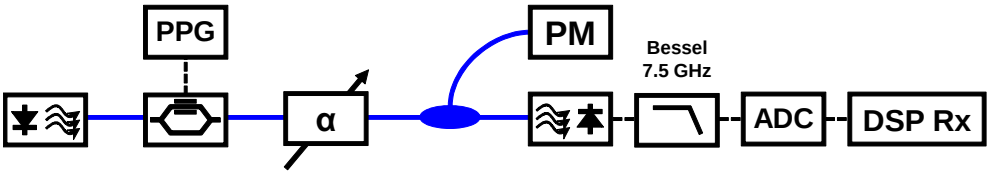

Figure 4.11: Experimental setup for the generation of optical packets at 10, 2.5, and 1.25 Gb/s. Because only one laser is used, the three optical packets have equal average power, which can be varied with the optical attenuator.

The digital polyphase receiver is tested by experimentally generating a repeating sequence of three optical packets, shown in figure 4.12, carrying NRZ modulated data at line-rates of 10 Gb/s, 2.5 Gb/s, and 1.25 Gb/s. The optical packet slot is 819.2 ns in duration and each optical packet is composed of a guard band of 12.8 ns (128 bits at 10 Gb/s), a 3.2 ns (32 bits at 10 Gb/s, 8 bits at 2.5 Gb/s, and 4 bits at 1.25 Gb/s) preamble for packet/line-rate detection, and a data payload of 803.2 ns (8 kbits at 10 Gb/s, 2 kbits at 2.5 Gb/s, and 1 kbits at 1.25 Gb/s). The payload data was an order

7 PRBS sequence, with period $L = 2^7 - 1$, which was chosen to mimic the spectral content of the `8B10B` line code.

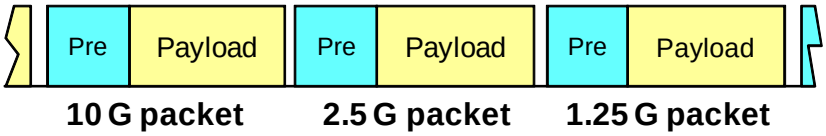

Figure 4.12: A diagram of the generated optical signal. It consists of a continuously repeating sequence having three optical packets at line-rates of 10, 2.5, and 1.25 Gb/s.

Experimental receiver performance

Figure 4.13 shows the characterised BER of the payload for line-rates of 10, 2.5, and 1.25 Gb/s with input optical powers ranging from −16 dBm to −28 dBm. At a BER of 1×10^{-3}, the sensitivity of the receiver is −22.92, −21.36, and −19.13 dBm for 10, 2.5 and 1.25 Gb/s, respectively. As expected, the lower line-rates have better performance due to the improved signal to noise ratio. This corresponds to a sensitivity worsening of 1.56 and 3.79 dB for 2.5 and 10 Gb/s, respectively, referred to the 1.25 Gb/s sensitivity, which closely approach the theoretical values of 1.505 and 4.51 dB obtained from equation 4.6. These results also show good agreement with the simulation carried out in section 4.5.1.

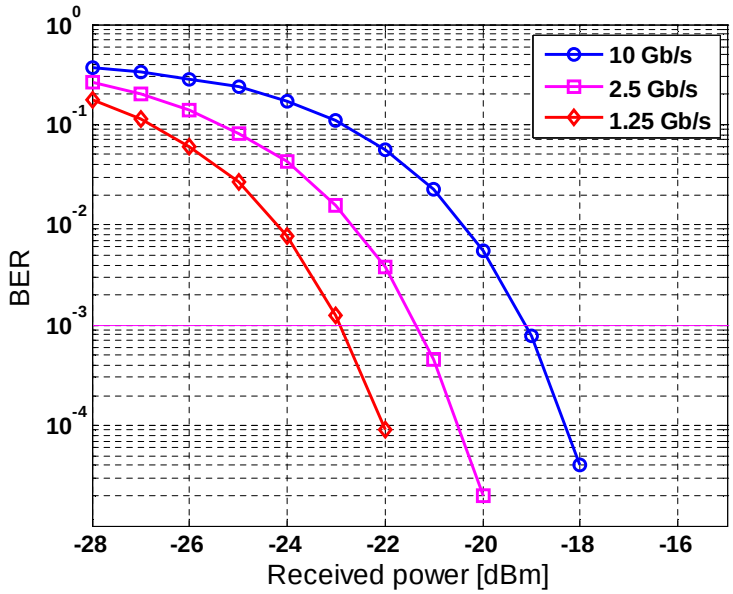

Figure 4.13: Digital polyphase receiver experimental BER performance as a function of the received power for 10, 2.5, and 1.25 Gb/s line-rates.

4.6 Multi-rate receiver design implementation

In section section 4.4, an algorithm for optical packet and line-rate detection, as well as two algorithms for CDR, were presented and discussed. A modelling study, described in section 4.5.1, concluded that a polyphase digital receiver is preferred over a LMS equaliser receiver. In this section, a complete digital dual-rate receiver design—intended for coexistence of 10G-EPON and 1G-EPON optical packets—is presented. This receiver combines the multi-rate packet detector described in section 4.3 with the polyphase CDR described on section 4.4.2 and analysed—in continuous-mode operation—in section 4.5.

In previous work [Thomsen et al., 2007], it has been shown that the sensitivity and dynamic range of an AC-coupled digital burst-mode receiver is limited by the resolution of the digitiser to about 7 dB when the received signal is maintained within the range of the digitiser. By inspection of table 4.3, this receiver dynamic range is insufficient for PON applications, where at least 23 dB is required. Here, a method to increase the dynamic range by letting the high power or loud packets exceed the range of the digitiser—such that they are nonlinearly clipped by the digitiser—is investigated. This clipping technique necessitates the use of a DC-coupled receiver front end, to avoid BLW which would result in the complete loss of part of the packets, and as such the performance of the receiver will depend not only on the range of the digitiser but also on the digitiser DC-offset.

The receiver discussed in this section will be experimentally characterised in section 4.7.

Dual-rate digital receiver architecture

Figure 4.14 shows a diagram of the digital dual-rate packet-mode receiver analysed in this section.

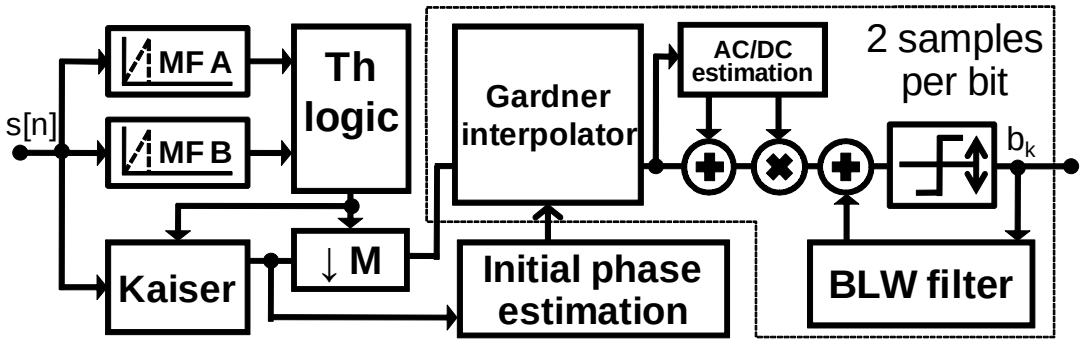

Figure 4.14: DSP architecture of the digital dual-rate burst-mode receiver designed for 10G-EPON and 1G-EPON coexistence.

The digital dual-rate receiver consists of a packet and line-rate detector which uses

the principles described in sections 4.2, 4.3, and 4.4.2 of this chapter. The CDR implementation follows a polyphase design, and it consists of two parts,

1. A **programmable downsampler**, consisting of a digital Kaiser filter and a decimator. The purpose of the downsampler is to reduce the sampling frequency of the received signal to 2 samples-per-bit, once the line-rate has been detected.

2. A **polyphase, 2 samples-per-bit CDR** enclosed in the dotted line in figure 4.14. The purpose of this module is to recover the clock of the incoming data stream, slice the bits into a $[1,0]$ space, and compensate for residual BLW.

All these architectural elements are described next.

Packet and line-rate detector

The packet and line-rate detection is realised with an array of two complex MFs whose outputs are fed to a digital threshold-logic block. A preamble of alternating ones and zeros, which produces a spectral component at a frequency of half the line-rate, was chosen. Thus, the MF kernels consist of the appropriate discrete-time Fourier coefficients at 5 GHz and 0.625 GHz for 10 Gb/s and 1.25 Gb/s line-rates, respectively. By exploiting the orthogonality of these frequencies among different line-rates, the output of the MF matched to the incoming packet is maximised, whilst the output of the other MF is minimised, as described in section 4.3.

The digital threshold-logic block uses this property and detects an incoming packet and line-rate only if one MF output is high and the other low. For simplicity, in this work an 800 ps threshold window centred about the MF peak was used when obtaining the PER measurements. This window length was chosen to be half of the 1.6 ns separation between the undesired periodic peaks in the unmatched output of the 10 Gb/s MF, shown in figure 4.6. However, in practise to remove the need for precise timing information at the receiver, the peak output from the MF would be determined using a peak search algorithm and the threshold logic applied at this point. The output decision from the presence and line-rate detector controls a programmable resampler, consisting of Nyquist anti-aliasing Kaiser filter followed by a decimator.

Polyphase clock and data recovery

Inside the dotted line in figure 4.14 is the clock and data recovery section, which works at 2 samples-per-bit independently of the line-rate. Firstly, the incoming samples are interpolated using the linear Gardner algorithm [Gardner, 1993; Erup et al., 1993]. The phase delay for the interpolator is estimated using the 2 sample-per-bit algorithm described in [Lee, 2002] for 10 Gb/s and the squaring algorithm [Oerder and Meyr,

1988] for lower line-rates where 16 samples per bit are available, thus increasing the robustness of the receiver.

After the interpolator, the packet DC-offset and amplitude are estimated in order to normalise the interpolated samples. In all cases, the estimation is done over a range of 128 bits, independently of the line-rate. This estimation length is equal to the PRBS period and, thus, the number of ones and zeros are balanced to ensure that the results are not biased. After this stage, a BLW correction coefficient is added [Baek et al., 2004], and samples are sliced using a variable-threshold decisor to further increase the receiver robustness [Kawai et al., 1989].

4.7 Digital dual-rate burst-mode receiver experimental characterisation

The design and subsystems of a digital dual-rate receiver have been described in section 4.6. Here, this receiver is experimentally characterised. This dual-rate receiver is intended for 10G-EPON and 1G-EPON coexistence and, thus, the receiver works at 10 and 1.25 Gb/s line-rates.

The key performance requirements of a packet receiver are the sensitivity and packet-to-packet power dynamic range. In order to fully explore these requirements, the dual-rate receiver was characterised in terms of both pBER and PER, as a function of the optical received power, where the PER is defined as the probability of incorrectly detecting the arrival and/or the line-rate of an optical packet. Given the high dynamic range demands of the EPON standards, digitiser clipping has been investigated in order to extend the packet-to-packet dynamic range. Thus, the electrical filtering between the TIA and the digitiser was removed in order to increase the signal bandwidth before digitalisation, and so allow for the detection of high power signals under strong clipping conditions. A DC-coupled photodiode was used in order to remove the BLW that arises in an AC-coupled photodiode. However, under hard clipping conditions there is a small residual BLW that will produce a power penalty.

The section firstly describes the experimental setup used to produce optical packets at different line-rates and variable powers. Then, to investigate the optimum digitiser range and offset, the impact of the digitiser range (in mV) on the sensitivity of the digital receiver under continuous-mode operation for 10 and 1.25 Gb/s line-rates is characterised. Then, the pBER in a packet-mode experiment, using the optimum range obtained in the previous step, is measured. Also, it is assessed the impact of the digitiser offset due to residual BLW. Once the digitiser optimal range and offset have been determined it is then necessary to optimise the packet and line-rate detector thresholds in order to maximise both the sensitivity and dynamic range. Finally, the packet and

line-rate performance of the digital dual-rate receiver is characterised when the packet and line-rate detector thresholds are optimised to match the payload for a sensitivity equal or better than BER $= 10^{-3}$.

4.7.1 Experimental set-up description

Figure 4.15 shows a diagram of the experimental setup used to simulate two ONU transmitters, labelled **A** and **B**, in the context of a dual line-rate PON.

The setup consists of two DFB lasers, which are coupled together with a 50/50 coupler and are externally modulated using a single Mach-Zehnder modulator. The DFB laser driving currents are independently driven with rectangular pulses to generate optical packets of 1.63 μs duration. Optical attenuators on each branch allow the transmit power of each ONU to be set to arbitrary values up to an upper level given by the DFB maximum output power. Whilst in practise each ONU transmitter would be modulated independently—which could have an impact on the orthogonality of the preambles, as a result of transmitter clock frequency drift, and extinction ratio variations—in this work a single modulator is used to modulate both lasers **A** and **B** to ensure that the performance of the transmitters is identical in terms of extinction ratio. This extinction ratio was measured and is about 14 dB in all the experiments described in this chapter.

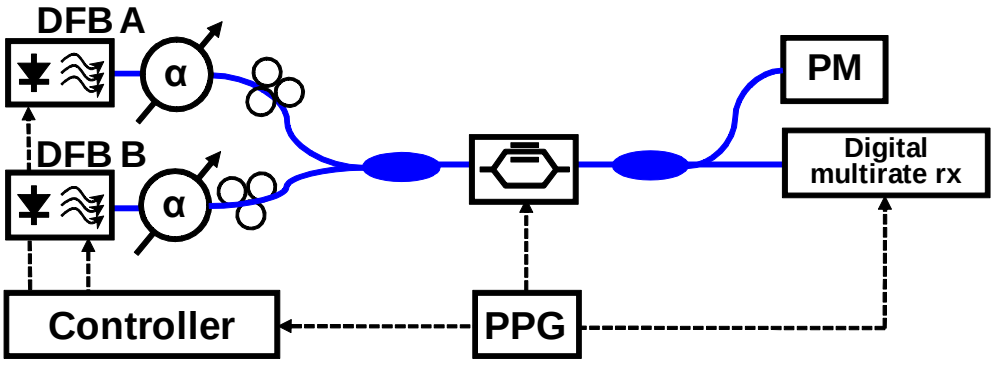

Figure 4.15: Experimental setup for the characterisation of the digital dual-rate receiver. This setup is capable of generating variable-power packets at 10 and 1.25 Gb/s.

One period of the continuously-repeating generated optical signal is shown in figure 4.16. This optical signal consists of 4 optical packets, each having a 6.4 ns preamble followed by a 1.47 μs payload, and a 153.6 ns gap band, which correspond to 64, 14,784 and 1,536 bits at 10 Gb/s, and 8, 1,848 and 192 bits at 1.25 Gb/s, respectively.

The optical packets in figure 4.16 are labelled 1-4 for convenience. The packet sequence can be decomposed into two sub-sequences, each containing a fixed power packet followed by a variable power packet, and also each sub-sequence having altern-

ate line-rates. Thus, packets 1 and 3, generated by branch **A**, have a constant power, while packets 2 and 4, generated by branch **B**, are power-swept over a range from +2.5 dBm to −30 dBm. Packets 1 and 4 have a line-rate of 10 Gb/s, and packets 2 and 3 have a line-rate of 1.25 Gb/s. This allows for the investigation of the packet-to-packet power performance, for both line-rates.

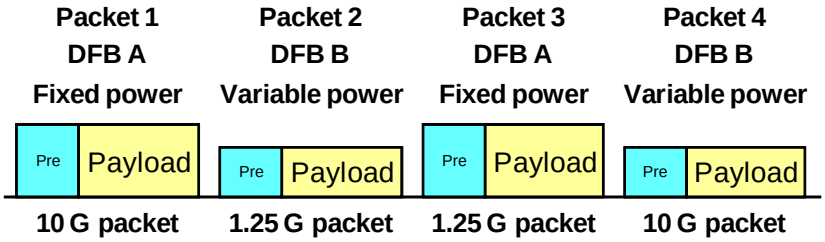

Figure 4.16: Diagram of the generated experimental packet sequence for the characterisation of the digital dual-rate burst-mode receiver.

4.7.2 Continuous-mode characterisation

Using one of the branches of the setup shown in figure 4.15, a set of continuous bit streams of either 10 or 1.25 Gb/s was generated. Each acquired stream had 100 kSamples at 25 GS/s. The optical power was swept from +2.5 to −30 dBm in variable steps. The acquired traces were processed with the same digital described in section 4.6 without the burst and line-rate detection section, in order to avoid DSP induced penalties. Figure 4.17 shows the BER characterisation for 10 Gb/s and 1.25 Gb/s, for digitiser ranges of 100, 200, 300 and 400 mV.

Sensitivity limit at low received power

For both line-rates, an expected increased sensitivity for lower digitiser ranges is observed. In addition, due to digital filtering of out of band noise by the digital Kaiser filtering, there is an extra sensitivity gain of 4.06 dB for the 1.25 Gb/s line-rate. PON receivers operate in a loss-limited regime and are dominated by the electrical thermal noise of the photodiode, TIA, and the electrical noise of the digitiser [Delgado Mendinueta et al., 2011c], and so the Q-factor is inversely proportional to the square root of the bandwidth for a constant received optical power, thus for the 1.25 Gb/s signal where the filter bandwidth is reduced by 8 times a theoretical sensitivity improvement of 4.51 dB is expected, as was deduced in section 4.5.1.

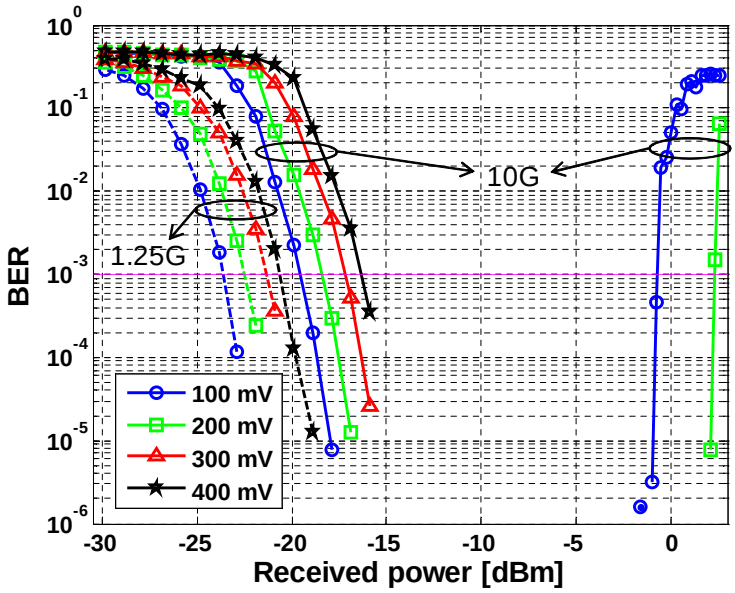

Figure 4.17: Continuous-mode digital dual-rate receiver sensitivity, for 10 and 1.25 Gb/s line-rates, and digitiser ranges of 100, 200, 300, and 400 mV.

Overshoot limit due to digitiser clipping

In order to extend the dynamic range of the receiver, the electrical signal is clipped by the digitiser. For the 100 and 200 mV ranges the onset of clipping occurs at received powers of -9 and -6 dBm respectively. Figure 4.18 shows the effects of hard clipping for a $+2.5$ dBm 10 Gb/s optical packet. Here is plotted the electrical signal after the digitiser, and it can be observed that an isolated `0` symbol surrounded by consecutive streams of `1` symbols is significantly reduced in amplitude, thus increasing the BER. It was experimentally found that removing the electrical Bessel filter before the digitiser, thus increasing the electrical signal bandwidth, improves the received signal quality under these conditions and the overall performance for low optical powers is also not significantly degraded, as the main noise source for this digital receiver is the electrical noise of the digitiser itself [Delgado Mendinueta et al., 2011c].

Figure 4.17 shows the receiver performance degradation that occurs at high powers due to clipping of the signal as the input signal power significantly exceeds the range of the digitiser. This effect is shown to occur at an input power of -1 dBm for the 100 mV range and $+2$ dBm for the 200 mV range. Thus, clipping increases the dynamic range by 8 dB under continuous-mode operation. As a result of the reduced bandwidth requirements for the 1.25 Gb/s signal the effects of clipping on the receiver performance are not observed up to the maximum received power of $+2.5$ dBm that was used in this experiment.

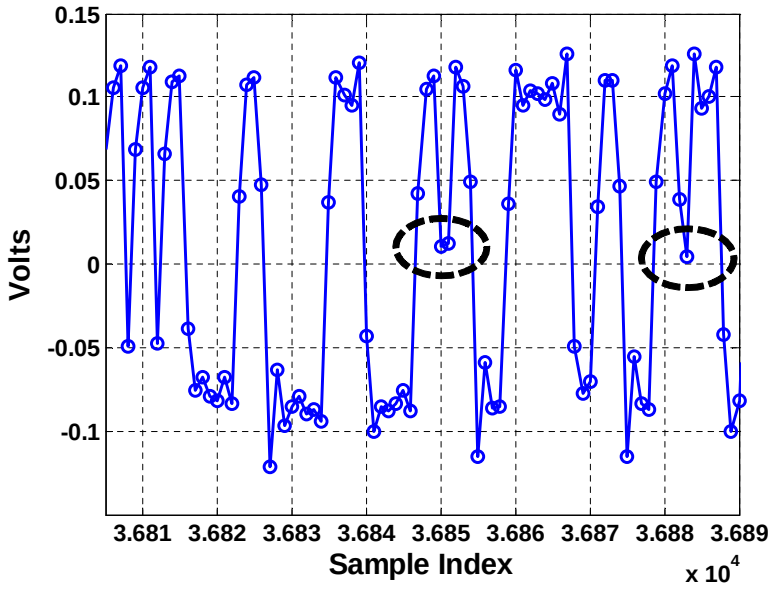

Figure 4.18: An illustration of the acquired electrical signal under hard clipping, for a $+2.5$ dBm 10 Gb/s optical packet. The dashed circles show two examples of an isolated `0` symbol preceded and followed by `1` symbols.

Optimum digitiser scale

As a compromise between sensitivity and dynamic range, a digitiser range of 200 mV was chosen for the subsequent experiments, which gives rise to a sensitivity and dynamic range of -18.5 dBm and 20.5 dB, respectively, for 10 Gb/s.

4.7.3 Packet-mode payload BER characterisation

Given a fixed digitiser range chosen to meet a particular payload sensitivity, the digitiser DC-offset should be optimised in order to minimise the receiver clipping at high received powers, and so minimise the overshoot of the receiver, whilst allowing for error free operation at low powers. In addition, the DC-coupled receiver introduces a residual BLW when operating in burst-mode, as illustrated in figure 4.19, which will affect the performance for low power bursts. In this figure, the red line represents the residual BLW level and has been obtained by applying a digital Butterworth low-pass filter to the received electrical signal (in blue).

Experimental methodology

In order to both quantify the BLW-induced penalty and to optimise the digitiser DC-offset, the pBER was measured in burst-mode operation by capturing a set of bit streams containing the worst case in terms of residual BLW, that is, a high-power packet preceded and followed by a low-power packet. In order to neglect the effects

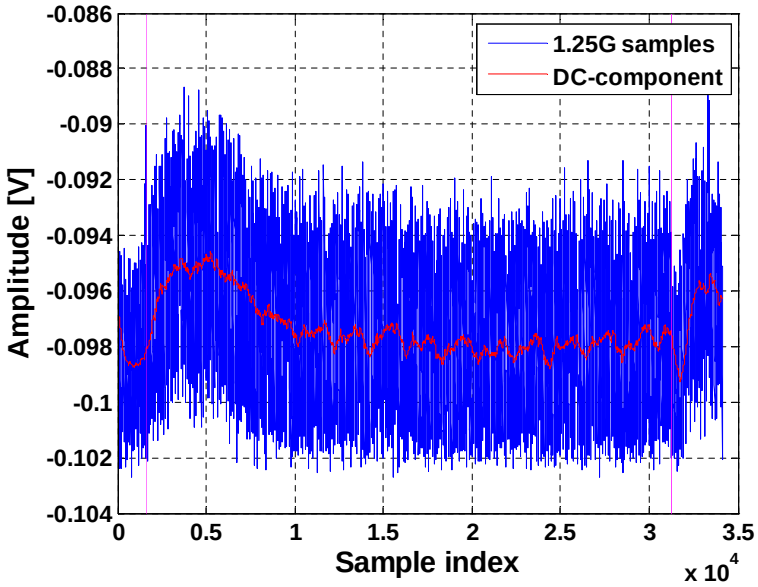

Figure 4.19: Baseline wander example resulting from a -22 dBm 1.25 Gb/s packet preceded and followed by $+0.5$ dBm packets. The red line represents the BLW trend, obtained by low-pass filtering the received electrical signal.

that may arise from packet detection in this experiment, the pBER of the variable-power packets was measured by simply chopping out the payload using the known packet timing. Then, the payload average amplitude and offset were determined by averaging across the entire payload before normalisation and thresholding, in order to get the best possible estimation of these values and thus not introduce an extra power penalty.

Experimental results

Figure 4.20 shows the sensitivity of the variable-power packets, for 10 and 1.25 Gb/s line-rates (refer to figure 4.16), in continuous and burst-mode operation. The sensitivity is defined here as the required received power for a BER/pBER better than 10^{-3}, for a digitiser range of 200 mV. A normalised offset of 0% corresponds to setting the digitiser offset equal to the bottom rail of the digitiser, with negative offset values falling below the digitiser screen. The impact of BLW under burst-mode operation is minimised if the offset is chosen to be 12% or higher. Under packet operation, the 10 Gb/s performance is equivalent to the continuous performance, however, at 1.25 Gb/s a degradation of 1 dB with respect to the continuous performance is observed as a result of residual BLW. This is due to the BLW compensator, that updates at the baud rate and thus the tracking performance depends on the ratio of the baud rate to the associated BLW time constant which is the same for both line-rates and thus the BLW filter is not as effective at lower line-rates.

The baseline wander, as shown in figure 4.19, predominately effects the start of

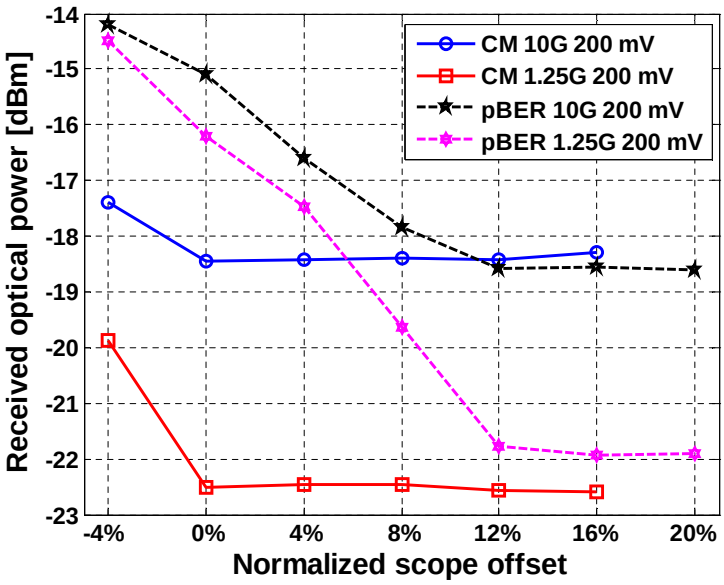

Figure 4.20: Sensitivity of the digital receiver, defined as the minimum received power to achieve a BER of 10^{-3}, for continuous and packet-mode transmission.

the burst. Thus, to determine that this additional penalty observed in the reception of the 1.25 Gb/s bursts arises from the tracking rate of the BLW compensator, the digital receiver was used just to process the second half of the burst where the effects of BLW are negligible. In this case the measured BER shows no penalty over the continuous-mode results shown in figure 4.20.

4.7.4 Packet-mode threshold optimisation

In this section, a method to optimise the two thresholds, λ_{10G} and $\lambda_{1.25G}$, required by the packet presence and line-rate detector is described. This method requires the knowledge of the output statistics (mean and variance) of the two matched filters, and it is realised by an exhaustive search over the range of possible optimisation values. It will be shown that a simplified method can also be used with near optimum results. The proposed threshold optimisation method has been applied to the dual-rate receiver. However, it can easily extended to digital receivers for three or more line-rates.

The thresholds λ_{10G} and $\lambda_{1.25G}$ need to be computed during the receiver prototyping, once a particular analog front-end has been chosen, and stored into the digital circuitry. To avoid this, adaptive thresholds algorithms could be feasible. However, the adaptive threshold optimisation process requires precise knowledge of the optical packet timing, which is precisely the problem the packet detector tackles. Peak search algorithms at the output of the MFs could be used for this task. However, this combined with the adaptive threshold algorithm packet detector will increase enormously the complexity of the DSP and thus price and energy consumption of the digital re-

ceiver. In the proposed solution, a calibration technique based on the collected statistics at the output of the MFs is described. This technique allows to choose fixed-values for the thresholds λ_{10G} and $\lambda_{1.25G}$ to be hard-coded into the digital implementation of the receiver and, thus, avoid the need of complex DSP algorithms.

Matched filter output statistics

Figure 4.21 shows the average MF output for matched and unmatched packets, corresponding A to 10 Gb/s and B to 1.25 Gb/s, as a function of the input packet power for packet header lengths of 16, 32, 48 and 64 bits at 10 Gb/s.

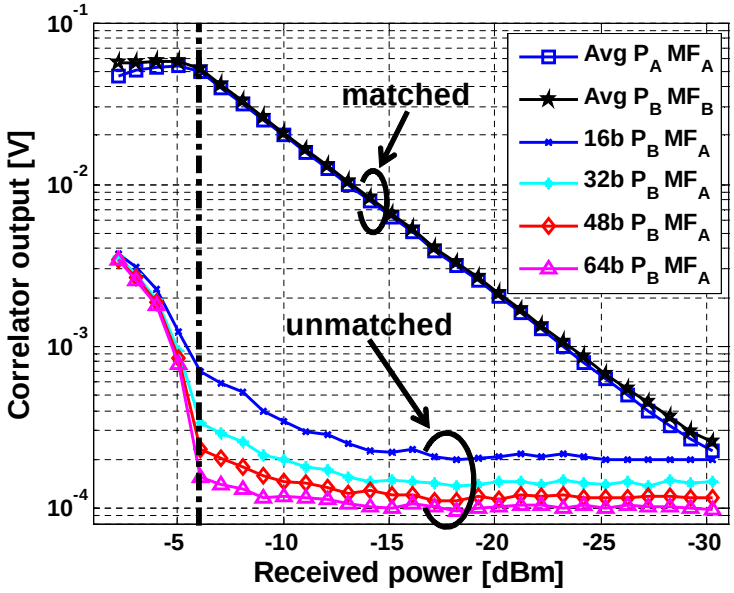

Figure 4.21: Average matched filter output at the optimum sampling point instant, for the matched and 10 Gb/s un-matched cases.

As expected, for a normalised MF the matched output is independent of both the line-rate and the header length, because the signal energy of the different preambles is exactly the same, so here we show the averaged result for clarity (■ and ★ lines for 10 and 1.25 Gb/s, respectively). For the unmatched outputs we only show the output of the 10 Gb/s MF when a 1.25 Gb/s packet is input as this represents the worse case performance, as the 1.25 Gb/s MF output when a 10 Gb/s packet is input is always lower (lines ×, +, ♦, and ▲).

Firstly, we see that increasing the header length reduces the noise floor of the unmatched output as the longer correlator more effectively filters out the noise. Secondly, we observe that signal clipping in the digitiser, which occurs for input powers greater than −6 dBm (as indicated by the vertical dotted line), significantly affects the 10 Gb/s line-rate detector performance. This occurs because the nonlinear clipping process generates harmonics of the clock tone, that the correlator is detecting, and this particu-

larly affects the performance of the 10 Gb/s MF as the 8^{th} harmonic of the 1.25 Gb/s preamble matches that of the 10 Gb/s MF.

Thresholds optimisation by PER scanning

The dual-rate packet and line-rate detector described in section 4.6 requires the optimisation of the two thresholds, λ_{10G} and $\lambda_{1.25G}$, after each MF in order to maximise the sensitivity and dynamic range of the receiver. To achieve this, it is first necessary to choose a soft power-level (P_{low}) for the matched burst and a loud power-level (P_{high}) for the unmatched burst, and then, using the mean and variance of the correlator outputs at these two power levels, the optimal threshold can be calculated using equation 4.7 [Agrawal, 2002, pag. 164],

$$\lambda_{opt} = \frac{\sigma_0 I_1 + \sigma_1 I_0}{\sigma_0 + \sigma_1} \tag{4.7}$$

In this equation, I_x represents the mean value of the soft/loud correlator output, as shown in figure 4.21, and σ_x represents the variance of the soft/loud correlator output (not plotted in the aforementioned figure for clarity). Equation 4.7 must be applied to both line-rates to derive the λ_{10G} and $\lambda_{1.25G}$ optimised values.

Once the thresholds have been determined then the packet receiver performance can be characterised in terms of PER and pBER by error counting. An example of this is shown in figure 4.22, where we define the **PER sensitivity** as the lowest received power were no errors were recorded, the **PER overshoot** as the highest received power were errors start, and the **PER dynamic range** as the difference of these two points. In this experiment, the PER is estimated using $2,048$ packets, which results in a minimum measurable packet error in the interval $[2.5\cdot 10^{-3}, 4\cdot 10^{-4}]$ with 95% confidence.

To investigate the impact of the choice of optimisation powers on the receiver performance, all possible combinations of P_{high} and P_{low} were scanned on a 1 dB grid. The result of this computation is, for every preamble length, two matrices containing the PER sensitivity and the PER overshoot, in dBm units. As en example, figure 4.23 shows the result of the described PER scanning for a preamble length of 64 bits. In order to choose an optimum (P_{low}, P_{high}) pair out of these matrices, two optimisation algorithms are described next.

PER sensitivity and PER dynamic range optimisation algorithms

In the previous section the scanning process to produce the PER sensitivity and PER overshoot matrices for every possible (P_{low}, P_{high}) pair combination was described. Here, two algorithms to calculate an optimum (P_{low}, P_{high}) are presented and analysed. These optimisation algorithms have the two matrices of figure 4.23 as input and produce an optimised (P_{low}, P_{high}) pair.

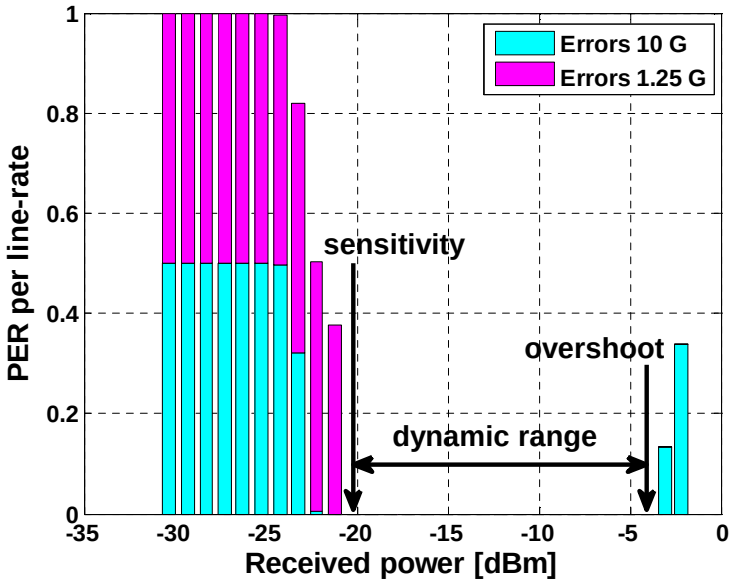

Figure 4.22: An example of a computed PER for a preamble of 64 bits with $P_{low} = -20.19$ dBm and $P_{high} = -4.02$ dBm. The three arrows point to the PER sensitivity, PER overshoot, and PER dynamic range.

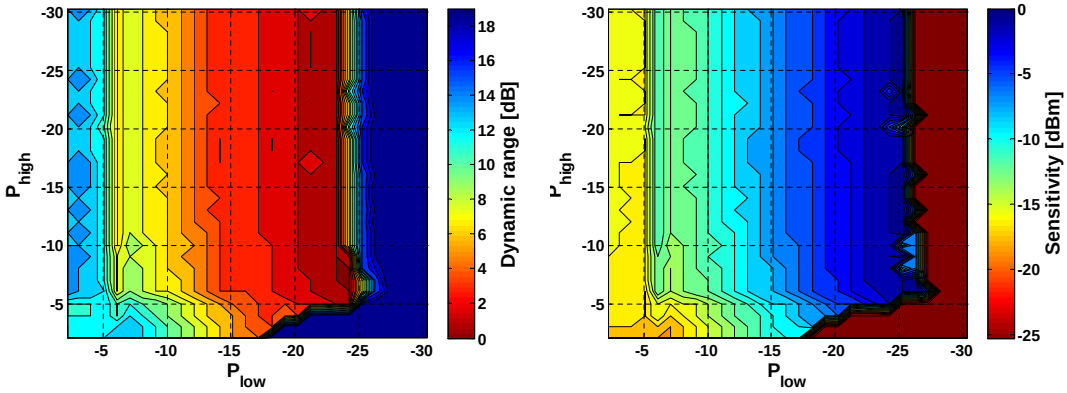

Figure 4.23: Results of the PER scanning for a preamble length of 64 bits, showing (left) the PER dynamic range in dB and (right) the PER sensitivity in dBm.

Both algorithms work as follows: firstly, the points that meet the PER sensitivity criteria, in this case a sensitivity better than -20 dBm, to ensure that the PER performance exceeds that of the pBER, are chosen from figure 4.23 (right). Let S be the set that contains the (P_{low}, P_{high}) pairs that meet the PER sensitivity. Then,

- Algorithm A: from the pairs belonging to the set S, pick the pair or pairs that have maximal PER overshoot. If there is more than one solution, pick a random one.
- Algorithm B: from the pairs belonging to the set S, pick the pair or pairs that have maximal PER dynamic range. If the solution is not unique, pick a random pair that maximises the PER dynamic range.

Figure 4.24 presents the results in terms of PER sensitivity, PER dynamic range, and PER overshoot for algorithms A and B. By inspection, algorithm A tends to fix the sensitivity at the specified pBER sensitivity constraint, while algorithm B tends to maximise the dynamic range by increasing the PER sensitivity as the number of preamble bits increases.

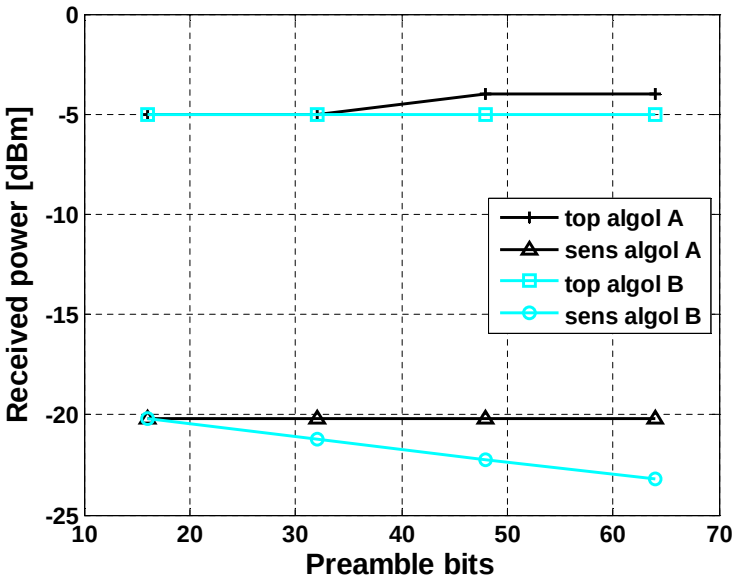

Figure 4.24: PER sensitivity and overshoot versus number of preamble bits, for optimisation algorithms A and B.

The best performance using this exhaustive search combined with the optimisation algorithms described was a sensitivity of -23 dBm and a dynamic range of 19 dB for a preamble of 64 bits at 10 Gb/s. Figure 4.24 shows that the PER sensitivity may be improved by increasing the preamble length. However, the PER overshoot point is limited by clipping regardless of the preamble length as a result of the nonlinear harmonics generated by the clipping process. Thus, a 16 bit preamble, at 10 Gb/s, is enough to reliably receive packets over a 16 dB dynamic range with a sensitivity of -18.5 dBm, guaranteeing a pBER better than 10^{-3} for this dual-rate receiver for both 10 and 1.25 Gb/s line-rates.

Simplified optimisation approach

Although the scanning method presented produces the optimum results, it is not practical as a general design method due to its large computational requirements. A large number of optical packets should be acquired and stored on disk for analysis and a long processing time is needed. However, using the average MF statistics, shown in figure 4.21, it is possible to estimate near-optimum results in a much shorter time.

The procedure, exemplified in figure 4.25, is as follows. Firstly, a soft burst power

value P_{low} is chosen giving a pBER sensitivity requirement. Next, an horizontal line is plotted, and the first high burst power value (denoted P_{high}) that lies down this line is chosen. This (P_{high}, P_{low}) pair can be used with equation 4.7 in order to obtain the optimised thresholds λ_{10G} and $\lambda_{1.25G}$. The performance achieved by this simplified method is similar to algorithm A (maximum overshoot), whose performance is shown in figure 4.24.

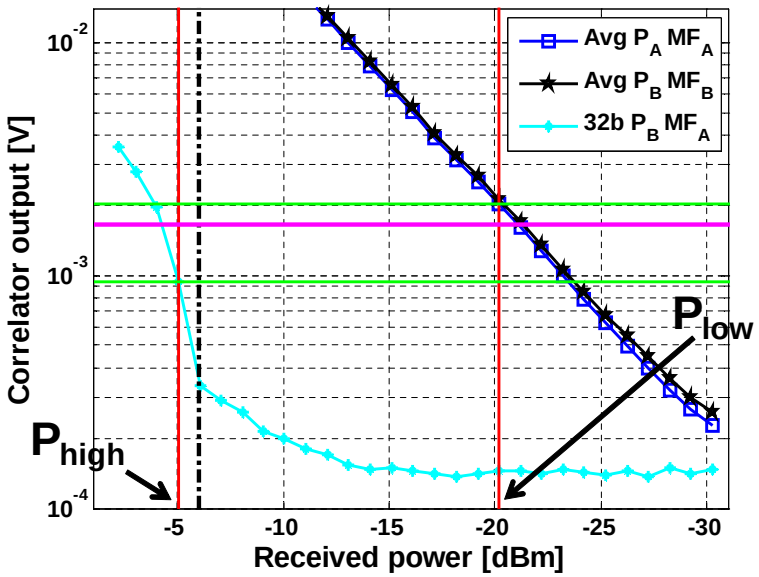

Figure 4.25: Zoomed version of figure 4.21 depicting the simplified threshold optimisation method.

4.7.5 Packet-mode combined PER and pBER characterisation

The last part of the digital dual-rate receiver characterisation was to study the pBER performance of the receiver, once an optimised pair of thresholds, λ_{10G} and $\lambda_{1.25G}$, were chosen. Figure 4.26 shows the pBER performance of the digital dual-rate receiver under the experimental conditions described in this section, compared with the pBER curves of figure 4.20, obtained under continuous-mode operation. The PER performance is not shown because it is identical to that already presented in figure 4.24.

By inspection of this figure, no penalty is observed for 1.25 Gb/s line-rate and for 10 Gb/s line-rate there is a negative penalty of approximately -0.325 dB. This negative penalty can be explained by considering that BLW is the main effect producing the penalty. The power of the fixed-power packet was -18.5 and $+2.5$ dBm for the PER experiment of this section and for the pBER digitiser offset optimisation experiment of section 4.7.3, respectively. Thus, the residual BLW in the PER experiment is less than the residual BLW in the pBER experiment, as the power difference between adjacent optical packets is smaller.

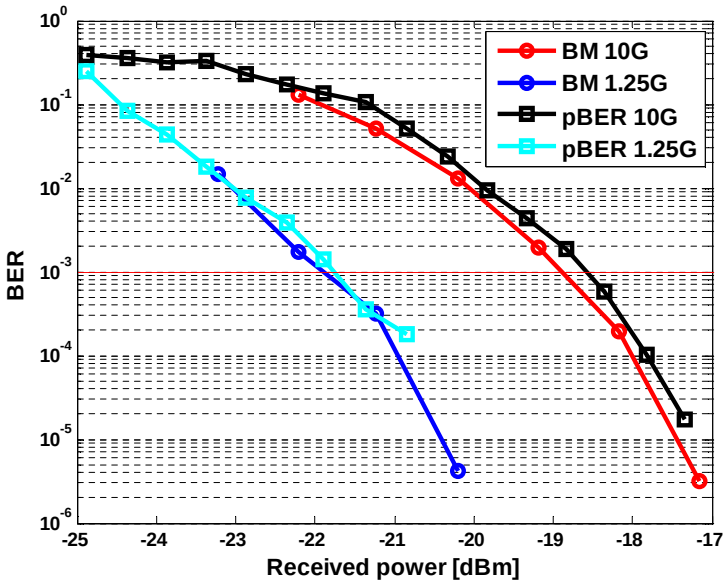

Figure 4.26: Payload BER comparison using the whole payload for DC-offset and amplitude estimation and the digital dual-rate burst-mode receiver. BM: burst-mode operation under conditions stated in this section. pBER: payload BER under conditions of section 4.7.3.

4.8 Chapter summary

In this chapter, a digital dual-rate burst-mode receiver, suitable for coexistence of the 10G-EPON and 1G-EPON standards, has been investigated. A multi-rate detection scheme, based on an array of MFs and relying on the orthogonality of the multiple line-rates, was devised. Two simple and cost-effective multi-rate CDR algorithms were investigated, the first one consisting of a variable length LMS fractionally spaced equaliser and the second one consisting on a polyphase, 2 samples-per-bit solution that works at the baud rate. Although the LMS equaliser solution outperforms the polyphase approach in terms of sensitivity, the polyphase approach is the preferred implementation because of its computational savings over the LMS equaliser. In addition, the LMS equaliser model assumed a very long time for tap convergence, which is totally unacceptable in a fast-response burst-mode receiver.

A complete receiver design was presented and experimentally demonstrated. This PIN based receiver provides a sensitivity of -18.5 dBm at 10 Gb/s for a pBER $= 10^{-3}$, and shows a 4.06 dB sensitivity gain when receiving 1.25 Gb/s line-rate. Clipping has been used to increase the burst-to-burst dynamic range to 20.5 dB in continuous-mode, an 8 dB improvement over that when clipping is not used. Under burst-mode operation a digitiser offset of 12% is required to minimise the penalty that arises from residual BLW and results in a penalty of 0 dB at 10 Gb/s and 0.6 dB at 1.25 Gb/s compared to continuous operation. It could be possible to further reduce the 1.25 Gb/s penalty by increasing the length of the BLW compensation filter. Also, by having two different

filters for 10 and 1.25 Gb/s. However, this would increase the complexity of the 2 samples-per-bit section of the receiver.

Clipping introduces an upper limit on the received power that is independent of the preamble length, as a result of nonlinearly generated harmonics which degrade the performance of the packet presence and line-rate detector. Nevertheless, the combination of both DC-coupling and clipping offers a significant improvement in terms of dynamic range for a given digitiser resolution. Hence, a 16/2 bit preamble for $10/1.25$ Gb/s line-rates is sufficient to reliably receive dual-rate optical packets at a pBER better than 10^{-3} over a 14.5 dB dynamic range using a digitiser range of 200 mV and 5 effective bits of resolution. Also, no sensitivity penalty was found in the payload BER for 1.25 Gb/s line-rate. However, a sensitivity improvement of -0.325 dB was observed for 10 Gb/s. This can be explained as the amount of BLW in the burst-mode characterisation was much less compared to the BLW present in the digitiser offset optimisation experiment.

5

Optical packet power equalisation and wavelength consolidation

WAVELENGTH Division Multiplexing is widely acknowledged as a key technology in the next generation of optical access networks, which will offer increased bit-rate and extended reach [Shea and Mitchell, 2007]. The evolution from Gigabit Passive Optical Networks (GPONs) to Next Generation Passive Optical Networks (NG-PONs) requires the integration of WDM architectures and the already deployed GPON infrastructure.

One potential solution introduces a centralised optical processing unit to be placed at the exchange site in a Wavelength Converting Optical Access Network (WCOAN) [Shea and Mitchell, 2009], allowing uncooled, colourless transmitters to be used in the customer's premises so that the access network is scalable and economically affordable to deploy. This unit will provide all-optical signal processing, including wavelength conversion, to consolidate the multiple burst-mode upstream optical signals from each PON segment, and will convert them to a set of stabilised WDM wavelengths for transmission over the back-haul fibre, which may consist of dual fibres for upstream and downstream directions. This approach reuses current locally deployed fibres and may or may not include optical amplification.

In this chapter, an experimental study of such a processing unit—consisting of a power equaliser and a wavelength converter—was carried out. The burst-mode transmitter and digital burst-mode receiver developed in chapter 4, working only at 10 Gb/s,

was used to experimentally validate this processing unit. This work was carried out in collaboration with Bowen Cao, who developed the Centralised Optical Processing Unit (COPU) used as device under test in the optical access network laboratory emulator built in chapter 4.

This chapter is structured as follows. In section 5.1, there is a brief introduction to next generation long-reach optical access networks. The centralised optical processing unit characterised in this chapter is described in section 5.2. After that, section 5.3 presents the experimental results for this COPU. The chapter concludes with a summary.

5.1 Long-reach optical access networks

Long-Reach Passive Optical Networks (LR-PONs) can increase the number of subscribers and decrease both network deployment and operational costs [Song et al., 2010]. Also, LR-PONs extend the coverage from 10-20 km to 100 km or more by means of optical amplification and WDM technologies [Song et al., 2010]. Hence, LR-PON reduces the need for SDH metro networks interconnecting several deployed PONs. A number of NG-PON networks are currently under research and they make use of advanced features as high order linear modulations and coherent receivers [Song et al., 2010; Lavery et al., 2010]. However, NG-PON are generally not compatible with currently deployed PONs, which is an important requisite tackled by LR-PONs.

In this chapter, a LR-PON approach that offers wavelength consolidation by wavelength conversion, extended reach by optical amplification, and compatibility with legacy PONs already deployed is described and experimentally characterised.

Long-reach WDM PON architectures

A typical LR-PON architecture has an extended reach, shared connection among many PONs segments and an optical processing unit which consolidates wavelengths and amplifies the optical signal [Song et al., 2010]. Thus, the optical processing unit acts as a wavelength demultiplexer in the downstream direction, an as a wavelength multiplexer (with possible wavelength conversion) in the upstream direction [Maier, 2009]. This is illustrated in figure 5.1, which shows how several different PONs are consolidated through wavelength conversion with optional power equalisation for back-haul WDM transmission to the central office by a local exchange.

A number of LR-PON architectures have been proposed recently in the literature. ACTS-PLANET SuperPON, intended for upgrading G.983 APON networks, makes use of EDFA amplification in the downstream direction and SOAs in the upstream direction. The inclusion of SOAs in the upstream direction, along with a gain-control

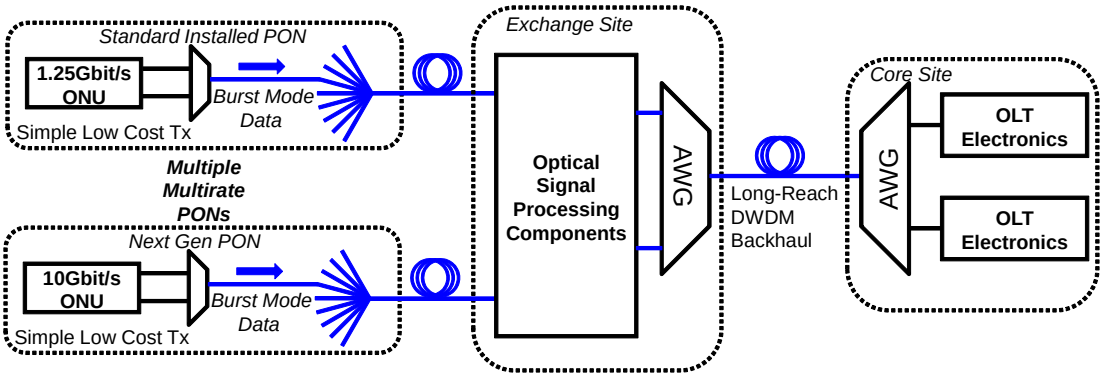

Figure 5.1: Proposed Long-Reach Passive Optical Network general architecture.

by MAC protocol inspection, allows for adaptation to power transients [Van de Voorde et al., 2000].

The University College Cork has demonstrated another LR-PON architecture that subdivides the C-band into a lower sub-band (used for downstream) and an upper sub-band (used for upstream). Each sub-PON uses one lower downstream sub-band channel and one upper upstream sub-band channel and, thus, the ONUs are colourless. In order to keep the wavelength stability required for WDM transmission, the local exchange contains an array of DFB lasers, which are shared by the ONUs. Every ONU contains a filter that separates downstream/upstream wavelengths and the shared DFB laser is modulated with an Electro-Absorption Modulator (EAM) modulator preceded and followed by SOAs for optical signal amplification [Talli and Townsend, 2006].

The two aforementioned LR-PONs use the tree topology. However, LR-PON demonstrators with ring topology also exist [Lázaro et al., 2008; An et al., 2004] and hybrid architectures, which combine ring and mesh topologies by inserting AWG routers and Passive Star Couplers (PSCs) into a ring [Maier et al., 2007].

University College London LR-PON architecture

The architecture developed at University College London by Bowen Cao, Dr. Darren Shea, and Dr. John Mitchell [Shea and Mitchell, 2009], is based on the architecture presented in figure 5.1. The key idea of this work is to reduce costs by keeping the current uncooled, cheap lasers at the customer premises ONUs. However, these uncooled lasers will have wavelength drifts, which makes them unsuitable for Dense Wavelength Division Multiplexing (DWDM) transmission. The proposed solution uses a Wavelength Converter (WC) which uses a cooled DFB laser as probe signal. This WC is shared among the PON segment ONUs and hence the cost is shared among the subscribers. The wavelength converted signal is stable enough to be combined in the local exchange with other PON segment signals, with a different wavelength allocated for every PON segment after conversion [Shea and Mitchell, 2009].

In this LR-PON architecture, the key component in the local exchange is the COPU and in the COPU itself the main component is the wavelength converter. The suitability of both Cross-Gain Modulation (XGM) and Cross-Phase Modulation (XPM) wavelength converting techniques has been already investigated [Cao et al., 2011b; Shea and Mitchell, 2009]. However, in these works only a continuous-mode transmitter and receiver was used and hence not all the penalties associated with a true burst-mode environment were investigated.

The purpose of this chapter, carried out in collaboration with Bowen Cao, is to experimentally investigate the local exchange COPU performance in a packet-mode environment using the packet transmitter developed in previous chapters of this thesis in conjunction with the digital burst-mode receiver technologies presented in chapters 3 and 4.

5.2 Centralised optical processing unit description

The COPU is expected to meet three different requirements, which are, namely, wavelength conversion, burst-to-burst power equalisation, and transmission distance enhancement. The wavelength conversion consolidates multiple Coarse-WDM ONUs wavelengths onto a set of fixed Dense-WDM wavelengths for efficient back-haul transmission over a WDM link and also compensates for the wavelength drift of uncooled, cheap ONU transmitters [Song et al., 2010]. Also, the unlevelled bursts coming from diverse ONUs at different distances from the exchange will need to be equalised to reduce the receiver burst-to-burst dynamic range requirement at the OLT. Moreover, the dynamic range of the wavelength converter is relatively small, so optical packets should be equalised in order to the wavelength converter to work properly. Optical packets coming from the ONUs would need regeneration to have a higher extinction ratio and possibly pre-chirping to enable dispersion tolerant transmission required in the long reach scenario [Cao et al., 2011a].

Figure 5.2 shows a diagram of the Centralised Optical Processing Unit. The COPU consists of two clearly differentiated sub-systems, namely, a power equaliser based on two cascaded SOAs, and a Wavelength Converter composed of two SOAs in a Mach-Zehnder architecture (known as a Semiconductor Optical Amplifier Mach-Zehnder Interferometer (SOA-MZI) configuration). Both elements will be described in detail next.

SOA-MZI wavelength converter

The key element in the optical processing unit is the WC based on XPM in a SOA-MZI. This device has previously been proposed for use in WDM enabled core and metro

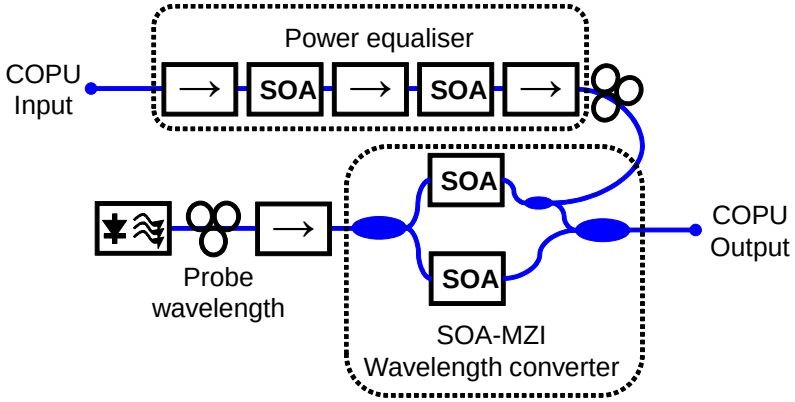

Figure 5.2: Centralised optical processing unit diagram. The COPU consists of a power equaliser and a SOA-MZI wavelength converter.

networks [Chung et al., 2005]. However, in access networks there are additional issues as the incoming wavelength is not stable and the optical signal is burst-mode and, thus, the packet-to-packet power is not constant.

The SOA-MZI device depicted in figure 5.2 works as follows: optical signals amplified by a SOA suffer from relatively large phase modulation. Thus, an optical signal that traverses one of the SOA in the interferometer modulates the phase of that interferometer branch and consequently the Mach-Zehnder interferometer modulates the intensity of the pump signal in accordance with this phase changes [Ben Yoo, 1996].

XPM wavelength conversion is considered the most effective because of its high conversion efficiency, extinction ratio enhancement, and negative chirp characteristics. It can also maintain the extinction ratio of incoming wavelengths that are less and greater than the output wavelength [Durhuus et al., 1994; Cao et al., 2011b].

SOA-based power equaliser

Generally, XPM wavelength converters have a limited operating range or input power dynamic range of 3-4 dB at 10 Gb/s [Danielsen et al., 1998]. This is because this power range is enough to change the phase of the signal by more than π radians and, thus, the interferometer does not work correctly if this range is exceeded. On the device used in this chapter, this input power dynamic range is only 2 dB under normal operating conditions. However, by using an all-optical packet-to-packet optical power equaliser, the dynamic range of the wavelength converter can be extended.

An all-optical technique to equalise optical bursts/packets can be realised by using a pre-amp SOA to amplify the ONU input signal power and a second booster SOA operating in the saturated regime to equalise the burst power [Pato et al., 2008, 2009]. However, the optical signal distortion caused by the saturated SOA is likely to require regeneration, which is provided by the SOA-MZI wavelength converter in the proposed COPU design.

5.3 Centralised optical processing unit experimental characterisation

This section presents the experimental setup used to generate and receive optical packets, the static power characterisation of the COPU, the COPU optimisation procedure, and finally the transmission characteristics of the system composed of burst-mode transmitter, COPU, and digital burst-mode receiver.

5.3.1 Experimental setup

Figure 5.3 shows the experimental setup used for the burst-mode characterisation of the COPU. Two ONUs were modelled with two externally modulated DFBs lasers at different wavelengths ($\lambda_1 = 1553.5$ nm and $\lambda_2 = 1556.3$ nm), with an extinction ratio of 14 dB. The COPU probe and pump signals are in a counter-propagation configuration, as this produces a better converted-signal performance in terms of higher extinction ratio and Q-factor [Cao et al., 2011b]. The probe, onto which the upstream traffic is converted, is a Continuous Wave (CW) laser at $\lambda_p = 1554.7$ nm. As this is a proof of concept experimental demonstration only commercially available C-band devices were available in our laboratory. Wavelength conversion from 1.3 μm to 1.5 μm using 1.3 μm SOAs has been previously demonstrated [Lacey et al., 1996]. Thus, the results of this experiment which show mapping of 1.5 μm Coarse Wavelength Division Multiplexing (CWDM) channels onto a 1.5 μm DWDM grid for back-haul will still hold for the 1.3 μm upstream wavelengths that are typically used in PONs. After the COPU, an optical filter removes out of band noise and simulates the transfer function of the AWG, shown in figure 5.1.

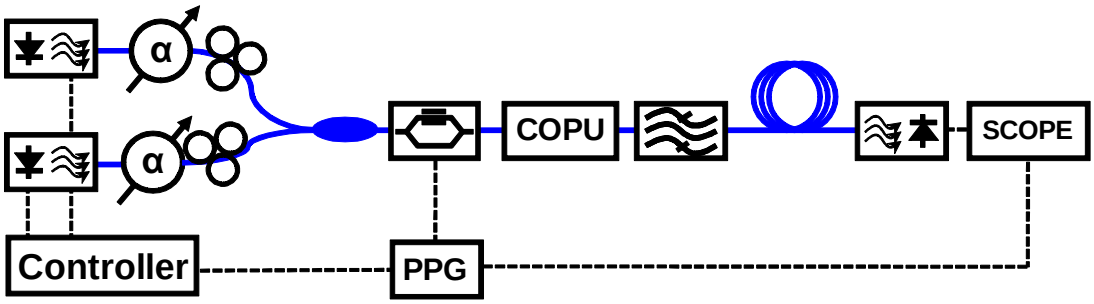

Figure 5.3: Experimental setup employed for the characterisation of the centralised optical processing unit.

Two optical packets, depicted in figure 5.4, were generated with this setup, creating a train composed of a loud and a soft packets, each having a 6.5 μs length with a guard time of 204 ns placed between packets.

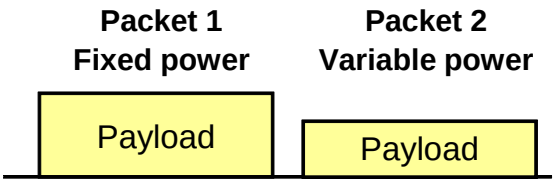

Figure 5.4: Generated optical packets for the COPU characterisation.

5.3.2 Digital burst-mode receiver

The burst-mode receiver, shown in figure 5.5, consisted of a digital burst-mode receiver based on a front-end having a DC-coupled PIN photodiode, electrical low-pass filter, and a fast ADC, in a similar way of the digital receiver presented in chapter 4.

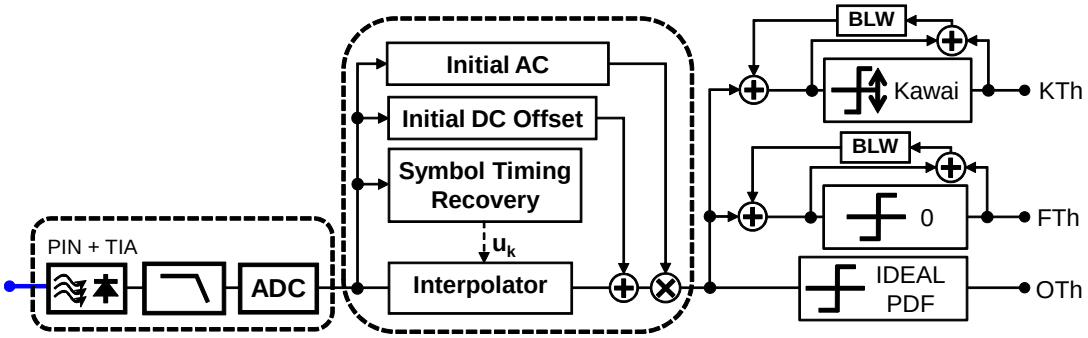

Figure 5.5: Diagram of the digital burst-mode receiver used in the characterisation of the COPU.

The power equaliser degrades the extinction ratio and also exhibits patterning effects in dynamic mode. To illustrate this, figure 5.6 shows two electrical eye diagrams produced after the output of the power equaliser booster SOA (figure 5.6.A) and after the SOA-MZI wavelength converter (figure 5.6.B), when a -15 dBm optical signal is input into the COPU.

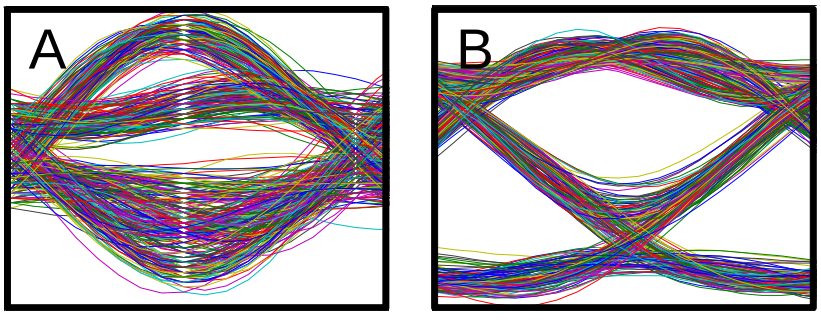

Figure 5.6: Electrical eye diagrams for a COPU input power of -15 dBm (A) after the power equaliser booster SOA and (B) after the SOA-MZI wavelength converter.

These distortions are partially compensated due to the regenerative properties of the nonlinear transfer function of the SOA-MZI WC [Cao et al., 2011b]. However, due to the large COPU input power variations, there are large variations on the output

signal extinction ratio and eye shape due to the saturated SOA patterning combined with the nonlinear transfer characteristics of the WC. In order to overcome this COPU-produced distortion, two digital-domain approaches were used

1. A **piecewise-parabolic interpolator**, controlled by a fractional delay estimator that can be efficiently implemented with a Farrow structure [Erup et al., 1993]. In this application, this interpolator produces an average of 0.5 dB improvement in terms of sensitivity over a linear interpolator used in previous chapters of this thesis. After the interpolator, the signal is normalised with an estimation of the burst DC-offset and amplitude.

2. An **adaptive threshold slicer**, based on [Kawai et al., 1989] and referred as (KTh), which includes a baseline-wander filter. Also, the performance of this approach was compared with a fixed-null threshold slicer (FTh) and an optimum slicer where the optimum threshold is determined with knowledge of the entire packet PDFs (OTh).

These algorithms are shown in the aforementioned figure 5.5. BER measurements up to 10^{-6} were carried out by error counting using offline processing. This allows for a good confidence interval measurement around the BER FEC limit of 10^{-3}.

5.3.3 Static COPU power equalisation

The input/output CW power characterisation of the COPU is shown in figure 5.7.

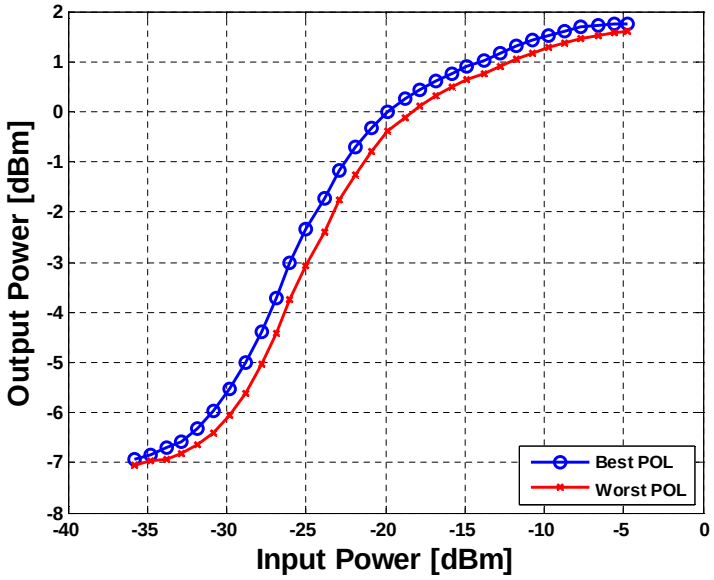

Figure 5.7: Centralised optical processing unit measured input/output power characteristic. The blue (○) and red (×) curves represent the best and worst input polarisation states, respectively.

For a PON with a 32-way optical splitter, the ≈ 15 dB insertion loss in the optical splitter limits the COPU input power to the range from −15 to −30 dBm. For this input power range, it was found that the output power range ranges in the interval from +1 dB to −6 dB, with a polarisation penalty of 1 dB. This compression in the power range can effectively reduce the loud/soft ratio of the bursty optical packets, thus extending the packet-to-packet dynamic range of the digital burst-mode receiver.

5.3.4 COPU optimisation procedure

The performance of the prototype COPU used in this work with respect to the input power range can be tuned by adjusting the WC bias point. The polarisation controller between the probe laser and the COPU was optimised in order to maximise the WC extinction ratio. Since the CW probe is physically located close to the SOA-MZI or even packaged together, once the polarisation for the probe is optimised it is not expected to change. However, in a real system the polarisation of the burst coming from the ONU is random. The SOAs used in the equalisation stage are polarisation insensitive but the SOA inside this prototype SOA-MZI device had a strong Polarization Dependent Gain (PDG). The PDG changes the signal power in one arm of the SOA-MZI, which affects the bias point of the WC and can result in an up to 2.5 dB dynamic polarisation penalty for the received BER sensitivity. It is expected that a production grade SOA-MZI device will be used in the real system, which will have an optimised SOA active region and is polarisation insensitive [Miyazaki et al., 2006]. Therefore, the bias point of a polarisation insensitive SOA-MZI device will not be affected by the random polarisation of the ONU packets.

The following procedure was used to adjust the ONU polarisation, i.e., the WC bias point, to overcome the polarisation penalty of this prototype device. Two packets of −15 (loud) and −25 dBm (soft) were generated and then three COPU optimisation cases, named A, B, and C, were chosen. These cases are illustrated in figure 5.8 for a back-haul transmission distance of 22 km, where the soft packet eye diagram was superimposed on the loud packet eye diagram.

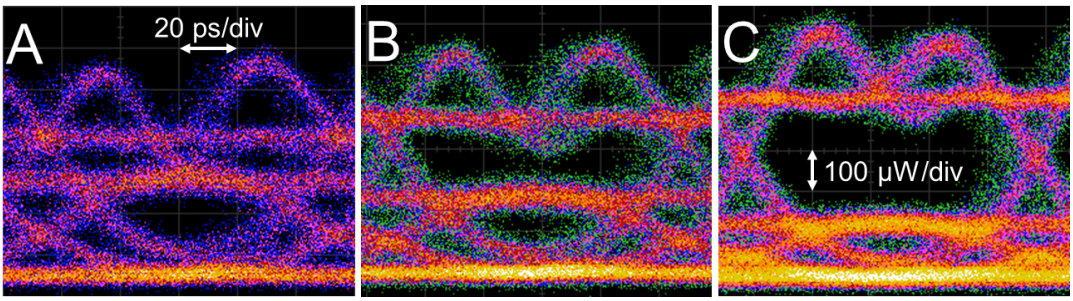

Figure 5.8: COPU output signal eye diagrams after 22 km of fibre for (A) polarisation case A, (B) polarisation case B, and (C) polarisation case C.

The loud packet eye exhibits a nonlinear distortion due to patterning-generated additional optical power before the SOA-MZI sinusoidal transfer function, which contrasts with the characterisation of figure 5.7 where no eye overload is noticeable in static CW mode. In case A, the optical eye diagram of the loud and soft packets was equalised as much as allowed. Ideally, this would be the case for the real system with a polarisation insensitive SOA-MZI device. Case C is the opposite and so the amplitude of the loud burst is maximised and the power of the soft packet is minimised. Case B is a compromise between cases A and C.

5.3.5 COPU BER characterisation

The four plots in figure 5.9 show the soft packet BER performance in burst-mode operation for COPU optimisation cases A and B. Case C, which follows the trend of increasing the overload point and reducing the sensitivity, is not plotted here for clarity. In these measurements, the optical power of the loud burst was fixed at -15 dBm in order to simulate the 32-way splitter loss, while the power of the soft burst was swept from -5 dBm to -35 dBm in 1 dB steps. The Back-to-Back (BB) curve in 5.9 indicates the DBMRx sensitivity in burst-mode operation and was measured by connecting the burst-mode transmitter straight into the DBMRx. In order to avoid quantisation clipping and consequently nonlinearities at the digital receiver, the quantiser range of the digital receiver and the optical attenuation was configured for every transmission distance to keep the maximum received electrical signal within quantisation limits. Consequently, a 4 dB optical attenuator was used for the BB case.

The sensitivity of the digital receiver is maximal for the 0 km case and diminishes with transmission distance due to fibre losses and dispersion. On the contrary, the overshoot of the receiver is worse for the 0 km case and improves with the transmission distance. The SOA-MZI device operating in non-inverting mode has the benefit of generating negative chirp. The pre-chirped converted signal reduces the impact of dispersion and so the results show that the overshoot improves when fibre distance increases from 0 km to 22 km. In addition, no significant benefit is observed between the variable-threshold slicer and the fixed threshold slicer, which leads to some DSP resources savings. There is a tradeoff between receiver sensitivity and overload, which can be observed in figure 5.9 (22 km transmission), where a reduction of 1 dB in sensitivity leads to a 5 dB improvement in overload switching from COPU optimisation case A to case B.

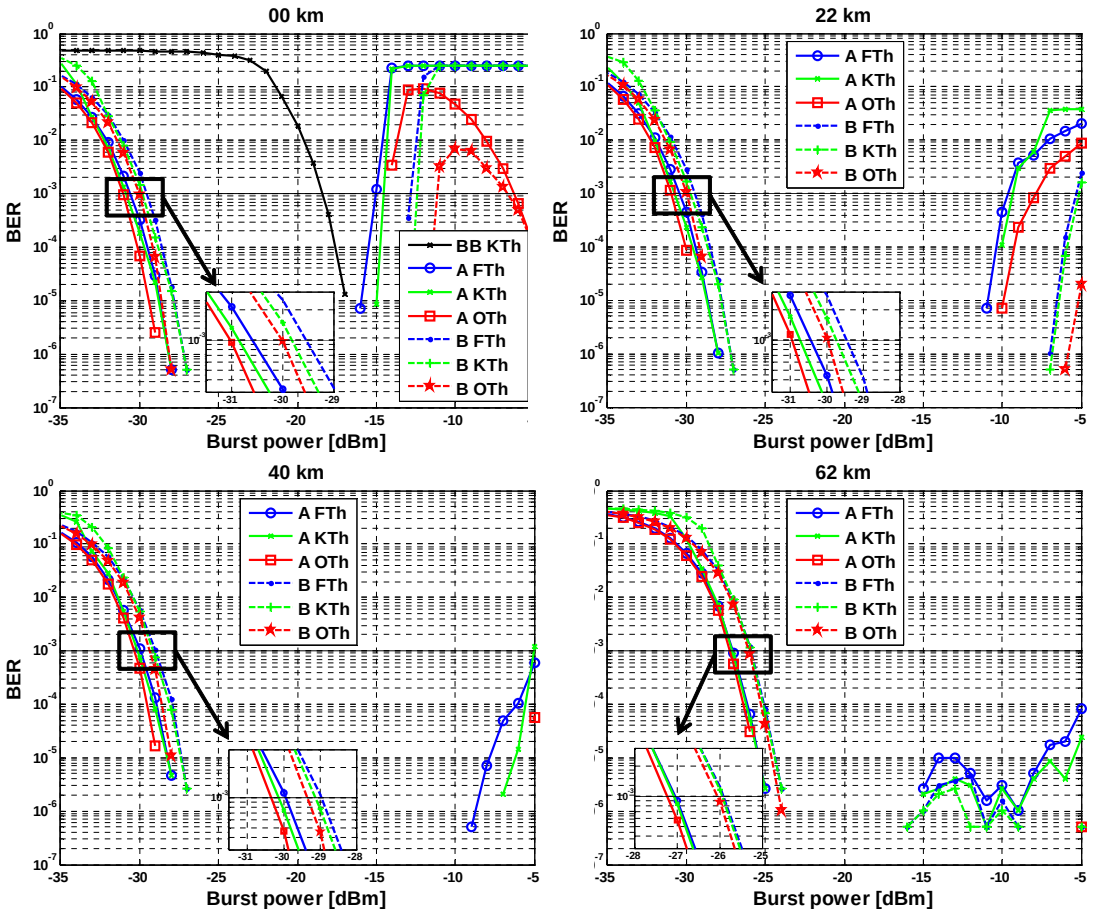

Figure 5.9: Experimental BER characterisation of the COPU for (FTh) fixed null threshold slicer, (KTh) Kawai variable-threshold slicer, and (OTh) optimum slicer for cases A and B for back-haul distances of (a) 00 km (COPU and no fibre), (b) 22 km, (c) 40 km, and (d) 62 km. The black line represent the back-to-back (neither COPU nor back-haul fibre) case.

5.4 Chapter summary

In this chapter, next-generation long-reach PON networks were introduced. Both capital and operational network costs can be reduced by introducing WDM and active optics in optical access networks. A new architecture, which consolidates several PON segments into a WDM link for long-distance transmission to the central office, was described. A critical component in this long-reach PON architecture is the Centralised Optical Processing Unit. The COPU equalises the burst-to-burst optical power of various ONUs, and then wavelength-convert this coarse wavelength upstream channel of the cheap ONU transmitters into a stable wavelength for the WDM back-haul transmission to the OLT, located in the central office.

A COPU, consisting of a cascaded SOA power equaliser and a SOA-MZI wavelength converter, has been experimentally characterised. The power equalisation of the cascaded SOAs was found to compress the input power range $(-30, -15)$ dBm into an output range of $(-6, +1)$ dBm, which increases the operational dynamic range of the

wavelength converter.

It was shown that there is a tradeoff between the maximum sensitivity of the receiver and the overload point which can be optimised by varying the operating point of the WC. The BER performance using a PIN-based DC-coupled digital burst-mode receiver at 22, 40, and 62 km of unamplified back-haul distances were compared and sensitivities of -30.94, -30.17, and -27.26 dBm with overload points of -9.3, -5, and > -5 dBm were found, respectively. Also, in this application a fixed null threshold slicer performs similarly to a more complex variable-threshold scheme used in previous chapters, which could lead to significant receiver DSP resource savings.

6

Conclusions and further work

In this thesis, the suitability of digital signal processing techniques at the optical receiver side—in order to overcome the physical layer impairments that arise in dynamic optical networks—was investigated. To re-conciliate the many protocol-simulation studies with the figures of merit produced in optical physical layer research, several studies with this digital receiver were conducted producing both payload bit-error rate and packet-error rate as figures of merit. This allows for a better understanding of the limits imposed by the analog optical medium and, thus, enable network designers to properly allocate network resources and calculate network limits (such as maximum reachable distance that meets a target packet-error rate or guarantees a maximum network throughput).

The rest of the chapter summarises the key points of this work and then offers the reader some future work guidelines in view of the work carried out in this thesis.

6.1 Summary of research

The complex concept of dynamic optical networking—and their different flavours—was introduced, along with the main advantages and disadvantages. It was shown that dynamic optical networks can be categorised into OCS and OPS, in increasing granularity order, and mimicking the classical classification of circuit-oriented networks and packet-oriented networks. OBS networks arise as a compromise between the flexibility to varying traffic demands and the granularity of OPS versus OCS networks, but

with relaxed optical component performance requirements, that allows for easier implementation and reduced costs. Furthermore, OBS Type-I and Type-II allow to vary the average burst-size and, thus, gradually adjust the optical component requirements as technology evolves.

The principal figures of merit—that allow the network designers to compare between several alternatives—were introduced and analysed. It was shown that research dealing with pure physical layer experiments mainly produces results in the form of bit-error rates or power penalties. On the other hand, research investigating network-wide resource allocation and dimensioning, or optical signalling protocols—better known as the *optical control plane*—prefer to measure the network performance using the packet-error rate or the network throughput. Consequently, it was shown that it is important to produce FOMs such as the packet-error rate when conducting dynamic network physical layer experiments or simulations and, thus, allow network designers to easily take into account the physical layer influence in the whole network design. The implementation of layer-2 and layer-3 functions into the optical domain leads to packetised optical networks and it was shown that this introduces a new set of impairments and challenges that should be addressed. A paramount problem in packetised optical networks is the ability of the receiver to correctly detect an incoming optical burst.

Dynamic optical networks require a set of optical components currently under research, that can be summarised into the categories of: a) burst-mode transmitters, b) burst-mode optical amplifiers, c) optical switching matrices, and d) burst-mode receivers. Generally, burst-mode optical components for dynamic optical networks offer less performance or are more complex or expensive than their continuous-mode counterparts. Also, physical layer impairments affecting continuous-mode networks (such as crosstalk) are accentuated due to dynamic operation of the network.

The main physical layer impairments in both core and access dynamic optical networks were identified and the burst-mode receiver requirements derived. In addition to the usual continuous-mode receiver requirements such as clock and data recovery, core dynamic optical networks require a burst-mode receiver with the following traits, in order of importance: a) packet detection, b) maximum noise immunity, c) gain excursions and BLW tolerance, d) high sensitivity and operating dynamic range, and e) fast response time. The burst-mode receiver requirements for optical access networks change slightly due to the different nature of the optical layer design—mainly, the absence of optical amplification and the presence of the high-loss optical splitter. These requirements are, in order of importance: a) high sensitivity, b) high dynamic range and overshoot point, c) immunity to consecutive identical digits, d) response time. Optionally, receivers for coexistence of current and legacy line-rates in the same passive segment will require to detect the line-rate and presence of incoming optical packets.

A survey of recent published work on burst-mode receivers was conducted. The conclusion of this survey is that the vast majority of the published work focuses on extending analog burst-mode techniques from 1 Gb/s to 10 Gb/s. Also, most of the research is concentrated on burst-mode receivers for optical access networks and in such networks the packet-error rate is not measured or considered negligible.

Digital burst-mode receiver and core networks

Due to the advent of ultra-fast analog-to-digital converters, it is now possible to use all-digital receiver techniques—which have been used in radio communications for more than 25 years—at optical line-rates. However, because of the high data rates of optical systems, the limited number of processing steps that can be carried out per-bit limits the amount of DSP that can be used in optical systems. Hence, simple and sub-optimum algorithms are preferred over more complex and better performing ones. The possibility of having an optical digital receiver with DSP capabilities allows for the compensation of impairments and thus relaxes the requirements of optical burst-mode mode amplifiers, transmitters, and optical switches.

The performance of a 10 Gb/s two-samples per bit digital optical receiver was investigated and it was shown that in an optical noise limited system, the receiver performance in terms of the packet-error rate can be increased by incrementing the preamble length and, thus, limiting the network total throughput. Also, in this AC-coupled receiver, it was shown that half the digitiser range should be reserved to allocate electrical signal drifts arising from BLW due to the AC-coupling.

This gave rise to a dynamic range of 7 dB, for an OSNR penalty of less than 1 dB, and this is mainly limited by the electrical noise from the digitiser front-end and ultimately from the quantisation noise of the digitiser. The best performance for this receiver was obtained for a -6 dBm received optical power with 10.85 dB OSNR. Burst preamble lengths of 32, 64, and 128 bits were investigated—of which only half of the preamble bits are used for burst-detection purposes and the remaining ones serve for DC-offset and burst amplitude estimation, and burst timing detection—and it was found that the PER was better than 0.06 for 64 preamble bits and 0.00065 for 128 preamble bits over the 7 dB dynamic range. The main conclusion of this is that in a noise-limited optical receiver, the PER can be made arbitrarily small by increasing the preamble length. However, this would not be practical due to the increasing number of resources consumed by the packet detector circuitry as the correlator length increases. Thus, a preamble length of 64 bits is optimal to ensure a PER better than 10^{-2} over the dynamic range of the receiver without significantly reducing the throughput.

A simulation model that can be applied to the study of digital optical receivers was developed. An experimental method to estimate the fundamental parameters of this receiver, namely, the photodiode responsivity R, the TIA gain G_{pd}, and the photodiode

and digitiser noises, σ^2_{rx} and σ^2_{scope}, was devised. It was found that the most significant noise contribution for this receiver is the electrical noise that the high-speed digitiser introduces, which degrades the signal particularly at low received powers. Also, the additive quantisation noise model was found to be accurate for a range of only 5 dB, and deviates markedly for lower received optical powers. The developed model showed good agreement with experimentally validated data at both high and low received optical powers.

The influence of the network load ρ and the traffic model sparsity on the PER was investigated using the aforementioned digital receiver. It was found that the traffic sparsity produces almost no effect on the packet error rate. Also, under the receiver physical layer protocol investigated, reducing the network load improves the performance of the packet detector. Thus, full network load offers a lower bound on the PER performance for this digital receiver.

Digital burst-mode receiver and access networks

Dynamic core optical networks and optical access networks receivers have many things in common due to the packetised nature of both kinds of networks. Thus, the investigation conducted for dynamic core optical networks was extended to include loss-limited optical systems, which is the main characteristic of optical access networks.

In order to facilitate the migration of legacy optical access systems, to reduce costs, and to allow different QoS, it is desirable to allow the coexistence between users working at several line-rates in the same passive optical networks segment. A critical component in this is the upstream burst-mode receiver that is capable of both detecting the optical packet presence and the line-rate. A new multi-rate packet detector, which exploits the orthogonality property of the burst preambles, was developed and experimentally validated.

To carry out multiple line-rate clock and data recovery, two algorithms were considered. The first one, named multi-fractional equaliser, consists of a variable length LMS equaliser that acts as signal filter and interpolator. The second algorithm, named polyphase-receiver, makes use of an *a priori* programmable digital anti-aliasing filter and then decimates the discrete signal into a two-samples-per-bit signal for all line-rates. A simulation modelling showed that the LMS equaliser outperforms slightly the polyphase approach, as the equaliser converges to the optimum Wiener filter. However, the long time required for the equaliser to converge is completely unacceptable in a real burst-mode receiver implementation. In addition, the polyphase CDR is computationally more efficient due to the polyphase decomposition of the anti-aliasing filter.

A dual-rate digital receiver, intended for 10G-EPON and 1G-EPON coexistence, consisting of a packet and line-rate detector and a polyphase CDR was developed and experimentally demonstrated. As stated above, dynamic range and receiver sensitivity

are critical parameters in optical access networks. In order to improve the dynamic range of 7 dB of the digital AC-coupled receiver, a DC-coupled receiver was used and non-linear signal clipping was allowed in the digitiser as a mechanism to extend the dynamic range. The experimental validation of this dual-rate received showed a sensitivity gain of 4.06 dB when receiving 1.25 Gb/s compared with 10 Gb/s, due to digital noise filtering. Also, by means of clipping, the burst-to-burst dynamic ranges was found to be 20.5 dB, a significant 8 dB improvement compared with non-clipped operation. A digitiser offset of 12% was found to be optimum and there was no penalty for 10 Gb/s when switching from continuous-mode to burst-mode operation. However, for the 1.25 Gb/s line-rate, a penalty of 0.6 dB was found and the cause is the residual BLW that affects this line-rate in particular, because the polyphase implementation of the BLW filter produces a variable time constant that is line-rate dependant.

The performance of the packet and line-rate detector was found to be the limiting factor for high received optical powers. The cause of this limitation is the non-linearly generated harmonics by the clipping process, which generate a frequency component that triggers the un-matched line-rate correlator and thus degrades the detector performance independently of the preamble length. Preamble sizes of 16, 32, 48, and 64 bits, referred to 10 Gb/s, were investigated and the PER of the receiver assessed. It was found that a 16 bit preamble is enough to correctly detect both packet presence and line-rate over a dynamic range of 14.5 dB. Thus, the packet and line-rate detector reduces the dynamic range from 20.5 to 14.5 dB, for 10 Gb/s line-rate, as a result of the signal distortion caused by non-linear clipping.

Long-reach optical access networks

Next generation dynamic optical access networks will use WDM techniques and optical amplification to extend the network reach to at least 100 km and to increase the maximum number of users (mainly limited by the splitting loses) per network segment. Several next-generation long-reach network architectures have been proposed and the principal ones found in the literature were reviewed.

A centralised optical processing unit, capable of both consolidating all the packets coming from a current PON segment into an specific wavelength channel for back-haul transmission and equalising the optical power—and thus allow for a receiver dynamic range relaxation—was characterised. This COPU consists of two SOAs that equalise the input optical power, followed by a SOA-MZI wavelength converter.

The experiments carried out showed that optical input powers ranging from -30 to -15 dBm get compressed into a range from -6 to $+1$ dBm by the COPU, which is within the dynamic range of the digital burst-mode receiver. The BER performance of the COPU was investigated for fibre transmission distances of 0 (back-to-back), 22, 40, and 62 km, over uncompensated standard fibre. For these distances, sensit-

ivities of -30.94, -30.17, and -27.26 dBm with overload points of -9.3, -5, and > -5 dBm were found, respectively. A fixed-null threshold slicer, which reduces receiver hardware resources, was found to perform similarly to more complex, variable thresholders.

6.2 Proposed future work

This section proposes some future work guidelines toward the realisation of dynamic optical networks. These recommendations have been split into three separate sections for better readability.

Development of a complete dynamic network testbed

The work carried out in this thesis has focused on the back-to-back investigation of digital receivers by characterising the main effects that arise in dynamical optical networks. However, additional dynamic network and continuous-mode transmission impairments should also be addressed. In order to do that, an improved dynamic optical network testbed should be designed and built in the laboratory. Figure 6.1 shows a possible design of such a testbed. The work carried out in this thesis included the optical burst transmitter and the burst-mode digital receiver.

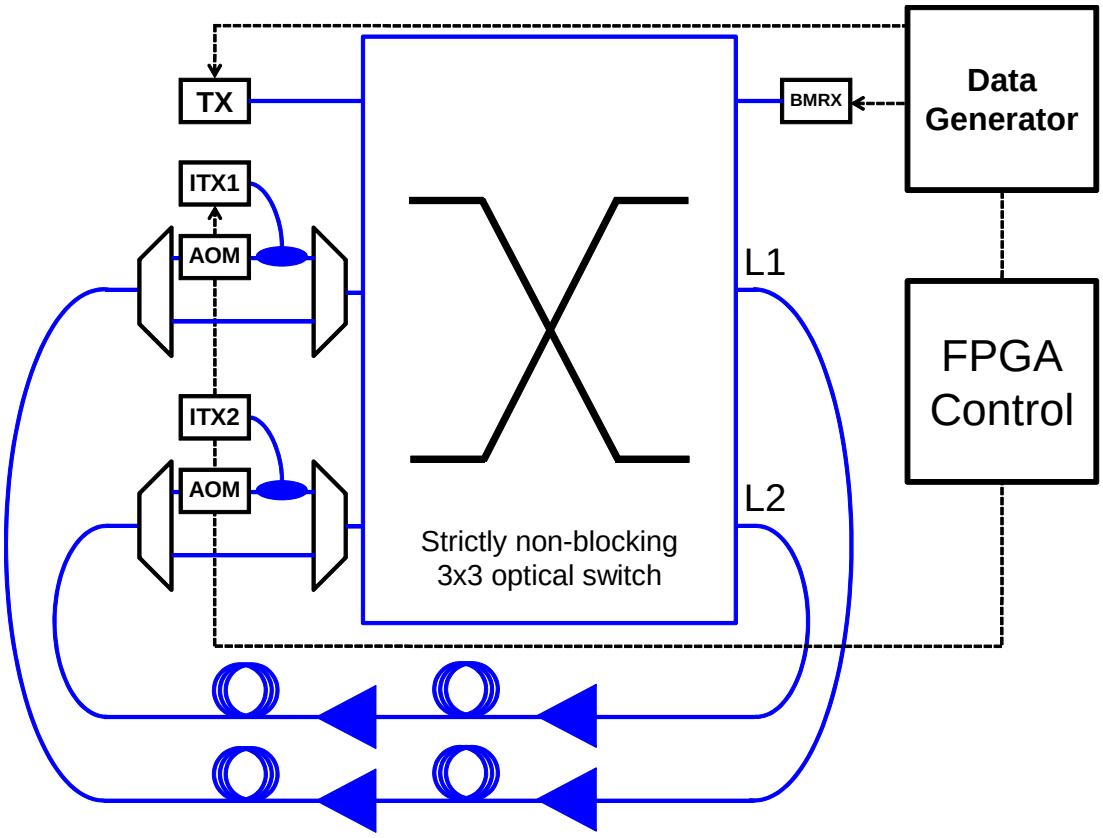

Figure 6.1: Diagram of a proposed dynamic optical network testbed.

The principal component of this testbed is a 3×3 strictly non-blocking optical switch fabric, which substitutes the AOM switches present in a classical optical recirculating loop. This switch fabric can be a crossbar PLZT switch, a SOA broadcast and select, SOA Clos switching matrix, or a wavelength-conversion plus AWG fabric.

The proposed testbed includes two loop branches, each consisting of some Single-Mode Fibre (SMF) optical fibre plus Dispersion Compensating Fibre (DCF). The link optical amplifiers are burst-mode optical amplifiers, such as gain-clamped EDFAs. Gain clamping the EDFAs allows for a simplified timing control of the testbed, because the problem of the loop loading is eliminated. Also, having two loop branches, L_1 and L_2, allows for investigating a diverse optical signal path. However, a simplified approach with just one branch and a 2×2 optical switch would be easier to implement. The multiplexer/demultiplexer at the inputs of the switch fabric allow for the add and drop of an optical dummy wavelength. Using this technique, the power variations that occur every time the optical signal traverses an optical switch can be simulated. The testbed would be controlled with a programmable data generator (such as the Tektronix DG-2030), with the help of an optional FPGA with a look up table to extend the number of channels and thus the number of elements under control.

Introduction of coherent techniques into dynamic optical networks

Coherent optical networks were initially investigated 30 years ago, in order to improve the sensitivity of the point-to-point optical links and thus increase the maximum transmission distance [Yamamoto, 1980]. However, the introduction of the optical amplifier imposed a revolution in the optical networking field, because the transmission distance could be increased by orders of magnitude at a very affordable price. Also, the fundamental limitation was no longer the receiver sensitivity (due to electrical noise) but the optical signal-to-noise ratio due to optical noise introduced by the optical amplifiers.

However, in spite of this, during the last years much research attention has been devoted to investigate high spectrally-efficient optical modulation formats, in order to keep up with the increasing demand for more transmission capacity and to upgrade the currently deployed WDM optical transmission links. As mentioned in the introductory chapter, these complex modulation formats make use of a coherent optical receiver. Typically, the coherent optical receiver consists of a local oscillator, an optical hybrid, a 4-channel high-speed ADC, and digital signal processing [Millar et al., 2010]. Component manufacturers are already developing commercial products that will allow coherent optical systems to become a reality [PMC-Sierra, 2011].

While the work presented in this thesis investigated only the simple OOK modulation format for both the preamble and the payload, it would be an interesting research topic to investigate the suitability of complex modulation formats in packetised dynamic optical networks. DSP in a coherent receiver can compensate for dispersion (no

DCF is needed), PMD, to some extend fibre non-linearities, and also increase the sensitivity. Due to the complex algorithms involved, a long preamble could be required for both detecting the optical packet and to initialise the adaptive equalisers. However, due to the superior spectral efficiency of complex optical modulation formats, more data can be allocated in the payload and, thus, the total network throughput could be kept constant or even being improved.

In summary, it would be very interesting to investigate the packet-error rate of a coherent digital receiver as a function of the preamble length and the fibre propagation distance. This is because most impairments (such as dispersion, PMD and non-linearities) increase with the transmission distance, among other variables as the bit/baud-rate.

High-scale optical component integration into photonic integrated circuits

Finally, the field of dynamic optical networking have been researched for more than two decades. However, dynamic optical networks have not yet become a reality in the form of commercially available off-the-shelf products. The main reason for that is the phenomenal development of electronics, both in electronic switching integrated circuits and in high parallel processing cores, which still comply with Moore's law [Moore, 1965] and are able to cope with the steadily increasing demand for more network bandwidth.

In order to compete with their electronic counterparts, dynamic optical networks should be able to deliver high-speed data at an affordable cost for telecommunication carriers. A key technological issue for lowering component costs is the integration and planar fabrication of many optical components into a single photonic chip [Coldren et al., 2011], and this is particularly important in the high-port count, high switching speed optical switching fabrics—which are essential components for the realisation of OBS and OPS—due to its complexity. Current suitable technologies for OCS already exist, such as Micro-Electro-Mechanical Systems (MEMS) [Yuan et al., 2008] and liquid crystal switches [Sorimoto et al., 2009]. Silicon photonics is a field which is being actively investigated and it is possible that in the medium term future the technology will mature enough to compete in an affordable way with electronics devices [Pavesi, 2003]. A good example of the current development of the integrated photonics field is the MOTOR Photonic Integrated Circuit (PIC) router by the University of Santa Clara, California [Nicholes et al., 2010]. Another example is the SOA switch fabric developed at Cambridge [Wonfor et al., 2011].

Whilst this work has gone some way toward addressing the required burst-mode receiver for dynamic optical networking, there is still some way to go with the development of an optical switching node that can compete with electronics.

References

G. P. Agrawal, *Fiber-Optic Communication Systems*, 3rd ed. Wiley Interscience, 2002. 33, 38, 42, 114

A. Albores-Mejía, K. A. Williams, T. de Vries, E. Smalbrugge, Y. S. Oei, M. K. Smit, and R. Nötzel, "Integrated 2 x 2 quantum dot optical crossbar switch in 1.55 μm wavelength range," *IET Electronic Letters*, vol. 45, no. 6, pp. 313–314, 2009. 40

F.-T. An, K. S. Kim, D. Gutiérrez, S. Yam, E. Hu, K. Shrikhande, and L. G. Kazovsky, "SUCCESS: a next-generation hybrid WDM/TDM optical access network architecture," *IEEE/OSA Journal of Lightwave Technology*, vol. 22, no. 11, pp. 2557–2569, Nov. 2004. 122

J. Aracil, N. Akar, S. Bjornstad, M. Casoni, K. Christodoulopoulos, D. Careglio, J. Fdez-Palacios, C. Gauger, O. G. de Dios, G. Hu, E. Karasan, M. Klinkowski, D. Morató, R. Nejabati, H. Overby, C. Raffaelli, D. Simeonidou, N. Stol, G. Tosi-Beleffi, and K. Vlachos, "Research in optical burst switching within the e-Photon/ONe network of excellence," *Elsevier Optical Switching and Networking*, vol. 4, pp. 1–19, 2007. 16, 36

Y. Awaji, H. Furukawa, B. J. Puttnam, N. Wada, P. Chan, and R. Man, "Burst-mode optical amplifier," in *Proceedings of the Optical Fiber Communication Conference and Exhibition (OFC)*, Mar. 2010, paper OThI4. 39

S. Azodolmolky, M. Klinkowski, E. Marin, D. Careglio, J. S. Pareta, and I. Tomkos, "A survey on physical layer impairments aware routing and wavelength assignment algorithms in optical networks," *Computer Networks*, vol. 53, no. 7, pp. 926–944, May 2009. 15

J. H. Baek, J. H. Hong, M. H. Sunwoo, and K. U. Kim, "Efficient digital baseline wander algorithm and its architecture for fast ethernet," in *IEEE Workshop on Signal Processing Systems (SIPS2004)*, Oct. 2004, pp. 136–141. 63, 106

D. Banerjee and B. Mukherjee, "Wavelength-routed optical networks: linear formulation, resource budgeting tradeoffs, and a reconfiguration study," *IEEE/ACM Transactions on Networking*, vol. 8, no. 5, pp. 598–607, Oct. 2000. 15

S. Baroni and P. Bayvel, "Wavelength requirements in arbitrarily connected wavelength-routed optical networks," *IEEE/OSA Journal of Lightwave Technology*, vol. 15, no. 2, pp. 242–251, Feb. 1997. 15, 19, 27

T. Battestilli and H. Perros, "An introduction to optical burst switching," *IEEE Communications Magazine*, vol. 41, no. 8, pp. S10–S15, Aug. 2003. 16, 29

P. Bayvel and M. Düser, "Optical burst switching: research and applications," in *Proceedings of the Optical Fiber Communication Conference and Exhibition (OFC)*, Feb. 2004, paper FO1. 17, 29, 51

S. J. Ben Yoo, "Wavelength conversion technologies for WDM network applications," *IEEE/OSA Journal of Lightwave Technology*, vol. 14, no. 6, pp. 955–966, Jun. 1996. 124

——, "Optical packet and burst switching technologies for the future photonic internet (Invited)," *IEEE/OSA Journal of Lightwave Technology*, vol. 24, no. 12, pp. 4468–4492, Dec. 2006. 15, 24, 25, 26, 28

Y. Benlachtar, S. J. Savory, B. C. Thomsen, G. Gavioli, P. Bayvel, and R. I. Killey, "Robust long-haul transmission utilizing electronic precompensation and MLSE equalization," in *Proceedings of the Optical Fiber Communication Conference and Exhibition (OFC)*, Anaheim, CA, USA, 2007, paper JWA52. 52

Y. Benlachtar, P. M. Watts, R. Bouziane, P. Milder, D. Rangaraj, A. Cartolano, R. Koutsoyannis, J. C. Hoe, M. Püschel, M. Glick, and R. I. Killey, "Generation of optical OFDM signals using 21.4 GS/s real time digital signal processing," *OSA Optics Express*, vol. 17, no. 20, pp. 17 658–17 668, Sep. 2009. 14

N. S. Bergano, F. W. Kerfoot, and C. R. Davidson, "Margin measurements in optical amplifier system," *IEEE Photonics Technology Letters*, vol. 5, no. 3, pp. 304–306, Mar. 1993. 33

J. Berthold, "Optical networking: Past, present, and future," *IEEE/OSA Journal of Lightwave Technology*, vol. 1, 1959, no. 9, pp. 269–1118, May 2008. 15, 16

A. Bianciotto, B. J. Puttnam, B. C. Thomsen, and P. Bayvel, "Optimization of wavelength-locking loops for fast tunable laser stabilization in dynamic optical networks," *IEEE/OSA Journal of Lightwave Technology*, vol. 27, no. 12, pp. 2117–2124, Jun. 2009. 37

D. J. Blumenthal, B.-E. Olsson, G. Rossi, T. E. Dimmick, L. Rau, M. Masanovic, O. Lavrova, R. Doshi, O. Jerphagnon, J. E. Bowers, V. Kaman, L. A. Coldren, and J. Barton, "All-optical label swapping networks and technologies," *IEEE/OSA Journal of Lightwave Technology*, vol. 18, no. 12, pp. 2058–2075, Dec. 2000. 15, 16, 28

D. J. Blumenthal, J. E. Bowers, L. Rau, H. F. Chou, S. Rangarajan, W. Wang, and K. N. Poulsen, "Optical signal processing for optical packet switching networks," *IEEE Communications Magazine*, vol. 41, no. 2, pp. S23–S29, Feb. 2003. 16

R. Bonk, P. Vorreau, D. Hillerkuss, W. Freude, G. Zarris, D. Simeonidou, F. Parmigiani, P. Petropoulos, R. Weerasuriya, S. Ibrahim, A. D. Ellis, D. Klonidis, I. Tomkos, and J. Leuthold, "An all-optical grooming switch for interconnecting access and metro ring networks (Invited)," *IEEE/OSA Journal of Optical Communications and Networking*, vol. 3, no. 3, pp. 206–214, Mar. 2011. 27

M. S. Borella, J. P. Jue, D. Banerjee, B. Ramamurthy, and B. Mukherjee, "Optical components for WDM lightwave networks," *Proceedings of the IEEE*, vol. 85, no. 8, pp. 1274–1307, Aug. 1997. 43

H. Buchta and E. Patzak, "Analysis of the physical impairments on maximum size and throughput of SOA-based optical burst switching nodes," *IEEE/OSA Journal of Lightwave Technology*, vol. 26, no. 13–16, pp. 2821–2830, Jul. 2008. 18, 36, 41

H. Buchta, C. M. Gauger, and E. Patzak, "Maximum size and throughput of SOA-based optical burst switching nodes with limited tuning-range wavelength converters and FDL buffers," *IEEE/OSA Journal of Lightwave Technology*, vol. 26, no. 13–16, pp. 2919–2927, Jul. 2008. 36

J. Buus and E. J. Murphy, "Tunable lasers in optical networks," *IEEE/OSA Journal of Lightwave Technology*, vol. 24, no. 1, pp. 5–11, Jan. 2006. 37

B. Cao, J. M. Delgado Mendinueta, J. E. Mitchell, and B. C. Thomsen, "Performance of an optical equaliser in a 10 Gbit/s wavelength converting optical access networks," in *Proceedings of the 37th European Conference and Exhibition on Optical Communications (ECOC)*, Geneva, Switzerland, Sep. 2011, paper Mo.1.C.1. 22, 123

B. Cao, D. P. Shea, and J. E. Mitchell, "Wavelength converting optical access network for 10 Gbit/s PON," in *Proceedings of the 15th International Conference on Optical Network Design and Modeling (ONDM 2011)*, Feb. 2011. 123, 124, 125, 126

S. Chandrasekhar and D. Kilper, "Using testbeds for optically-transparent mesh network experimentation (Invited)," in *IEEE LEOS Annual Meeting Conference Proceedings*, Oct. 2006, pp. 771–772. 34

Y. F. Chang, "Uplink burst-mode transmissions using EPON physical-layer chipset for broadband optical Ethernet access networks," *OSA Journal of Optical Networking*, vol. 6, no. 7, p. 937, 2007. 44

S.-Y. Cheng and J. B. Evans, "Implementation of signal power estimation methods," *IEEE Transactions on Circuits and Systems II: Analog and Digital Signal Processing*, vol. 44, no. 3, pp. 240–250, Mar. 1997. 61

M. C. Chia, D. K. Hunter, I. Andonovic, P. Ball, and I. Wright, "Optical packet switches: A comparison of designs," in *Proceedings of the IEEE International Conference on Networks (ICON)*, Sep. 2000, pp. 365–369. 41

M. C. Chia, D. K. Hunter, I. Andonovic, P. Ball, I. Wright, S. P. Ferguson, K. M. Guild, and M. J. O'Mahony, "Packet loss and delay performance of feedback and feed-forward arrayed-waveguide gratings-based optical packet switches with WDM inputs-outputs," *IEEE/OSA Journal of Lightwave Technology*, vol. 19, no. 9, pp. 1241–1254, Sep. 2001. 40

D. Chiaroni, M. Sotom, C. Chauzat, D. D. Bouard, F. Masetti, J. C. Jacquinot, J. L. Moncelet, M. Bachmann, P. Doussirire, M. Goix, and E. Grard, "Feasibility issues of a high-speed photonic packet switching fabric based on WDM subnanosecond optical gates," in *Proceedings of the 22nd European Conference and Exhibition on Optical Communications (ECOC)*, vol. 4, Oslo, 1996, paper ThD.1.7, pp. 127–130. 40

I. Chlamtac, A. Ganz, and G. Karmi, "Lightpath communications: an approach to high bandwidth optical WAN's," *IEEE Transactions on Communications*, vol. 40, no. 7, pp. 1171–1182, Jul. 1992. 15

R. Choy and A. Edelman, "Parallel MATLAB: Doing it right," *Proceedings of the IEEE*, vol. 93, no. 2, pp. 331–341, Feb. 2005. 66, 67

H. S. Chung, R. Inohara, K. Nishimura, and M. Usami, "All-optical multi-wavelength conversion of 10 Gbit/s NRZ/RZ signals based on SOA-MZI for WDM multicasting," *Electronics Letters*, vol. 41, no. 7, pp. 432–433, Mar. 2005. 124

Cisco Systems, "Cisco CRS-1 multishelf system," Sep. 2011. [Online]. Available: http://www.cisco.com/en/US/products/ps5842/index.html 15

L. A. Coldren, "Monolithic tunable diode lasers," *IEEE Journal of Selected Topics in Quantum Electronics*, vol. 6, no. 6, pp. 988–999, Nov. 2000. 37

L. A. Coldren, S. C. Nicholes, L. Johansson, S. Ristic, R. S. Guzzon, E. J. Norberg, and U. Krishnamachari, "High performance InP-based photonic ICs — A tutorial," *IEEE/OSA Journal of Lightwave Technology*, vol. 29, no. 4, pp. 554–570, Feb. 2011. 139

R. E. Crochiere and L. R. Rabiner, "Interpolation and decimation of digital signals — A tutorial review," *Proceedings of the IEEE*, vol. 69, no. 3, pp. 300–331, Mar. 1981. 59

R. E. Crochiere, L. R. Rabiner, and R. R. Shively, "A novel implementation of digital phase shifters," *Bell System Technical Journal*, vol. 54, no. 8, pp. 1497–1502, Oct. 1975. 59

S. L. Danielsen, P. B. Hansen, K. E. Stubkjaer, M. Schilling, K. Wunstel, W. Idler, P. Doussiere, and F. Pommerau, "All optical wavelength conversion schemes for increased input power dynamic range," *IEEE Photonics Technology Letters*, vol. 10, no. 1, pp. 60–62, Jan. 1998. 124

R. Davey, T. D. Ridder, X.-Z. Qiu, P. Ossieur, H. Krimmel, D. Smith, L. Lealman, A. Poustie, G. Talli, C. Chow, P. Townsend, S. Randel, and H. Rohde, "Progress in IST project PIEMAN towards a 10 Gbit/s, multi-wavelength long reach PON," in *Proceedings of BroadBand Europe Conference*, 2006, paper Th3A3. 38

I. Dedic, "56GS/s ADC: Enabling 100GbE," in *Proceedings of the Optical Fiber Communication Conference and Exhibition (OFC)*, Mar. 2010. 14

J. M. Delgado Mendinueta, P. Bayvel, and B. C. Thomsen, "Impact of burst header length in the performance of a 10 Gb/s digital burst mode receiver," in *Proceedings of the Optical Fiber Communication Conference and Exhibition (OFC)*, Mar. 2009, paper OWA7. 22

——, "Dynamic optical networks demonstrators: Reviewed and classified," in *London Communications Symposium (LCS)*, London, U. K., Sep. 2009. 22

——, "Impact of network load and traffic sparsity on the performance of a digital burst-mode receiver," in *Proceedings of the 36th European Conference and Exhibition on Optical Communications (ECOC)*, Sep. 2010. 22

——, "Cluster processing for the study of optical burst-mode digital signal processing receivers and subsystems for dynamic optical burst switching networks," in *5th International Conference on Broadband Communications, Networks and Systems (BROADNETS)*, Sep. 2008, pp. 77–81. 22

——, "Digital lightwave receivers: An experimentally validated system model," *IEEE Photonics Technology Letters*, vol. 23, no. 6, pp. 338–340, Mar. 2011. 22, 108, 109

J. M. Delgado Mendinueta, B. Cao, B. C. Thomsen, and J. E. Mitchell, "Performance of an optical equaliser in a 10G wavelength converting optical access network," *OSA Optics Express*, vol. 19, no. 26, pp. B229–B234, Dec. 2011. 21

J. M. Delgado Mendinueta, J. E. Mitchell, P. Bayvel, and B. C. Thomsen, "Digital multi-rate receiver for 10GE-PON and GE-PON coexistence," in *Proceedings of the Optical Fiber Communication Conference and Exhibition (OFC)*, Los Angeles, CA, Mar. 2011, paper NTuD4. 22

——, "Digital dual-rate burst-mode receiver for 10G and 1G coexistence in optical access networks," *OSA Optics Express*, vol. 19, no. 15, pp. 14 060–14 066, Jul. 2011. 22

T. Durhuus, C. Joergensen, B. Mikkelsen, R. J. S. Pedersen, and K. E. Stubkjaer, "All optical wavelength conversion by SOA's in a Mach-Zehnder configuration," *IEEE Photonics Technology Letters*, vol. 6, no. 1, pp. 53–55, Jan. 1994. 124

M. Düser and P. Bayvel, "Analysis of a dynamically wavelength-routed optical burst switched network architecture," *IEEE/OSA Journal of Lightwave Technology*, vol. 20, no. 4, pp. 574–585, Apr. 2002. 37

M. Düser, "Investigation of advanced optical packet-routed network architectures," Ph.D. dissertation, Department of Electronic and Electrical Engineering, University College London (UCL), Jan. 2003. 16, 19, 27, 28, 32, 37

F. Effenberger, D. Clearly, O. Haran, G. Kramer, R. D. Li, M. Oron, and T. Pfeiffer, "An introduction to PON technologies," *IEEE Communications Magazine*, vol. 45, no. 3, pp. S17–S25, Mar. 2007. 43

F. Effenberger and T. S. El-Bawab, "Passive optical networks (PONs): Past, present, and future," *Elsevier Optical Switching and Networking*, vol. 6, no. 3, pp. 143–150, 2009. 18, 43, 86, 87

T. S. El-Bawab, Ed., *Optical Switching*, 1st ed. Springer, 2006. 24, 25, 39

C. A. Eldering, "Theoretical determination of sensitivity penalty for burst mode fiber optic receivers," *IEEE/OSA Journal of Lightwave Technology*, vol. 11, no. 12, pp. 2145–2149, Dec. 1993. 41

L. Erup, F. M. Gardner, and R. A. Harris, "Interpolation in digital modems—Part II: Implementation and performance," *IEEE Transactions on Communications*, vol. 41, no. 6, pp. 998–1008, Jun. 1993. 59, 60, 100, 105, 127

H. Esmaeilzadeh, E. Blem, R. S. Amant, K. Sankaralingam, and D. Burger, "Dark silicon and the end of multicore scaling," in *Proceedings of the 38th International Symposium on Computer Architecture*, Jun. 2011. 15

C. W. Farrow, "A continuously variable digital delay element," in *IEEE International Symposium on Circuits and Systems*, Jun. 1988. 59

C. R. S. Fludger, T. Duthel, D. van den Borne, C. Schulien, E.-D. Schmidt, T. Wuth, J. Geyer, E. De Man, K. Giok-Djan, and H. de Waardt, "Coherent equalization and POLMUX-RZ-DQPSK for robust 100-GE transmission," *IEEE/OSA Journal of Lightwave Technology*, vol. 26, no. 1, pp. 64–72, Jan. 2008. 51

I. Foster, *Designing and Building Parallel Programs*. Addison-Wesley, 1995. 67

P. Gambini, M. Renaud, C. Guillemot, F. Callegati, I. Andonovic, B. Bostica, D. Chiaroni, G. Corazza, S. L. Danielsen, P. Gravey, P. B. Hansen, M. Henry, C. Janz, A. Kloch, R. Krähenbühl, C. Raffaelli, M. Schilling, A. Talneau, and L. Zucchelli, "Transparent optical packet switching: Network architecture and demonstrators in the KEOPS project," *IEEE Journal on Selected Areas in Communications*, vol. 16, no. 7, pp. 1245–1259, Sep. 1998. 29

F. M. Gardner, "Interpolation in digital modems—Part I: Fundamentals," *IEEE Transactions on Communications*, vol. 41, no. 3, pp. 501–507, Mar. 1993. 59, 97, 98, 105

——, *Phaselock Techniques*, 3rd ed. Wiley-Interscience, Jul. 2005. 59

C. A. Gauger, H. Buchta, and E. Patzak, "Integrated evaluation of performance and technology-throughput of optical burst switching nodes under dynamic traffic," *IEEE/OSA Journal of Lightwave Technology*, vol. 26, no. 13, pp. 1969–1979, Jul. 2008. 36

D. Geer, "Chip makers turn to multicore processors," *Computer*, vol. 38, no. 5, pp. 11–13, May 2005. 15

A. Gerber and R. Doverspike, "Traffic types and growth in backbone networks," in *Proceedings of the Optical Fiber Communication Conference and Exhibition (OFC)*, Mar. 2011. 14

A. H. Gnauck, P. J. Winzer, S. Chandrasekhar, X. Liu, B. Zhu, and D. W. Peckham, "Spectrally efficient long-haul WDM transmission using 224-Gb/s polarization-multiplexed 16-QAM," *IEEE/OSA Journal of Lightwave Technology*, vol. 29, no. 4, pp. 373–377, Feb. 2011. 14

P. E. Green, *Fiber to the Home. The New Empowerment*, 1st ed. Wiley-Interscience, 2006. 30, 87, 88

J. Gripp, J. E. Simsarian, J. D. LeGrange, P. G. Bernasconi, and D. T. Neilson, "Architectures, components, and subsystems for future optical packet switches," *IEEE Journal of Selected Topics in Quantum Electronics*, vol. 16, no. 5, pp. 1394–1404, Sep. 2010. 40

C. Guillemot, M. Renaud, P. Gambini, C. Janz, I. Andonovic, R. Bauknecht, B. Bostica, M. Burzio, F. Callegati, M. Casoni, D. Chiaroni, F. Clérot, S. L. Danielsen, F. Dorgeuille, A. Dupas, A. Franzen, P. B. Hansen, D. K. Hunter, A. Kloch, R. Krähenbühl, B. Lavigne, A. L. Corre, C. Raffaelli, M. Schilling, J.-C. Simon, and L. Zucchelli, "Transparent optical packet switching: The european ACTS KEOPS project approach," *IEEE/OSA Journal of Lightwave Technology*, vol. 16, no. 12, pp. 2117–2134, Dec. 1998. 28

K. Hara, S. Kimura, H. Nakamura, N. Yoshimoto, and H. Hadama, "New AC-coupled burst-mode optical receiver using transient-phenomena cancellation techniques for 10 Gbit/s-class high-speed TDM-PON systems," *IEEE/OSA Journal of Lightwave Technology*, vol. 28, no. 19, pp. 2775–2782, Oct. 2010. 47, 48

S. Haykin, "Cognitive radio: brain-empowered wireless communications," *IEEE Journal on Selected Areas in Communications*, vol. 23, no. 2, pp. 201–220, Feb. 2005. 19

——, *Communications Systems*, 4th ed. Wiley, 2001. 55

——, *Adaptive Filter Theory*, 4th ed. Prentice Hall, 2002. 64, 96

W.-P. Huang, X. Li, C.-Q. Xu, X. Hong, C. Xu, and W. Liang, "Optical transceivers for fiber-to-the-premises applications: System requirements and enabling technologies," *IEEE/OSA Journal of Lightwave Technology*, vol. 25, no. 1, pp. 11–27, Jan. 2007. 30, 44

D. K. Hunter and I. Andonovic, "Approaches to optical internet packet switching," *IEEE Communications Magazine*, vol. 38, no. 9, pp. 116–122, Sep. 2000. 15

E. Hyytiä, "Heuristic algorithms for the generalized routing and wavelength assignment problem," in *Proceedings of the Seventeenth Nordic Teletraffic Seminar (NTS-17)*, Fornebu, Norway, Aug. 2004. 15

Amendment 1: Physical Layer Specifications and Management Parameters for 10 Gb/s Passive Optical Networks, IEEE Standard 802.3av-2009, Oct. 2009. [Online]. Available: http://standards.ieee.org/about/get/802/802.3.html 43

Part 3: Carrier sense multiple access with Collision Detection (CSMA/CD) Access Method and Physical Layer Specifications, IEEE Standard 802.3-2008, Dec. 2008. [Online]. Available: http://standards.ieee.org/about/get/802/802.3.html 43

E. Igawa, M. Nogami, N. Ohata, N. Suzuki, and J. Nakagawa, "Symmetric 10G-EPON ONU tranceiver integrated with newly-developed burst-mode pre-bias timing control IC," in *Proceedings of the Optical Fiber Communication Conference and Exhibition (OFC)*, Mar. 2010, paper NMC1. 48

E. Ip, A. P. T. Lau, D. J. F. Barros, and J. M. Kahn, "Coherent detection in optical fiber systems," *OSA Optics Express*, vol. 16, no. 2, pp. 753–791, Jan. 2008. 14

Gigabit-capable passive optical networks (GPON): General characteristics, ITU-T Recommendation G.984.1, Mar. 2008. [Online]. Available: http://www.itu.int/rec/T-REC-G.984.1/en 43

P. Jaranowski and A. Królak, "Gravitational-wave data analysis. Formalism and sample applications: The gaussian case," *Living Reviews in Relativity*, vol. 8, no. 3, Mar. 2005. [Online]. Available: http://www.livingreviews.org/lrr-2005-3 55

V. Jayaraman, Z.-M. Chuang, and L. Coldren, "Theory, design, and performance of extended tuning range semiconductor lasers with sampled gratings," *IEEE Journal of Quantum Electronics*, vol. 29, no. 6, pp. 1824–1834, Jun. 1993. 37

M. C. Jeruchim, "Techniques for estimating the bit error rate in the simulation of digital communication systems," *IEEE Journal on Selected Areas in Communications*, vol. SAC–2, no. 1, pp. 153–170, Jan. 1984. 66, 67, 82

J. P. Jue, W. H. Yang, Y. C. Kim, and Q. Zhang, "Optical packet and burst switched networks: A review," *IET Communications*, vol. 3, no. 3, pp. 334–352, Mar. 2009. 15, 16

J. Kaiser and R. Schafer, "On the use of the I_0-sinh window for spectrum analysis," *IEEE Transactions on Acoustics, Speech and Signal Processing*, vol. 28, no. 1, pp. 105–107, Feb. 1980. 99

M. Kawai, H. Watanabe, T. Ohtsuka, and K. Yamaguchi, "Smart optical receiver with automatic decision threshold setting and retiming phase alignment," *IEEE/OSA Journal of Lightwave Technology*, vol. 7, no. 11, pp. 1634–1640, Nov. 1989. 9, 41, 64, 106, 127

M. Klinkowski, M. Pióro, D. Careglio, M. Marciniak, and J. Solé-Pareta, "Non-linear optimization for multi-path source routing in OBS networks," *IEEE Communications Letters*, vol. 11, no. 12, pp. 1016–1018, Dec. 2007. 66

A. M. J. Koonen, N. Yan, J. J. Vegas Olmos, I. T. Monroy, C. Peucheret, E. Van Breusegem, and E. Zouganeli, "Label-controlled optical packet routing—Technologies and applications," *IEEE Journal of Selected Topics in Quantum Electronics*, vol. 13, no. 5, pp. 1540–1550, Sep. 2007. 16

G. Kramer, "10G-EPON: Drivers, challenges, and solutions," in *Proceedings of the 35th European Conference and Exhibition on Optical Communications (ECOC)*, Vienna, Austria, Sep. 2009, paper 5.7.2. 43, 51

B. Krogfoss, G. Hanson, and R. J. Vale, "Impact of consumer traffic growth on mobile and fixed networks: Business model and network quality impact," *Bell Labs Technical Journal*, vol. 16, no. 1, pp. 105–120, 2011. 14

J.-W. Kwon, J.-H. Lee, J.-M. Baek, J.-C. Cho, J.-W. Seo, S.-S. Park, J.-K. Lee, Y.-K. Oh, and D.-H. Jang, "AC-coupled burst-mode OLT SFP transceiver for gigabit ethernet PON systems," *IEEE Photonics Technology Letters*, vol. 17, no. 7, pp. 1519–1521, Jul. 2005. 47

J. P. R. Lacey, G. J. Pendock, and R. S. Tucker, "All-optical 1300-nm to 1550-nm wavelength conversion using cross-phase modulation in a semiconductor optical amplifier," *IEEE Photonics Technology Letters*, vol. 8, no. 7, pp. 885–887, Jul. 1996. 125

D. Lavery, E. Torrengo, and S. Savory, "Bidirectional 10 Gbit/s long-reach WDM-PON using digital coherent receivers," in *Proceedings of the Optical Fiber Communication Conference and Exhibition (OFC)*, Mar. 2011, paper OTuB4. 14

D. Lavery, M. Ionescu, S. Makovejs, E. Torrengo, and S. J. Savory, "A long-reach ultra-dense 10 Gbit/s WDM-PON using a digital coherent receiver," *OSA Optics Express*, vol. 18, no. 25, pp. 25 855–25 860, Dec. 2010. 121

J. A. Lázaro, J. Prat, P. Chanclou, G. M. Tosi Beleffi, A. Teixeira, I. Tomkos, R. Soila, and V. Koratzinos, "Scalable extended reach PON," in *Proceedings of the Optical Fiber Communication Conference and Exhibition (OFC)*, Feb. 2008, paper OThL2. 122

S.-H. Lee, J. Kim, Q. Le, M. Lee, H. Kim, and C.-S. Park, "A single-chip 2.5-Gb/s burst-mode optical receiver with wide dynamic range," *IEEE Photonics Technology Letters*, vol. 23, no. 2, pp. 85–87, Jan. 2011. 47, 48

S. J. Lee, "A new non-data-aided feedforward symbol timing estimator using two samples per symbol," *IEEE Communications Letters*, vol. 6, no. 5, pp. 205–207, May 2002. 60, 97, 105

B. Li, L. S. Tamil, D. Wolfe, and J. Plessa, "10 Gbps burst-mode optical receiver based on active phase injection and dynamic threshold level sett," *IEEE Communications Letters*, vol. 10, no. 10, pp. 722–724, Oct. 2006. 47

X. Liu, D. M. Gill, and S. Chandrasekhar, "Optical technologies and techniques for high bit rate fiber transmission," *Bell Labs Technical Journal*, vol. 11, no. 2, pp. 83–104, 2006. 39

G. Luo, J. L. Zyskind, J. A. Nagel, and M. A. Ali, "Experimental and theoretical analysis of relaxation-oscillations and spectral hole burning effects in all-optical gain-clamped EDFA's for WDM networks," *IEEE/OSA Journal of Lightwave Technology*, vol. 16, no. 4, pp. 527–533, Apr. 1998. 38

J. P. Mack, H. N. Poulsen, E. F. Burmeister, B. Stamenic, G. Kurczveil, J. E. Bowers, and D. J. Blumenthal, "Demonstration of contention resolution for labeled packets at 40 Gb/s using autonomous optical buffers," in *Proceedings of the Optical Fiber Communication Conference and Exhibition (OFC)*, Mar. 2009. 29

M. Maier, M. Herzog, and M. Reisslein, "STARGATE: The next evolutionary step toward unleashing the potential of WDM EPONs," *IEEE Communications Magazine*, vol. 45, no. 5, pp. 50–56, May 2007. 122

M. Maier, *Optical Switching Networks*, 1st ed. Cambridge University Press, 2008. 24, 25, 28

——, "WDM passive optical networks and beyond: the road ahead (Invited)," *OSA Journal of Optical Networking*, vol. 1, no. 4, pp. 1–16, Aug. 2009. 121

D. G. Manolakis, V. K. Ingle, and S. M. Kogon, *Statistical and Adaptive Signal Processing*, 1st ed. Artech House, 2005. 61

D. Marco and D. L. Neuhoff, "The validity of the additive noise model for uniform scalar quantizers," *IEEE Transactions on Information Theory*, vol. 51, no. 5, pp. 1739–1755, May 2005. 76, 79

F. Masetti, D. Chiaroni, R. Dragnea, R. Robotham, and D. Zriny, "High-speed high-capacity packet-switching fabric: a key system for required flexibility and capacity (Invited)," *OSA Journal of Optical Networking*, vol. 2, no. 7, pp. 255–265, Jul. 2003. 40

(2009, Aug.) MATLAB and Simulink for Technical Computing. The MathWorks, Inc. [Online]. Available: http://www.mathworks.com 66

C. F. Mélange, X. Yin, B. Baekelandt, T. D. Ridder, X.-Z. Qiu, J. Bauwelinck, J. Gillis, P. Demuytere, and J. Vandewege, "Fully DC-coupled 10Gb/s burst-mode PON prototypes and upstream experiments with 58ns overhead," in *Proceedings of the Optical Fiber Communication Conference and Exhibition (OFC)*, Mar. 2010, paper OWX2. 47, 48

H. Meyr, M. Moeneclaey, and S. A. Fechtel, *Digital Communication Receivers: Synchronization, Channel Estimation, and Signal Processing*, 1st ed. Wiley-Interscience, Oct. 1997, vol. 2. 19, 32

V. Mikhailov, "Investigation of high-speed wavelength-division-multiplexed (WDM) optical fibre transmission systems and devices using recirculating loop techniques," Ph.D. dissertation, Department of Electronic and Electrical Engineering, University College London (UCL), Sep. 2003. 33

D. S. Millar, S. Makovejs, C. Behrens, S. Hellerbrand, R. I. Killey, P. Bayvel, and S. J. Savory, "Mitigation of fiber nonlinearity using a digital coherent receiver," *IEEE Journal of Selected Topics in Quantum Electronics*, vol. 16, no. 5, pp. 1217–1226, Sep. 2010. 138

Y. Miyazaki, T. Miyahara, K. Takagi, K. Matsumoto, S. Nishikawa, T. Hatta, T. Aoyagi, and K. Motoshima, "Polarization-insensitive SOA-MZI monolithic all-optical wavelength converter for full C-band 40Gbps-NRZ operation," in *Proceedings of the 32nd European Conference and Exhibition on Optical Communications (ECOC)*, Sep. 2006. 128

E. Modiano and A. Narula-Tam, "Mechanisms for providing optical bypass in WDM-based networks," *SPIE Optical Networks*, vol. 1, pp. 9–16, Jan. 2000. 15

I. T. Monroy, E. van Breusegem, A. M. J. Koonen, J. J. Vegas Olmos, J. van Berkel, J. Jennen, C. Peucheret, and E. Zouganeli, "Optical label switched networks: laboratory trial and network emulator in the IST-STOLAS project," *IEEE Communications Magazine*, vol. 44, no. 8, pp. 43–51, Aug. 2006. 28

G. E. Moore, "Cramming more components onto integrated circuits," *Electronics*, vol. 38, no. 8, pp. 114–117, Apr. 1965. 139

T. Myouraku, S. Takahashi, and A. Tajima, "AC-coupled reset-less 10 Gbps burst-mode 3R receiver using an internal scrambling scheme," in *Proceedings of the Optical Fiber Communication Conference and Exhibition (OFC)*, Mar. 2011, paper NTuD3. 47, 48

J. Nakagawa, M. Noda, N. Suzuki, S. Yoshima, K. Nakura, and M. Nogami, "Demonstration of 10G-EPON and GE-PON coexisting system employing dual-rate burst-mode 3R transceiver," *IEEE Photonics Technology Letters*, vol. 22, no. 24, pp. 1841–1843, Dec. 2010. 48

J. Nakagawa, M. Nogami, N. Suzuki, M. Noda, S. Yoshima, and H. Tagami, "10.3-Gb/s burst-mode 3R receiver incorporating full AGC optical receiver and 82.5-GS/s over-sampling CDR for 10G-EPON systems," *IEEE Photonics Technology Letters*, vol. 22, no. 7, pp. 471–473, Apr. 2010. 48

——, "10.3Gb/s burst-mode 3R receiver incorporating full AGC optical receiver and 82.5GS/s sampling CDR for 10G-EPON systems," in *Proceedings of the 35th European Conference and Exhibition on Optical Communications (ECOC)*, Vienna, Austria, Sep. 2009. 48

J. Nakagawa, M. Noda, N. Suzuki, S. Yoshima, K. Nakura, and M. Nogami, "First demonstration of 10G-EPON and GE-PON co-existing system employing dual-rate burst-mode 3R transceiver," in *Proceedings of the Optical Fiber Communication Conference and Exhibition (OFC)*, Mar. 2010, paper PDPD10. 47, 48, 85, 86

M. Nakamura, N. Ishihara, and Y. Akazawa, "A 156-Mb/s CMOS optical receiver for burst-mode transmission," *IEEE Journal of Solid-State Circuits*, vol. 33, no. 8, pp. 1179–1187, Aug. 1998. 48

M. Nakamura, Y. Imai, Y. Umeda, J. Endo, and Y. Akatsu, "1.25-Gb/s burst-mode receiver ICs with quick response for PON systems," *IEEE Journal of Solid-State Circuits*, vol. 40, no. 12, pp. 2680–2688, Dec. 2005. 45, 47, 48

S. C. Nicholes, M. L. Masanovic, B. Jevremovic, E. Lively, L. A. Coldren, and D. J. Blumenthal, "The world's first InP 8×8 monolithic tunable optical router (MOTOR) operating at 40 Gbps line rate per port (Postdeadline)," in *Proceedings of the Optical Fiber Communication Conference and Exhibition (OFC)*, Mar. 2009, paper PDPB1. 40

——, "An 8×8 InP monolithic tunable optical router (MOTOR) packet forwarding chip," *IEEE/OSA Journal of Lightwave Technology*, vol. 28, no. 4, pp. 641–650, Feb. 2010. 139

S. Nishihara, S. Kimura, T. Yoshida, M. Nakamura, J. Terada, K. Nishimura, K. Kishine, K. Kato, Y. Ohtomo, N. Yoshimoto, T. Imai, and M. Tsubokawa, "A burst-mode 3R receiver for 10-Gbit/s PON systems with high sensitivity, wide dynamic range, and fast response," *IEEE/OSA Journal of Lightwave Technology*, vol. 26, no. 1, pp. 99–107, Jan. 2008. 47, 48

V. O'Byrne, "Verizon's fiber-to-the-premises and lessons learned," in *Proceedings of the Optical Fiber Communication Conference and Exhibition (OFC)*, Mar. 2010. 14

M. Oerder and H. Meyr, "Digital filter and square timing recovery," *IEEE Transactions on Communications*, vol. 36, no. 5, pp. 605–612, May 1988. 75, 105

Y.-H. Oh, S.-G. Lee, Q. Le, H.-Y. Kang, and T.-W. Yoo, "A CMOS burst-mode optical transmitter for 1.25-Gb/s ethernet PON applications," *IEEE Transactions on Circuits and Systems II: Express Briefs*, vol. 52, no. 11, pp. 780–783, Nov. 2005. 37

Y. Ohtomo, H. Kamitsuna, H. Katsurai, K. Nishimura, M. Nogawa, M. Nakamura, S. Nishihara, T. Kurosaki, T. Ito, and A. Okada, "High-speed circuit technology for 10-Gb/s optical burst-mode transmission," in *Proceedings of the Optical Fiber Communication Conference and Exhibition (OFC)*, Mar. 2010, paper OWX1. 44, 45, 47, 48

M. J. O'Mahony, C. Politi, D. Klonidis, R. Nejabati, and D. Simeonidou, "Future optical networks," *IEEE/OSA Journal of Lightwave Technology*, vol. 24, no. 12, pp. 4684–4696, Dec. 2006. 28

M. J. O'Mahony, D. Simeonidou, D. K. Hunter, and A. Tzanakaki, "The application of optical packet switching in future communication networks," *IEEE Communications Magazine*, vol. 39, no. 3, pp. 128–135, Mar. 2001. 28

M. J. O'Mahony, C. T. Politi, and G. Hill, "Roadmap on optical transport network technologies," in *Proceedings of the 10th International Conference on Transparent Optical Networks (ICTON)*, vol. 1, Athens, Greece, Jun. 2008, pp. 165–168. 15

A. V. Oppenheim, A. S. Willsky, and S. Hamid, *Signals and Systems*, 2nd ed. Prentice Hall, 1996. 58, 98, 99

P. Ossieur, D. Verhulst, Y. Martens, W. Chen, J. Bauwelinck, X. Z. Qiu, and J. Vandewege, "A 1.25-Gb/s burst-mode receiver for GPON applications," *IEEE Journal of Solid-State Circuits*, vol. 40, no. 5, pp. 1180–1189, May 2005. 47, 48, 51

P. Ossieur, T. D. Ridder, J. Bauwelinck, C. Mélange, B. Baekelandt, X.-Z. Qiu, J. Vandewege, G. Talli, C. Antony, P. Townsend, and C. Ford, "A 10 Gb/s burst-mode receiver with automatic reset generation and burst detection for extended reach PONs," in *Proceedings of the Optical Fiber Communication Conference and Exhibition (OFC)*, 2009, paper OWH3. 47, 48, 85

S. V. Pato, R. Meleiro, D. Fonseca, P. Andre, P. Monteiro, and H. Silva, "All-optical burst-mode power equalizer based on cascaded SOAs for 10-Gb/s EPONs," *IEEE Photonics Technology Letters*, vol. 20, no. 24, pp. 2078–2080, Dec. 2008. 124

S. V. Pato, P. Monteiro, and H. Silva, "On using all-optical burst-mode power equalization in converged metro-access networks," in *Proceedings of the 11th International Conference on Transparent Optical Networks (ICTON 2009)*, Jul. 2009. 124

L. Pavesi, "Will silicon be the photonic material of the third millenium?" *Journal of Physics: Condensed Matter*, vol. 15, no. 26, p. R1169, Jun. 2003. 139

P. Z. Peebles, *Probability, Random Variables, and Random Signal Principles*, 2nd ed. McGraw-Hill, 1987. 32

S. Peng, K. J. Hinton, J. Baliga, R. S. Tucker, Z. Li, and A. Xu, "Burst switching for energy efficiency in optical networks," in *Proceedings of the Optical Fiber Communication Conference and Exhibition (OFC)*, Mar. 2010, p. OWY5. 15

S. D. Personick, "Receiver design for digital fiber optic communication systems, Part I," *Bell System Technical Journal*, vol. 52, no. 6, pp. 843–874, Jul. 1973. 101

——, "Receiver design for digital fiber optic communication systems, Part II," *Bell System Technical Journal*, vol. 52, no. 6, pp. 875–886, Jul. 1973. 101

PMC-Sierra, "PM6373 POLO 40G integrated FEC, DSP, and ADC coherent device," Sep. 2011. [Online]. Available: http://www.pmc-sierra.com/products/details/pm6373/ 138

L. Ponnampalam, N. D. Whitbread, R. Barlow, G. Busico, A. J. Ward, J. P. Duck, and D. J. Robbins, "Dynamically controlled channel-to-channel switching in a full-band DS-DBR laser," *IEEE Journal of Quantum Electronics*, vol. 42, no. 3, pp. 223–230, Mar. 2006. 37

B. Puttnam, B. C. Thomsen, R. Muckstein, A. Bianciotto, and P. Bayvel, "Nanosecond tuning of a DS-DBR laser for dynamic optical networks," in *Proceedings of the European Conference on Lasers and Electro-Optics and European Quantum Electronics Conference (CLEO/EQEC)*, Jun. 2009. 37

B. J. Puttnam, B. C. Thomsen, and P. Bayvel, "Performance of an adaptive threshold receiver in a dynamic optical burst-switched network," *IEEE Photonics Technology Letters*, vol. 20, no. 3, pp. 223–225, Feb. 2008. 52

B. J. Puttnam, B. C. Thomsen, A. López, and P. Bayvel, "Experimental investigation of optically gain-clamped EDFAs in dynamic optical-burst-switched networks," *OSA Journal of Optical Networking*, vol. 7, no. 2, pp. 151–159, Feb. 2008. 38, 51, 62, 81

B. J. Puttnam, Y. Awaji, N. Wada, and S. Zsigmond, "Investigating the limits of optical packet transmission through cascaded transient-suppressed EDFAs without regeneration or active gain control," in *Proceedings of the Optical Fiber Communication Conference and Exhibition (OFC)*, 2010, paper OThI6. 39

B. J. Puttnam, "Investigation of sub-systems for dynamic wavelength-routed optical networks," Ph.D. dissertation, Department of Electronic and Electrical Engineering, University College London (UCL), Mar. 2008. 17, 19, 52

C. M. Qiao and M. S. Yoo, "Optical burst switching (OBS) — A new paradigm for an optical Internet," *Journal of High Speed Networks*, vol. 8, no. 1, pp. 69–84, 1999. 16, 29

——, "Choices, features and issues in optical burst switching," *Optical Networks Magazine*, vol. 1, no. 2, pp. 36–44, Jul. 2000. 16, 29

C. M. Qiao, M. A. González-Ortega, A. Suárez-González, X. Liu, and J.-C. López-Ardao, "On the benefit of fast switching in optical networks," in *Proceedings of the Optical Fiber Communication Conference and Exhibition (OFC)*, Mar. 2010. 15

Y. Qin, S. Azodolmolky, M. Gunkel, R. Nejabati, and D. Simeonidou, "Hardware accelerated impairment-aware control plane for future optical networks," *IEEE Communications Letters*, vol. 15, no. 9, pp. 1004–1006, Sep. 2011. 28

X. Z. Qiu, C. Mélange, T. De Ridder, B. Baekelandt, J. Bauwelinck, X. Yin, and J. Vandewege, "Evolution of burst mode receivers," in *Proceedings of the 35th European Conference and Exhibition on Optical Communications (ECOC)*, Sep. 2009. 44

X.-Z. Qiu, P. Ossieur, J. Bauwelinck, Y. Yi, D. Verhulst, J. Vandewege, B. De Vos, and P. Solina, "Development of GPON upstream physical-media-dependent prototypes," *IEEE/OSA Journal of Lightwave Technology*, vol. 22, no. 11, pp. 2498–2508, Nov. 2004. 18, 43, 44, 45, 89

L. Rabiner, J. Cooley, H. Helms, L. Jackson, J. Kaiser, C. Rader, R. Schafer, K. Steiglitz, and C. Weinstein, "Teminology in digital signal processing," *IEEE Transactions on Audio and Electroacoustics*, vol. 20, no. 5, pp. 322–337, Dec. 1972. 99

C. Raffaelli, K. Vlachos, N. Andriolli, D. Apostolopoulos, J. Buron, R. van Caenegem, G. Danilewicz, J. M. Finochietto, J. Garcia-Haro, D. Klonidis, M. J. O'Mahony, G. Maier, A. Pattavina, P. Pavón-Marino, S. Ruepp, M. Savi, M. Scaffardi, I. Tomkos, A. Tzanakaki, L. Wosinska, O. Zourarakim, and F. Neri, "Photonics in switching: Architectures, systems and enabling technologies," *Computer Networks*, vol. 52, no. 10, pp. 1873–1890, Jul. 2008. 26, 40

R. Ramaswami and K. N. Sivarajan, "Routing and wavelength assignment in all-optical networks," *IEEE/ACM Transactions on Networking*, vol. 3, no. 5, pp. 489–500, Oct. 1995. 15, 27

R. Ramaswami, "Optical networking technologies: What worked and what didn't," *IEEE Communications Magazine*, vol. 44, no. 9, pp. 132–139, Sep. 2006. 16, 25, 26, 29

F. Ramos, E. Kehayas, J. M. Martinez, R. Clavero, J. Marti, L. Stampoulidis, D. Tsiokos, H. Avramopoulos, J. Zhang, P. V. Holm-Nielsen, N. Chi, P. Jeppesen, N. Yan, I. T. Monroy, A. M. J. Koonen, M. T. Hill, Y. Liu, H. J. S. Dorren, R. Van Caenegem, D. Colle, M. Pickavet, and B. Riposati, "IST-LASAGNE: towards all-optical label swapping employing optical logic gates and optical flip-flops," *IEEE/OSA Journal of Lightwave Technology*, vol. 23, no. 10, pp. 2993–3011, Oct. 2005. 16, 28

S. Rangarajan, Z. Hu, L. Rau, and D. J. Blumenthal, "All-optical contention resolution with wavelength conversion for asynchronous variable-length 40 Gb/s optical packets," *IEEE Photonics Technology Letters*, vol. 16, no. 2, pp. 689–691, Feb. 2004. 16

D. H. Richards, J. L. Jackel, and M. A. Ali, "A theoretical investigation of dynamic all-optical automatic gain control in multichannel EDFA's and EDFA cascades," *IEEE Journal of Selected Topics in Quantum Electronics*, vol. 3, no. 4, pp. 1027–1036, Aug. 1997. 38

J. J. P. C. Rodrigues, M. M. Freire, N. M. Garcia, and P. M. N. P. Monteiro, "Enhanced just-in-time: A new resource reservation protocol for optical burst switching networks," in *Proceedings of the IEEE Symposium on Computers and Communications*, Jul. 2007. 66

E. Säckinger, *Broadband Circuits for Optical Fiber Communication*, 1st ed. Wiley-Interscience, 2005. 45, 46

N. Sato, K. Ota, N. Mishima, Y. Oikawa, and N. Shiga, "Less than 0.19-dB transient gain excursion AGC-EDFA with digital control for 20-channel add/drop equivalent operation," in *Proceedings of the Optical Fiber Communication Conference and Exhibition (OFC)*, Mar. 2011, paper OMH3. 39

S. J. Savory, "Digital coherent optical receivers: Algorithms and subsystems," *IEEE Journal of Selected Topics in Quantum Electronics*, vol. 16, no. 5, pp. 1164–1179, Sep. 2010. 14, 51

——, "Digital filters for coherent optical receivers," *OSA Optics Express*, vol. 16, no. 2, pp. 804–817, Jan. 2008. 51

R. Schneiderman, "Mobile computing has a growing impact on DSP apps and markets [special reports]," *IEEE Signal Processing Magazine*, vol. 28, no. 4, pp. 8–11, Jul. 2011. 14

R. Scholtz, "Frame synchronization techniques," *IEEE Transactions on Communications*, vol. 28, no. 8, pp. 1204–1213, Aug. 1980. 65

B. J. Shastri and D. V. Plant, "5/10-Gb/s burst-mode clock and data recovery based on semiblind oversampling for PONs: Theoretical and experimental," *IEEE Journal of Selected Topics in Quantum Electronics*, vol. 16, no. 5, pp. 1298–1320, Sep. 2010. 47, 49

D. P. Shea and J. E. Mitchell, "Long-reach optical access technologies," *IEEE Network*, vol. 21, no. 5, pp. 5–11, Sep. 2007. 120

——, "Architecture to integrate multiple pons with long reach dwdm backhaul," *IEEE Journal on Selected Areas in Communications*, vol. 27, no. 2, pp. 126–133, Feb. 2009. 120, 122, 123

P. W. Shumate, "Fiber-to-the-home: 1977–2007," *IEEE/OSA Journal of Lightwave Technology*, vol. 26, no. 9, pp. 1093–1103, May 2008. 43

H. Song, B.-W. Kim, and B. Mukherjee, "Long-reach optical access networks: A survey of research challenges, demonstrations, and bandwidth assignment mechanisms," *IEEE Communications Surveys and Tutorials*, vol. 12, no. 1, pp. 112–123, 2010. 121, 123

K. B. Song, S. T. Chung, G. Ginis, and J. M. Cioffi, "Dynamic spectrum management for next-generation dsl systems," *IEEE Communications Magazine*, vol. 40, no. 10, pp. 101–109, Oct. 2002. 19

K. Sorimoto, H. Tsuda, H. Ishikawa, T. Hasama, H. Kawashima, K. Kintaka, M. Mori, and H. Uetsuka, "Demonstration of a wavelength selective switch using an LCOS and a stacked arrayed waveguide grating," in *Proceedings of the 35th European Conference and Exhibition on Optical Communications (ECOC)*, Vienna, Austria, Sep. 2009. 139

C. E. Spurgeon, *Ethernet — The Definitive Guide*, 1st ed. O'Reilly & Associates, Inc., Feb. 2000. 48

A. K. Srivastava, Y. Sun, J. L. Zyskind, and J. W. Sulhoff, "EDFA transient response to channel loss in WDM transmission system," *IEEE Photonics Technology Letters*, vol. 9, no. 3, pp. 386–388, Mar. 1997. 39

A. Stavdas, S. Sygletos, M. J. O'Mahoney, H. L. Lee, C. Matrakidis, and A. Dupas, "IST-DAVID: Concept presentation and physical layer modeling of the metropolitan area network," *IEEE/OSA Journal of Lightwave Technology*, vol. 21, no. 2, pp. 372–383, Feb. 2003. 28

C. Su, L.-K. Chen, and K.-W. Cheung, "Theory of burst-mode receiver and its applications in optical multiaccess networks," *IEEE/OSA Journal of Lightwave Technology*, vol. 15, no. 4, pp. 590–606, Apr. 1997. 41

A. Sugama, T. Akahoshi, K. Sato, S. Aoki, Y. Kai, Y. Takita, M. Kato, and H. Onaka, "Integrated 8×8 electro-optic high-speed switch for optical burst transport networks," in *Proceedings of the Optical Fiber Communication Conference and Exhibition (OFC)*, Mar. 2007, paper OWV2. 40

J. Sugawa, D. Mashimo, and H. Ikeda, "10.3Gbps burst-mode receiver capable of upstream transmission with short overhead for 10G-EPON," in *Proceedings of the 36th European Conference and Exhibition on Optical Communications (ECOC)*, Torino, Italy, Sep. 2010, paper Mo.2.B.4. 47, 49, 85

S. Takahashi, T. Okamura, and A. Tajima, "The fastest response burst-mode transmission scheme using small redundant scrambler and AC-coupled receiver with fast baseline response," in *Proceedings of the Optical Fiber Communication Conference and Exhibition (OFC)*, Mar. 2010, paper OThE7. 47, 48

G. Talli and P. D. Townsend, "Hybrid DWDM-TDM long-reach PON for next-generation optical access," *IEEE/OSA Journal of Lightwave Technology*, vol. 24, no. 7, pp. 2827–2834, Jul. 2006. 122

K. Tanaka, A. Agata, and Y. Horiuchi, "IEEE 802.3av 10G-EPON standardization and its research and development status," *IEEE/OSA Journal of Lightwave Technology*, vol. 28, no. 4, pp. 651–661, Feb. 2010. 10, 43, 51, 85, 87, 88, 89, 90

A. S. Tanenbaum, *Computer Networks*, 3rd ed. Prentice-Hall, Inc., 1996. 25, 30

S. Tariq, M. K. Dhodhi, J. C. Palais, and R. E. Ahmed, "Next generation DWDM networks: demands, capabilities and limitations," in *Proceedings of the Canadian Conference on Electrical and Computer Engineering*, vol. 2, 2000, pp. 1003–1007. 15

H. Teimoori, D. Apostolopoulos, K. Vlachos, C. Ware, D. Petrantonakis, K. Yiannopoulos, L. Stampoulidis, H. Avramopoulos, and D. Erasme, "Physical architectures for packet-switching network nodes based on nonlinear logic gates," in *Proceedings of the 6th International Symposium on Communication Systems, Networks and Digital Signal Processing (CNSDSP 2008)*, Jul. 2008, pp. 676–679. 26

J. Terada, K. Nishimura, S. Kimura, H. Katsurai, N. Yoshimoto, and Y. Ohtomo, "A 10.3 Gb/s burst-mode CDR using a $\Delta\Sigma$ DAC," *IEEE Journal of Solid-State Circuits*, vol. 43, no. 12, pp. 2921–2928, Dec. 2008. 97

B. C. Thomsen, B. J. Puttnam, and P. Bayvel, "Optically equalized 10 Gb/s NRZ digital burst-mode receiver for dynamic optical networks," *OSA Optics Express*, vol. 15, no. 15, pp. 9520–9526, Jul. 2007. 52, 104

V. Tintor, P. Matavulj, and J. Radunovic, "Analysis of blocking probability in optical burst switched networks," *Springer Photonic Network Communications*, vol. 15, no. 3, pp. 227–236, Jun. 2008. 66

R. W. Tkach, "Scaling optical communications for the next decade and beyond," *Bell Labs Technical Journal*, vol. 14, no. 4, pp. 3–9, Feb. 2010. 14

A. V. Tran, C.-J. Chae, R. S. Tucker, and Y. J. Wen, "EDFA transient control based on envelope detection for optical burst switched networks," *IEEE Photonics Technology Letters*, vol. 17, no. 1, pp. 226–228, Jan. 2005. 39

R. S. Tucker, "Optical packet switching meets mythbusters," in *Proceedings of the Optical Fiber Communication Conference and Exhibition (OFC)*, Mar. 2011, paper OTuG4. 28

——, "Optical packet switching: A reality check," *Optical Switching and Networking*, vol. 5, no. 1, pp. 2–9, Mar. 2008. 28

G. L. Turin, "An introduction to matched filters," *IRE Transactions on Information Theory*, vol. 6, no. 3, pp. 311–329, Jun. 1960. 55, 56

——, "Introduction to digital matched-filters," *Proceedings of the IEEE*, vol. 64, no. 7, pp. 1092–1112, Jul. 1976. 55, 56

J. S. Turner, "Terabit burst switching," *Journal of High Speed Networks*, vol. 8, no. 1, pp. 3–16, Jan. 1999. 16, 29

I. Van de Voorde, C. M. Martin, I. Vandewege, and X. Z. Oiu, "The superPON demonstrator: an exploration of possible evolution paths for optical access networks," *IEEE Communications Magazine*, vol. 38, no. 2, pp. 74–82, Feb. 2000. 122

J. J. Vegas Olmos, N. Chi, G. Zervas, D. Simeonidou, S. Yu, I. T. Monroy, and A. M. J. Koonen, "Optical node with time-space-and-wavelength domain contention resolution, deflection and dropping capability," *OSA Optics Express*, vol. 14, no. 24, pp. 11 545–11 550, Nov. 2006. 40

H. Wang, A. Wonfor, K. A. Williams, R. V., Penty, and I. H. White, "Demonstration of a lossless monolithic 16×16 QW SOA switch," in *Proceedings of the 35th European Conference and Exhibition on Optical Communications (ECOC)*, Vienna, Austria, Sep. 2009. 40

Y. Wang, E. Serpedin, and P. Ciblat, "An alternative blind feedforward symbol timing estimator using two samples per symbol," *IEEE Transactions on Communications*, vol. 51, no. 9, pp. 1451–1455, Sep. 2003. 97

A. Ward, D. Robbins, G. Busico, E. Barton, L. Ponnampalam, J. Duck, N. Whitbread, P. Williams, D. Reid, A. Carter, and M. Wale, "Widely tunable DS-DBR laser with monolithically integrated SOA: design and performance," *IEEE Journal of Selected Topics in Quantum Electronics*, vol. 11, no. 1, pp. 149–156, Jan. 2005. 37

B. Widrow, J. R. Glover, J. M. McCool, J. Kaunitz, C. S. Williams, R. H. Hearn, J. R. Zeidler, E. Dong, and R. C. Goodlin, "Adaptive noise cancelling: Principles and applications," *Proceedings of the IEEE*, vol. 63, no. 12, pp. 1692–1716, Dec. 1975. 101

A. Wonfor, H. Wang, R. V. Penty, and I. H. White, "Large port count high-speed optical switch fabric for use within datacenters (Invited)," *IEEE/OSA Journal of Optical Communications and Networking*, vol. 3, no. 8, pp. A32–A39, Aug. 2011. 139

Y. Yamamoto, "Receiver performance evaluation of various digital optical modulation-demodulation systems in the 0.5-10 μm wavelength region," *IEEE Journal of Quantum Electronics*, vol. 16, no. 11, pp. 1251–1259, Nov. 1980. 138

J. Yang, B. Xiang, T. He, A. Karalar, X. Ye, and S. J. Ben Yoo, "All-optical contention resolution with TTL-aware selective 3R regeneration in optical-label switching router networks," in *Proceedings of the Optical Fiber Communication Conference and Exhibition (OFC)*, Feb. 2008, paper OMG3. 29

S. Yao, B. Mukherjee, S. J. B. Yoo, and S. Dixit, "A unified study of contention-resolution schemes in optical packet-switched networks," *IEEE/OSA Journal of Lightwave Technology*, vol. 21, no. 3, pp. 672–683, Mar. 2003. 17, 29, 35, 36, 41

X. Yin, X. Z. Qiu, B. Baekelandt, C. Mélange, T. De Ridder, J. Bauwelinck, and J. Vandewege, "5 Gbit/s burst-mode experiments for high split extended reach PONs," *Electronics Letters*, vol. 46, no. 1, pp. 54–55, Jul. 2010. 47, 48

C. J. Youn, X. Liu, S. Chandrasekhar, Y.-H. Kwon, J.-H. Kim, J.-S. Choe, D.-J. Kim, K.-S. Choi, and E. S. Nam, "Channel estimation and synchronization for polarization-division multiplexed CO-OFDM using subcarrier/polarization interleaved training symbols," *OSA Optics Express*, vol. 19, no. 17, pp. 16 174–16 181, Aug. 2011. 14

S. Yuan, N. Madamopoulos, R. Helkey, V. Kaman, J. Klingshirn, and J. Bowers, "Fully integrated $N \times N$ MEMS wavelength selective switch with 100% colorless add-drop ports," in *Proceedings of the Optical Fiber Communication Conference and Exhibition (OFC)*, Feb. 2008, paper OWC2. 139

A. Zalesky, "To burst or circuit switch?" *IEEE/ACM Transactions on Networking*, vol. 17, no. 1, pp. 305–318, Feb. 2009. 29

A. Zapata-Beghelli, "Resource allocation and scalability in dynamic waveband-routed optical networks," Ph.D. dissertation, Department of Electronic and Electrical Engineering, University College London (UCL), Aug. 2006. 19

A. Zapata-Beghelli and P. Bayvel, "Dynamic versus static wavelength-routed optical networks," *IEEE/OSA Journal of Lightwave Technology*, vol. 26, no. 20, pp. 3403–3415, Oct. 2008. 29

J. R. Zeidler, "Performance analysis of LMS adaptive prediction filters," *Proceedings of the IEEE*, vol. 78, no. 12, pp. 1781–1806, Dec. 1990. 101

W.-P. Zhu, Y. Yan, M. O. Ahmad, and M. N. S. Swamy, "Feedforward symbol timing recovery technique using two samples per symbol," *IEEE Transactions on Circuits and Systems I: Regular Papers*, vol. 52, no. 11, pp. 2490–2500, Nov. 2005. 97

A
Acronyms

AC	Alternating Current
ADC	Analog to Digital Converter
ADM	Add-Drop Multiplexer
ADSL	Asymmetrical Digital Subscriber Line
APD	Avalanche PhotoDiode
ASE	Amplified Spontaneous Emission
ASIC	Application-Specific Integrated Circuit
ATM	Asynchronous Transfer Mode
AOM	Acousto-Optical Modulator
AON	Active Optical Network
AVC	Active Vertical Coupler
AWG	Arrayed Waveguide Grating
AWGN	Additive White Gaussian Noise
BB	Back-to-Back
BD	Burst Detector
BER	Bit Error Rate
BERT	Bit Error-Rate Tester
BLW	Base-Line Wander

BS Broadcast and Select

BSE Baud Spaced Equaliser

CD Chromatic Dispersion

CDR Clock and Data Recovery

CID Consecutive Identical Digits

COPU Centralised Optical Processing Unit

CWDM Coarse Wavelength Division Multiplexing

CW Continuous Wave

DBMRx Digital Burst-Mode Receiver

DC Direct Current

DD Direct Detection

DCF Dispersion Compensating Fibre

DFB Distributed Feedback Laser

DFT Discrete Fourier Transform

DMBRx Digital Multi line-rate Burst-mode receiver

DON Dynamic Optical Network

DPLL Digital Phase-Locked Loop

DPO Digital Phosphor Oscilloscope

DSDBR Digital Supermode Distributed Bragg Reflector

DSP Digital Signal Processing

DTFT Discrete Time Fourier Transform

DUT Device Under Test

DWDM Dense Wavelength Division Multiplexing

EAM Electro-Absorption Modulator

EDFA Erbium Doped Fibre Amplifier

EPON Ethernet Passive Optical Network

FDL Fibre Delay Line

FEC Forward Error Correction

FIR Finite Impulse Response

FOM Figure Of Merit

FPGA Field Programmable Gate Array

FSE Fractionally Spaced Equaliser

FSM Finite State Machine

FTTX Fibre to the Node, Curb, Building, or Home

FWC Fixed Wavelength Converter

FWHM Full Width at Half Maximum

GEM G-PON Encapsulation Method

GPIB General Purpose Interface Bus

GPON Gigabit Passive Optical Network

IC Integrated Circuit

IEEE Institute of Electrical and Electronics Engineers

IP Internet Protocol

ISI Inter-Symbol Interference

ITU International Telecommunication Union

LAN Local Area Network

LMS Least Mean Squares

LR-PON Long-Reach Passive Optical Network

MAC Media Access Control

MAN Metropolitan Area Network

MEMS Micro-Electro-Mechanical Systems

MF Matched Filter

MZI Mach-Zehnder Interferometer

NG-PON Next Generation Passive Optical Network

NRZ Non-Return to Zero

OADM Optical Add-Drop Multiplexer

OBS Optical Burst Switching

OCS Optical Circuit Switching

O/E/O Optical-Electrical-Optical

OLS Optical Label Swapping

OLT Optical Line Terminal

ONU Optical Network Unit

OOK On-Off Keying

OPS Optical Packet Switching

ORL Optical Recirculating Loop

OSNR Optical Signal-to-Noise Ratio

OTDM Optical Time Division Multiplexing

OXC Optical Cross-Connect

pBER Payload Bit-Error Rate

PC Personal Computer

PDF Probability Density Function

PDG Polarization Dependent Gain

PER Packet Error Rate

PIC Photonic Integrated Circuit

PLC Planar Lightwave Circuit

PLL Phase-Locked Loop

PLZT Lead Lanthanum Zirconate Titanate

PM Performance Metric

PMD Polarisation Mode Dispersion

PMF Probability Mass Function

PON Passive Optical Network

PRBS Pseudo-Random Binary Sequence

PSC Passive Star Coupler

PSD Power Spectral Density

PPG Pulsed Pattern Generator

PPP Point-to-Point Protocol

RIN Relative Intensity Noise

ROADM Reconfigurable Optical Add-Drop Multiplexer

ROSNR Required Optical Signal-to-Noise Ratio

RWA Routing and Wavelength Assignment

SDH Synchronous Digital Hierarchy

SGDBR Sampled Grating Distributed Bragg Reflector

SMF Single-Mode Fibre

SNB Strictly Non-Blocking

SNR Signal-to-Noise Ratio

SOA Semiconductor Optical Amplifier

SOA-MZI Semiconductor Optical Amplifier Mach-Zehnder Interferometer

SONET Synchronous Optical NETworking

TCP Transmission Control Protocol

TDM Time Division Multiplexing

TDMA Time Division Multiple Access

TIA Trans-Impedance Amplifier

TWC Tunable Wavelength Converter

VHDL Very-high-speed-integrated-circuit Hardware Description Language

VISA Virtual Instrument Software Architecture

WC Wavelength Converter

WC/AWG Wavelength Converter and Arrayed Wavelength Grating

WCOAN Wavelength Converting Optical Access Network

WDM Wavelength Division Multiplexed

WR-OBS Wavelength Routed Optical Burst Switching

WRON Wavelength Routed Optical Network

WSNB Wide-Sense Non-Blocking

WSS Wavelength Selector Switch

WXC Wavelength Cross-Connect

XGM Cross-Gain Modulation

XPM Cross-Phase Modulation